

Making a Deal with the Devilfish: Biometric-Informed Screening Technology - CRADA 514 (Final Report)

2020 Fish Protection Prize: Team Mater

March 2022

Benjamin D. Mater¹
Charles C. Coutant¹
Kenneth D. Ham
William A. Perkins
Josef F. Christ
David M. Anderson
Rajesh K. Singh
Andre A. Rahrooh
Brittany L. Taruffelli
Robert P. Mueller

¹Alden Research Laboratory, LLC.

DISCLAIMER

This report was prepared as an account of work sponsored by an agency of the United States Government. Neither the United States Government nor any agency thereof, nor Battelle Memorial Institute, nor any of their employees, makes **any warranty, express or implied, or assumes any legal liability or responsibility for the accuracy, completeness, or usefulness of any information, apparatus, product, or process disclosed, or represents that its use would not infringe privately owned rights.** Reference herein to any specific commercial product, process, or service by trade name, trademark, manufacturer, or otherwise does not necessarily constitute or imply its endorsement, recommendation, or favoring by the United States Government or any agency thereof, or Battelle Memorial Institute. The views and opinions of authors expressed herein do not necessarily state or reflect those of the United States Government or any agency thereof.

PACIFIC NORTHWEST NATIONAL LABORATORY
operated by
BATTELLE
for the
UNITED STATES DEPARTMENT OF ENERGY
under Contract DE-AC05-76RL01830

Printed in the United States of America

Available to DOE and DOE contractors from the
Office of Scientific and Technical Information,
P.O. Box 62, Oak Ridge, TN 37831-0062;
ph: (865) 576-8401
fax: (865) 576-5728
email: reports@adonis.osti.gov

Available to the public from the National Technical Information Service
5301 Shawnee Rd., Alexandria, VA 22312
ph: (800) 553-NTIS (6847)
email: orders@ntis.gov <<https://www.ntis.gov/about>>
Online ordering: <http://www.ntis.gov>

Making a Deal with the Devilfish: Biometric-Informed Screening Technology - CRADA 514 (Final Report)

2020 Fish Protection Prize: Team Mater

March 2022

Benjamin D. Mater¹
Charles C. Coutant¹

¹Alden Research Laboratory, LLC.

Prepared for
the U.S. Department of Energy
under Contract DE-AC05-76RL01830

Pacific Northwest National Laboratory
Richland, Washington 99354

Cooperative Research and Development Agreement (CRADA) Final Report

Report Date:

In accordance with Requirements set forth in the terms of the CRADA, this document is the CRADA Final Report, including a list of Subject Inventions, to be provided to PNNL Information Release who will forward to the DOE Office of Scientific and Technical Information as part of the commitment to the public to demonstrate results of federally funded research.

Parties to the Agreement:

Battelle Memorial Institute, Operator of Pacific Northwest National Laboratory under its U.S. Department of Energy Contract No.DE-AC05-76RL01830

and

Alden Research Laboratory, LLC

CRADA number: 514

CRADA Title: Making a Deal with the Devilfish: Biometric-Informed Screening Technology – Fish Protection Prize

Responsible Technical Contact at DOE Lab: Kenneth Ham, kenneth.ham@pnnl.gov

Name and Email Address of POC at Company: Ben Mater, bmater@aldenlab.com

DOE Program Office: Water Power Technologies Office

Joint Work Statement Funding Table showing DOE funding commitment:

- 1. Marketability Study (\$10K PNNL w/ Alden support):** PNNL will perform market research to determine (i) number of candidate sites, (ii) species/life stages of concern at these sites, (iii) typical hydraulic conditions at these sites, including approximate sweeping and approach velocity magnitudes, and (iv) approximate revenue potential for retrofitting candidate sites.
- 2. CFD Baseline Simulations (\$30K PNNL w/ Alden guidance):** PNNL will perform Computational Fluid Dynamics (CFD) simulations of the baseline concept and a conventional analog on PNNL's HPC system with Alden guidance. Simulations will be used to (i) determine utility of CFD as design optimization tool and (ii) analyze entrainment and head loss performance of the baseline concept compared to a conventional analog screen.
- 3. CFD Design Refinement Simulations (\$30K PNNL w/ Alden guidance):** Following review of baseline simulation results, Alden will develop refined prototype designs. PNNL will perform simulations of select design refinements on PNNL's HPC system. Simulations will be used to (i) further optimize the prototype design and (ii) identify optimal flow regimes (e.g., optimal sweep/approach velocity ratio range).
- 4. Prototype Fabrication (\$20K PNNL w/ Alden guidance):** Refined prototype designs and conventional analogs will be fabricated by PNNL (e.g., using additive manufacturing) for laboratory flume testing to be conducted at Alden. It is assumed that approximately twelve screen panels will be fabricated, each being approximately 12 inches by 12-36 inches in size, with as small as ~1 mm-wide screen bars and slots.
- 5. Laboratory Prototype Testing (Alden):** A testing apparatus (flume) will be designed, fabricated, and used by Alden to analyze flow patterns associated with the refined prototype designs. The apparatus will allow for flow patterns to be visualized and particle (e.g., surrogate egg) entrainment and impingement rates to be quantified. The goal of the laboratory testing is to analyze entrainment/impingement performance of the refined prototype designs using a conventional analog screen design as the basis for comparison.
- 6. Hydraulic/Biologic Consulting (\$10K PNNL):** PNNL will provide hydraulic and biologic consulting support to support interpretation of numerical and laboratory results.
- 7. Reporting (Alden with PNNL support/review):** Alden will develop the following deliverables and submit them to NREL, PNNL, DOE-WPTO, and Reclamation:
 - a. 1-page monthly progress updates from the date of CRADA execution through one year from the date of CRADA execution.
 - b. Presentation at a 2021 or 2022 conference or workshop detailing the progress made to date during the CRADA period of performance. DOE-WPTO and Reclamation will select the venue, but potential venues could include the HydroVision Annual Conference or the American Fisheries Society Annual Meeting.
 - c. Final technical paper no more than 25 pages, excluding references and appendices, describing the progress made over the CRADA period of performance as well as advances toward the goals of the Fish Protection Prize. Due: one year from the date of CRADA execution.
 - d. One PowerPoint slide summarizing the award (concept, team, and progress) and labeled for external use.

Executive Summary

This report documents an investigation into the performance of a novel fish-protection screen intended to prevent small aquatic and marine organisms from entering water intakes in free-flowing water bodies. The proposed prototype screen resembles conventional, slotted fish-protection screens with parallel wires or bars; however, the prototype bars are shaped to mimic the filter elements in the mouths of filter-feeding fishes such as the devil ray (*Mobula tarapacana*). Millions of years of evolution have perfected these structures to provide energetically efficient and clog-resistant filtering of zooplankton from seawater. The intent of the prototype is to exploit these mechanisms for the protection of similarly sized, or larger, organisms in settings where the freely flowing current is approximately parallel with the screen face (i.e., sweeping flow) and perpendicular to the screen bars.

Using computer modeling and laboratory flume testing, the prototype screen was compared to a conventional screen type (wedge wire bars) of similar porosity (~30%) and slot size (1.75-mm) for a variety of flow conditions. The interactions of 1-mm spherical particles (surrogate fish eggs) with the screen face were of primary focus. The study did not reveal meaningful differences between the prototype and the conventional analog; however, a wealth of information was generated that will be used to refine the proposed design. More broadly, many of the new insights are generally applicable to conventional screens – especially findings related to entrainment risk versus flow velocity. These findings may prove useful to fish-protection agencies that regulate water intakes. As such, the project outcomes may benefit the environment, water users, and the general public through better-informed regulation of intakes. Key findings that are broadly applicable to fish-protection screens in sweeping flow include:

- Near 100% entrainment of sub-slot-sized particles when the sweeping velocity across the screen face is less than 5 times the bulk velocity approaching the screen (1-mm particles, 1.75-mm slots).
- Decreasing entrainment risk for sweep-to-approach velocity ratios from 5 to 20. Saltation (skipping) of particles along the screen face is an important mechanism to reduce entrainment.
- Near 0% entrainment for sweep-to-approach velocity ratios ≥ 20 , with all particles saltating along the screen face to avoid entrainment.
- 0% impingement of particles which were slightly larger than screen slot size for a sweep-to-approach velocity ratio of 10 (2.5-mm particles, 1.75-mm slots).
- *Increasing* porosity from ~30% to ~50% was shown to *decrease* entrainment of 1-mm particles through 1.75-mm slots by more than a factor of two (half the entrainment at 50% porosity vs. 30% porosity) – likely due to decreased slot velocity at higher porosity. An optimal porosity likely exists that minimizes slot velocity while maximizing particle-screen interactions that prevent entrainment.

Contents

Executive Summary	v
1.0 Introduction: A Nature-Inspired Fish Protection Screen	1
2.0 Project Activities	3
3.0 Computer Modeling of Particle-Screen Interactions	4
3.1 Objectives	4
3.2 Methodology	4
3.3 Results	8
4.0 Prototype Performance in a Laboratory Flume	19
4.1 Objectives	19
4.2 Methodology	20
4.3 Results	23
5.0 Is It Worth It? Marketability	28
5.1 Objectives	28
5.2 Methodology	28
5.3 Results	29
6.0 Discussion of Findings	29
7.0 Future Research	30
8.0 References	31
Appendix A CFD Evaluation of Devilfish-Inspired Fish Exclusion Screening	A.1
Appendix B Additive Manufacturing	B.1
Appendix C Fish Screen Life-Cycle Cost Model	C.1

Figures

Figure 1.1.	Three-dimensional rendering of baseline, fine-scale prototype and a hypothetical wedge wire screen of matching slot size and porosity	2
Figure 3.1.	Schematic of CFD flume which closely resembled laboratory flume.....	5
Figure 3.2.	Example of local flow disturbance by a sub-slot-sized particle and particle-screen interaction for wedge wire and prototype	6
Figure 3.3.	Schematic of entrainment calculation approach.....	8
Figure 3.4.	Vortex shedding and oscillatory through-screen flow observed in simulation of prototype in wing orientation	9
Figure 3.5.	Bin-wise approach velocity along the length of the prototype in spoiler mode and wedge wire screen types	11
Figure 3.6.	Simulated flow patterns through prototype slots for increasing sweep-to-approach velocity ratio	13
Figure 3.7.	Simulated flow patterns through wedge wire slots for increasing sweep-to-approach velocity ratio	13
Figure 3.8.	Simulated flow patterns through prototype slots for increasing sweep-to-approach velocity ratio	14
Figure 3.9.	Simulated flow patterns through wedge wire slots for increasing sweep-to-approach velocity ratio	14
Figure 3.10.	Simulated particle trajectories for prototype for increasing sweep-to-approach velocity ratio	16
Figure 3.11.	Simulated particle trajectories for wedge wire for increasing sweep-to-approach velocity ratio	16
Figure 3.12.	Simulated particle trajectories for prototype for increasing sweep-to-approach velocity ratio	17
Figure 3.13.	Simulated particle trajectories for wedge wire for increasing sweep-to-approach velocity ratio	17
Figure 3.14.	Comparison of trajectories for prototype and wedge wire at sweep-to-approach velocity ratio of 20 and a sweep velocity of only 1 ft/s.....	17
Figure 3.15.	Comparison of particle entrainment in central screen bins.....	19
Figure 4.1.	Plan view schematic of Alden test flume.	20
Figure 4.2.	Photographs of Alden laboratory flume prior to testing.	20
Figure 4.3.	Fine-scale prototype test panel fabricated by PNNL and two conventional wedge wire analogs.....	22
Figure 4.4.	Photograph of dye injection revealing considerable turbulent mixing in laboratory flume.....	24
Figure 4.5.	Photograph of dye injection revealing considerable turbulent mixing in front of wing-oriented prototype.....	24
Figure 4.6.	Photographs of two bead sizes immediately upon injection into Alden flume.....	25
Figure 4.7.	Comparison of 1-mm bead entrainment in laboratory flume testing of prototype and two wedge wire panels for flow Scenario #5	26

Tables

Table 2.1.	Originally-proposed work under CRADA and notes on actual task performance.	3
Table 3.1.	Flow conditions simulated with CFD model for both prototype and wedge wire.....	7
Table 3.2.	Comparison of particle entrainment in central screen bins.....	18
Table 4.1.	Comparison of 1-mm bead entrainment and 2.5-mm bead impingement in laboratory flume testing of prototype and two wedge wire panels for flow Scenario #5	27

1.0 Introduction: A Nature-Inspired Fish Protection Screen

In FY20, the National Renewable Energy Laboratory (NREL) initiated a prize competition with support from Pacific Northwest National Laboratory (PNNL), and sponsored by the U.S. Department of Energy Water Power Technologies Office (DOE WPTO) and United States Bureau of Reclamation (USBR), to support the development of innovative methods for excluding fish from water diversions and intakes: the Fish Protection Prize. This report documents the prize-winning concept and preliminary research made possible by direct financial support from DOE WPTO and USBR and technical voucher support from PNNL during FY21 under CRADA 514.

The prize-winning concept, developed by Benjamin Mater of Alden Research Laboratory, LLC (Alden) and Charles Coutant, is for a novel fish exclusion screen that mimics the filter elements in the mouths of filter-feeding fishes. Millions of years of evolution have perfected these structures to provide energetically efficient and clog-resistant filtering, making use of detailed micro-hydraulics that we are just now coming to understand. Recently, Divi et al. (2018) used laboratory testing and numerical modeling to show that the buccal filter elements of manta rays (*Mobula birostris*) and devil rays (*Mobula tarapacana*) can efficiently separate zooplankton particles from seawater, even if the particles are smaller than the openings between filter elements. Rather than basic sieve-like filtering wherein particles are filtered solely on the basis of size relative to filter pores, the fish rely upon small-scale flow patterns at filter elements and a particle ricochet mechanism to exclude even sub-pore scale particles.

The concept screen seeks to exploit these biological mechanisms to prevent aquatic organisms – especially ichthyoplankton and small life stages of fish – from entering water withdrawals (e.g., irrigation-water diversions, desalination plant intakes, power station cooling-water intakes, and hydropower turbine intakes) while minimizing debris fouling. The baseline conceptual design replaces the bars of a traditional slotted fish protection screen (e.g., typically constructed from parallel wedge-wire bars) with bars that resemble the filter elements of the devil ray (Figure 1.1.). The bars' cross-sectional geometry was scaled up from the 1.1-mm slot size reported in Divi et al. to a 1.75-mm slot size to match the minimum slot size requirement of the National Marine Fisheries Service (NMFS). The screen bars are intended to be bi-directional, working in both “spoiler” and “wing” orientation (tilted away from or toward the source of water flowing parallel to the array of filter elements, respectively). Already approved and installed infrastructures which feature mesh and wedge wire screens, louvers, and bar racks could be readily retrofitted with the prototype screen.

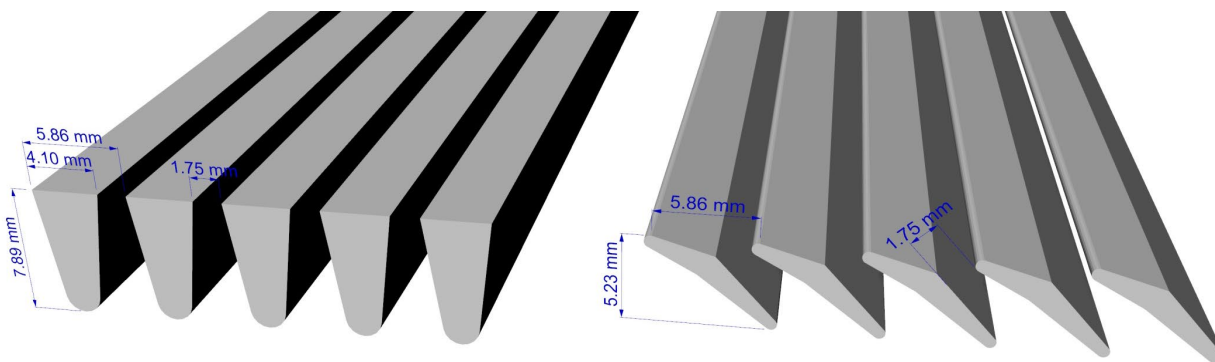


Figure 1.1. Three-dimensional rendering of baseline, fine-scale prototype (right) and a hypothetical wedge wire screen of matching slot size (1.75 mm) and porosity (29.9%). Both tested with PNNL CFD model.

The goal of the CRADA work was to arrive at a final hydraulic-based design (bar shape and spacing) for both fine and coarse-scale versions of the prototype. The fine-scale version was to have similar dimensions to devil fish morphology for exclusion of eggs and larval fish (~1.75-mm clear spacing). The dimensions of the coarse-scale version were to target protection of larger fish (e.g., river-migrating juvenile salmon, shad, or river herring; ~1-10 cm clear spacing). Research and development objectives for the CRADA work included:

- i. Investigation of the prototype at both fine and coarse scales using computer modeling.
- ii. Comparison of the prototype and conventional screen design(s) using laboratory testing.

Both computer modeling and laboratory testing were accomplished during the CRADA period. However, the ultimate goal of refining the baseline concept at fine and coarse scales was not fully realized. Rather, the unrefined, fine-scale concept (Figure 1.1., right) was thoroughly modeled and tested alongside a conventional wedge-wire analog (Figure 1.1., left) in order to develop a firm understanding of performance over a range of flow conditions. The data developed will serve as a sound foundation for post-CRADA work investigating design refinement and coarse-scale performance.

The remainder of this report documents the numerical and experimental approaches used to investigate the baseline, fine-scale concept, the data developed pertaining to particle entrainment/exclusion performance, and the implications for future research and development. A market analysis tool developed by PNNL is also discussed.

2.0 Project Activities

The originally proposed scope of work (SOW) is summarized in Table 2.1. along with a note on the extent to which each task was addressed during the CRADA period. The tasks can be generally categorized into those related to computer modeling, those related to laboratory testing, and the marketability study. Accomplished work in these three areas is discussed further in the subsequent sections of this report.

Table 2.1. Originally-proposed work under CRADA and notes on actual task performance.

Task	Proposed Work	Accomplishments or Deviations
1	Marketability Study (PNNL w/ Alden support)	PNNL developed a spreadsheet-based tool for estimating return on investment based on existing candidate sites, both screened and unscreened, in the western US (see Section 5.0).
2	CFD Baseline Simulations (PNNL w/ Alden guidance)	PNNL successfully developed CFD models of the baseline concept and a conventional analog at the fine-scale (1.75 mm slot size). The two screen types were simulated and compared for a range of flows as envisioned (see Section 3.0); however, only a single particle size (dia. 1 mm) was investigated. Time did not allow for investigation of the coarse-scale prototype.
3	CFD Design Refinement Simulations (PNNL w/ Alden guidance)	Time did not afford for testing alternative screen designs; however, the wealth of data generated under Task 2 will serve as a strong foundation for design refinement.
4	Prototype Fabrication (PNNL w/ Alden guidance)	PNNL fabricated a single 18-inch by 40-inch test panel of the fine-scale baseline prototype screen. Conventional analog test panels were purchased by Alden directly from an established screen vendor (see section 4.0).
5	Laboratory Prototype Testing (Alden)	An 8-inch-wide, 18-inch-deep acrylic flume was constructed at Alden as envisioned. Testing was performed to compare the fine-scale prototype test panel with two competing conventional wedge-wire panels. Entrainment of 1-mm and impingement of 2.5-mm beads were evaluated. Only a single flow regime was tested during the CRADA period; however, future testing is possible (see Section 4.0)
6	Hydraulic/Biologic Consulting (PNNL)	Helpful hydraulic discussions were held on a bi-weekly basis with PNNL scientists and engineers.
7	Reporting (Alden with PNNL support/review)	Monthly progress reports were submitted The current report will serve as technical documentation. A summary slide was prepared.

3.0 Computer Modeling of Particle-Screen Interactions

3.1 Objectives

Under Alden guidance, PNNL performed CFD simulations of flow and particles interacting with the fine-scale baseline prototype and a wedge wire analog of matching slot size (1.75 mm) and porosity (29.9%). The simulated screen bar geometry is shown in Figure 1.1.. Highlights of the study are summarized here, with details provided in Appendix A. Key objectives were (i) to determine utility of CFD as design optimization tool and (ii) analyze entrainment and head loss performance of the baseline concept compared to a conventional analog screen.

3.2 Methodology

PNNL employed the commercial CFD software StarCCM+ by Siemens Digital Industries to develop a numerical model closely resembling a laboratory test flume constructed by Alden for this study (Figure 3.1.). Both real and computer-generated flumes featured a long channel with a 40-inch-long screened “test section” along one of the flume walls, mid-way down the flume. Water was withdrawn through this test section to mimic a fish-exclusion intake screen oriented parallel to the current in a river, canal, or estuary.

Per NMFS terminology, the component of flow parallel to the screen face was referred to as “sweeping flow,” while the component normal to the screen face was referred to as “approach flow.” The “nominal” value of sweep velocity was the value prescribed uniformly across the flume at the upstream boundary of the model and directed down the flume. The nominal value of approach velocity was the suction flow rate divided by the total (bulk) screen area. These nominal values are equivalent to cross-sectional averages. Flow orientations are sketched in Figure 3.1. for clarity.

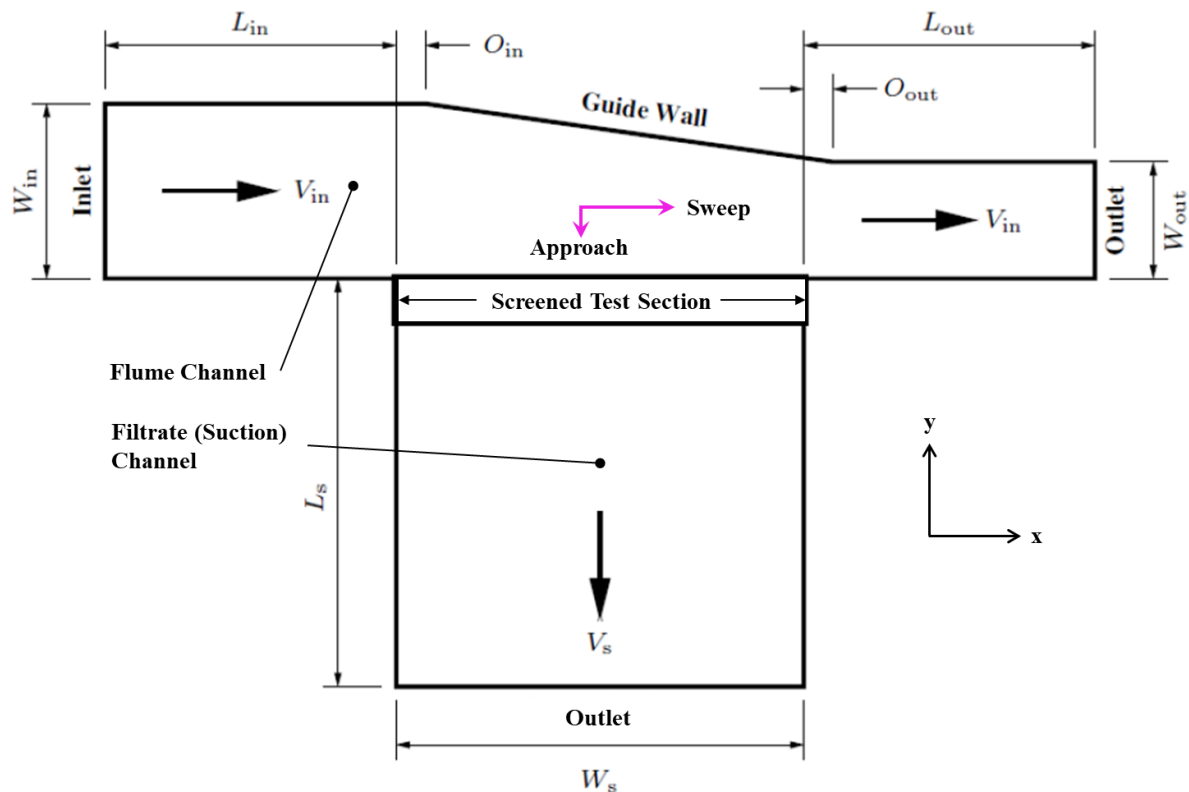


Figure 3.1. Schematic of CFD flume which closely resembled laboratory flume. Test section length held constant for all simulations ($W_s = 40$ inches). Flume dimensions varied to maintain constant average sweep velocity in all flow scenarios as defined in Appendix A.

3.2.1 A Virtual Flume

Unlike the actual flume, which featured a three-dimensional, rectangular channel and a free surface, the CFD domain was simplified to a horizontal, two-dimensional slice at mid-depth of the flume (i.e., variations with depth, or z-direction, were neglected). Thus, the domain extent represented the flume footprint when viewed from above (Figure 3.1). Within the test section, screen bars were oriented perpendicular to the sweeping flow in the flume (into the page in Figure 3.1.). The flume wall opposing the screen face was angled, reducing the width of the flume through the test section to maintain a constant sweeping velocity.

CFD models solve the governing equations for fluid flow at discrete points in space (and time) on a computational mesh. To ensure that small-scale flow patterns through the screen slots were adequately resolved, a mesh sensitivity study was performed. Mesh resolution was increased until sweep, approach, and through-slot velocities became insensitive to further increases in resolution (see Appendix A for details). The mesh that best balanced accuracy and computational expense featured at least ten computation cells across the 1.75-mm screen slot openings.

3.2.2 Simulation of Fish Eggs (Particles)

The CFD model was used to simulate steady-state flow patterns around and through the screen as well as particle interactions with the screen. In many fish protection applications, the particles of interest (e.g., eggs and small life stages) are comparable in size to the screen slots and, as such, are influenced by, but also disturb the local flow field as they approach the screen face (e.g., see Figure 3.2). To capture this two-way coupling, StarCCM+'s Discrete Element Method (DEM) was used to simulate passive spherical particles with a diameter of 1 mm to mimic small fish eggs and the beads used in the laboratory flume. The DEM approach allowed for realistic particle-screen interactions such as the ricochet phenomenon reported by Divi et al. (2018). Over one thousand particles were released across the width of the flume upstream of the test section for each simulation (different distances from the wall on the screen side of the channel).

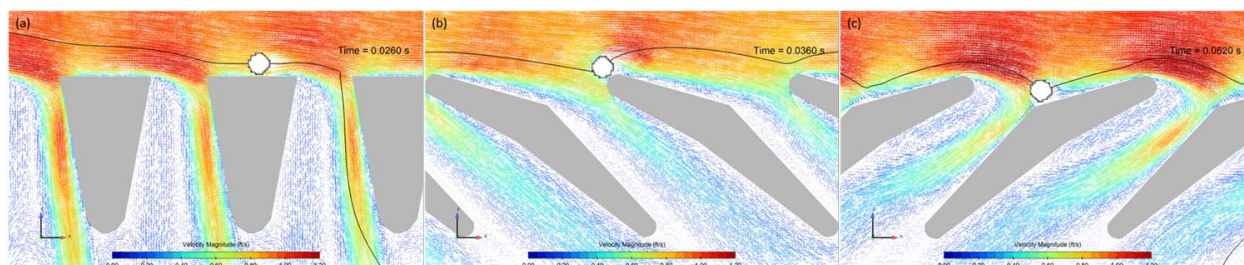


Figure 3.2. Example of local flow disturbance by a sub-slot-sized particle and particle-screen interaction for wedge wire (a) and prototype in wing (b) and spoiler (c) orientation. Both mechanisms need to be captured in CFD simulations to accurately assess screen performance. Images from Alden's preliminary CFD study as part of Fish Protection Prize application.

3.2.3 Simulated Flow Conditions

To capture the wide range of hydraulic conditions that might be experienced by a fish exclusion screen, nominal sweeping and approach velocity were varied across several CFD simulations. Ten separate flow scenarios were tested as listed in Table 3.1. The sweep-to-approach velocity ratio was varied from as low as 2.5 (1 ft/s sweep velocity and maximum allowable approach velocity per NMFS of 0.4 ft/s) to 33.3 (typical flow regime in the buccal cavity of a devil ray swimming at 1 ft/s). The slot-Reynolds number (relative importance of inertial forces to viscous forces through the slot) ranged from approximately 60 to 800, suggesting that slot flow was in the transitional regime between laminar and fully turbulent conditions.

The prototype was tested in “spoiler” orientation for all ten flow scenarios, as was the wedge wire analog. The prototype was tested in “wing” mode for Scenario #5 only due to complications of a vortex-shedding phenomenon (see Section 3.3.1). Head loss across the prototype (spoiler orientation only) and wedge wire screen was estimated for each flow scenario by integrating static pressure head on either side of the screen.

Table 3.1. Flow conditions simulated with CFD model for both prototype (spoiler orientation) and wedge wire.

Scenario #	Sweeping Velocity (fps)	Approach Velocity (fps)	Slot Velocity @ 30% por. (fps)	Sweep: Approach Velocity	Note
1*	1	0.4	1.33	2.5	Very Low Sweep:Approach Ratio; Mod. Sweep Vel. (Max allowable approach velocity per NMFS)
2*	1	0.2	0.67	5	Low Ratio; Moderate Sweep
3*	2	0.4	1.33	5	Low Ratio; High Sweep
4	0.5	0.05	0.17	10	Moderate Ratio; Low Sweep
5†	1	0.1	0.33	10	Moderate Ratio; Moderate Sweep
6	2	0.2	0.67	10	Moderate Ratio; High Sweep
7	1	0.05	0.17	20	High Ratio; Moderate Sweep
8	2	0.1	0.33	20	High Ratio; High Sweep
9	3	0.15	0.50	20	High Ratio; Very High Sweep
10	1	0.03	0.10	33.3	Very High Ratio; Moderate Sweep (devil ray swimming regime)

*simulation not possible with Alden's 8-inch-wide physical flume and 40-inch-long test section (screen flow rate \geq flume flow rate); CFD model "flume" width > 8 inches for these simulations.

†Basis for CFD mesh and turbulence model sensitivity studies on baseline conceptual screen design.

3.2.4 Calculating Entrainment

In principle, estimating entrainment would involve simply counting the number of particles that were sucked through the screen and dividing by the total number of particles released into the flume to get the percent entrained. However, there are two major issues with this simplistic approach if we are interested in screen exclusion mechanisms: (i) Some particles released into the flume may never get close enough to ever have a chance to interact with the screen face or become entrained. Inclusion of these non-interacting particles in the simple entrainment ratio calculation would bias the estimate low. (ii) The second issue has to do with flow patterns. In an ideal simulation, the test screen would be infinitely long so as to avoid anomalous flow patterns near the leading and trailing edges of the screen. As will be shown in the results, the 40-inch-long test screen demonstrated considerably non-uniform through-flow near its upstream and downstream regions. These non-uniformities were not consistent between screen types or flow regimes and could bias the entrainment estimates in unpredictable ways.

These two potential sources of bias were mitigated by only considering particles that got within 5-diameters' distance (5 mm) of the screen face within the middle 60% of the test section (center 24 inches). If a particle never got within 5 mm of the screen face, that particle was considered to have never interacted and was ignored. If a particle did get within 5 mm of the screen face but had its first "interaction" with the screen in the upstream or downstream-most 8 inches of the test section, that particle was also ignored. The interaction scenarios are sketched in Figure 3.3.

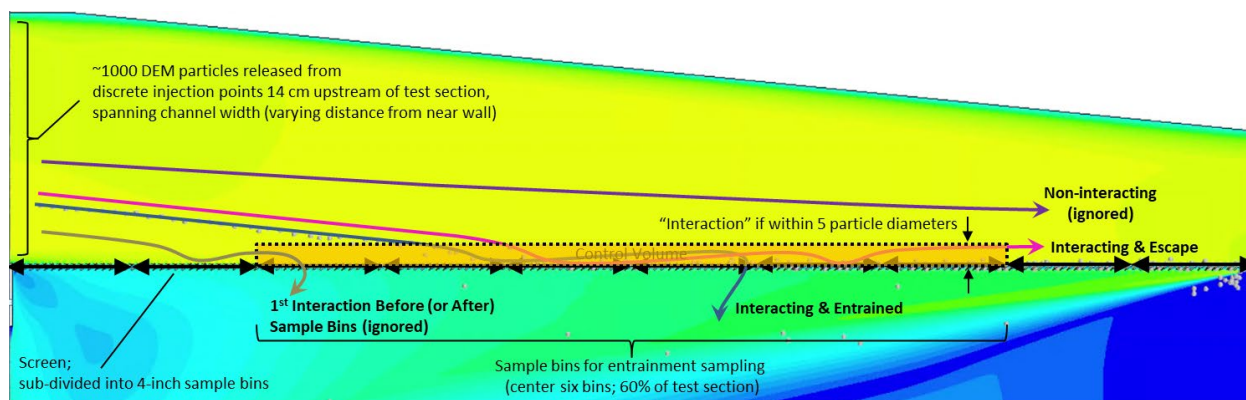


Figure 3.3. Schematic of entrainment calculation approach. Hypothetical particle trajectories sketched relative to test section. Particles that got within five diameters' distance of the screen face were considered to have "interacted." Only particles whose first "interaction" occurred within the center 60% of the test section were considered in the calculation of entrainment percentage.

The entrainment ratios calculated using this approach may be interpreted as the percentage of *interacting* particles that were entrained through the screen assuming nearly-uniform sweeping and approach velocity. This kind of data filtering is not easily accomplished in less controlled laboratory studies (present one included), therefore, the entrainment calculation defined above likely yielded values that were higher than those typically reported from physical flume studies (because interacting particles are more likely to become entrained than particles that simply drift by the screen at a safe distance).

3.3 Results

3.3.1 Vortex Shedding and Near-Screen Turbulence?

Preliminary "shakedown" CFD simulations were carried out for the fine-scale baseline prototype in both wing and spoiler-orientation as well as the wedge wire analog using the flow regime of Scenario #5 (1 ft/s nominal sweep velocity, 0.1 ft/s nominal approach velocity).

For this flow condition an interesting phenomenon was observed when the prototype screen was simulated in wing orientation. The shakedown simulation indicated that the wing-oriented screen bars drive flow through the screen similar to a hood scoop driving air flow into a car induction system. This "forced induction" was predicted to occur even with no applied suction, i.e., in pure sweeping flow. For flow Scenario #5, the applied suction could essentially not "keep up" with the water being forced through the screen by the screen bars. This competition manifested as a flow instability at the screen face. The instability was characterized by vortices emanating from the leading edge of the screen. The vortices were predicted to grow and migrate down the screen face, forcing flow upward and downward through the screen in an oscillating pattern as shown in Figure 3.4. A quick test with Flow Scenario #7 (1 ft/s sweep velocity, 0.05 ft/s approach velocity) indicated that the stability is exacerbated when suction/approach velocity is reduced.

This finding suggests that the wing orientation may induce considerable turbulence near the screen face. Near-screen turbulence may have both negative implications (e.g., screen vibration) and positive implications (e.g., behavioral deterrence or guidance of fish). However,

because turbulence was not explicitly simulated by the model, the wing orientation was excluded from further CFD investigation. Future work may investigate the positive potential for the prototype in generating beneficial near-screen turbulence.

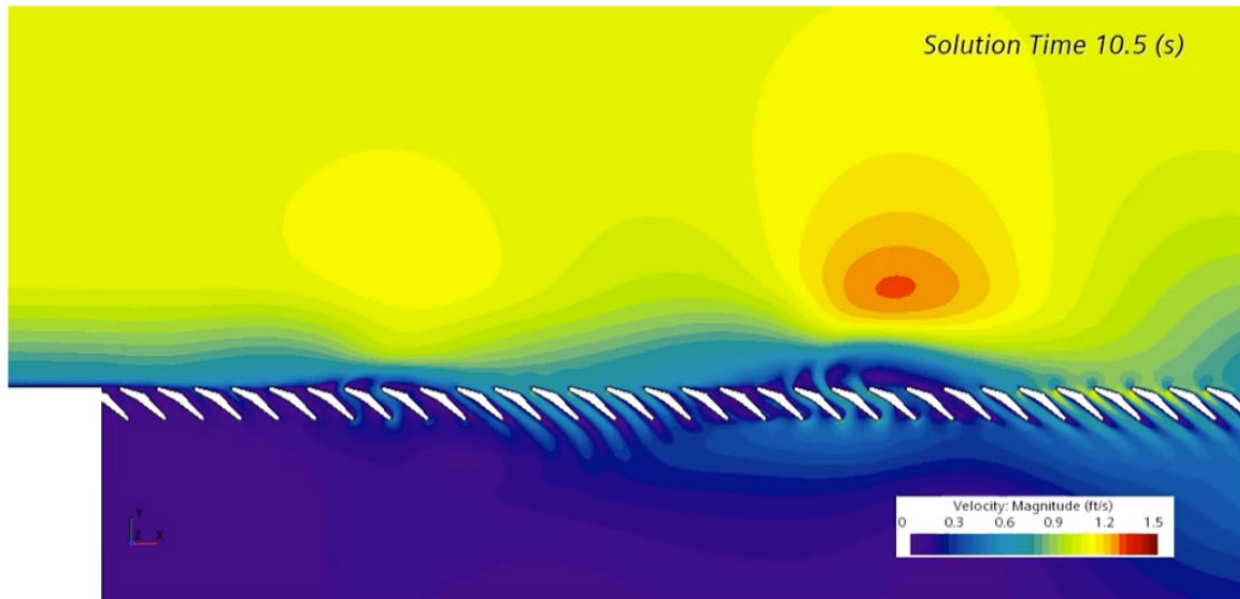


Figure 3.4. Vortex shedding and oscillatory through-screen flow observed in simulation of prototype in wing orientation (flow scenario #5). Sweeping flow is left to right in image.

3.3.2 Flow Patterns

3.3.2.1 Streamwise Flow Distribution

The remainder of the CFD analysis focused on the spoiler orientation of the prototype and the wedge wire screen only (wing-orientated prototype excluded). Simulated flow patterns were evaluated at both the scale of the test section (40-inches in length) and that of the individual screen slots (1.75-mm openings). With regard to the former, the 40-inch test section was subdivided into ten 4-inch bins, and flow through each of the bins was monitored to check flow distribution through the screen. The flow rate (volume per time per unit depth in the 2D model) through each bin was divided by the bin length (area per unit depth) to give an average bulk velocity through the bin, normal to the screen face. Although sampled right at the screen face, these values are close estimations of the approach velocity.

The approach velocity estimates for each bin of both the prototype (spoiler orientation) and the wedge wire are plotted in Figure 3.5 as percentages of the overall average approach velocity for the entire screen. This figure shows only flow Scenarios #1, #2, #5, and #10 (all scenarios shown in Appendix A). These scenarios were selected to demonstrate the influence of sweep-to-approach velocity ratio on flow distribution; all four scenarios shown featured a sweep velocity of 1 ft/s but have approach velocity varying from 0.4 ft/s (maximum allowed by NMFS) to 0.03 ft/s (approximate approach velocity for *M. Tarapacana* filter elements).

When the sweep-to-approach velocity ratio is low, as in the case of Scenario #1 (ratio of 2.5; Figure 3.5a) and Scenario #2 (ratio of 5; Figure 3.5b), approach velocity was predicted to

increase monotonically along the length of the screen for both the prototype and wedge wire. The trend, however, was most pronounced with the prototype, with bin-wise values exceeding 20% of the overall nominal/overall average value in the first and last two bins.

The relatively non-uniform flow distribution demonstrated by the prototype at low sweep-to-approach velocity ratio likely has to do with hydraulic resistance of the screen elements: The pore-scale flow path in the spoiler-oriented prototype is more tortuous than in the wedge wire. As such, head loss is somewhat higher for the prototype (as will be discussed in Section 3.3.3). The pressure gradient required to get flow through the screen thus takes more streamwise distance to develop. By the time flow gets to the downstream portion of the screen, the local approach velocity must increase above the average value to satisfy mass conservation (recall, the total suction flow rate is fixed).

As approach velocity (suction) decreases, so does screen head loss and, by extension, flow distribution improves. Flow distribution becomes more even and similar between the prototype and wedge wire in Scenario #5 (sweep-to-approach ratio of 10; Figure 3.5c) and Scenario #10 (sweep-to-approach ratio of 33.3; Figure 3.5d).

Note that the trend in approach velocity distribution at low sweep-to-approach velocity ratios is unique to screens in cross flow filtration; in other applications, increased screen resistance often leads to more uniform flow distribution, not less. The trend at may also be influenced by geometry of the filtrate channel (downstream of the screen) for the simulated model domain and could perhaps be made more uniform by inclusion of backing structures such as vanes, baffles, or perforated plate to better condition the flow on the downstream side of the screen.

What does this flow distribution finding have to do with fish protection? In general, more uniform flow is preferred in order to avoid “hot spots” in approach velocity that could entrain or impinge fish. The test section simulated here is somewhat short compared to actual fish protection screens and, therefore, the flow distribution simulated may be somewhat extreme, with entrainment/impingement risk highest near the downstream portion of the screen. A longer test section would have likely shown better flow distribution. Nonetheless, these findings suggest that the prototype may require additional optimization and/or flow conditioning measures (e.g., perforated plate backing the screen).

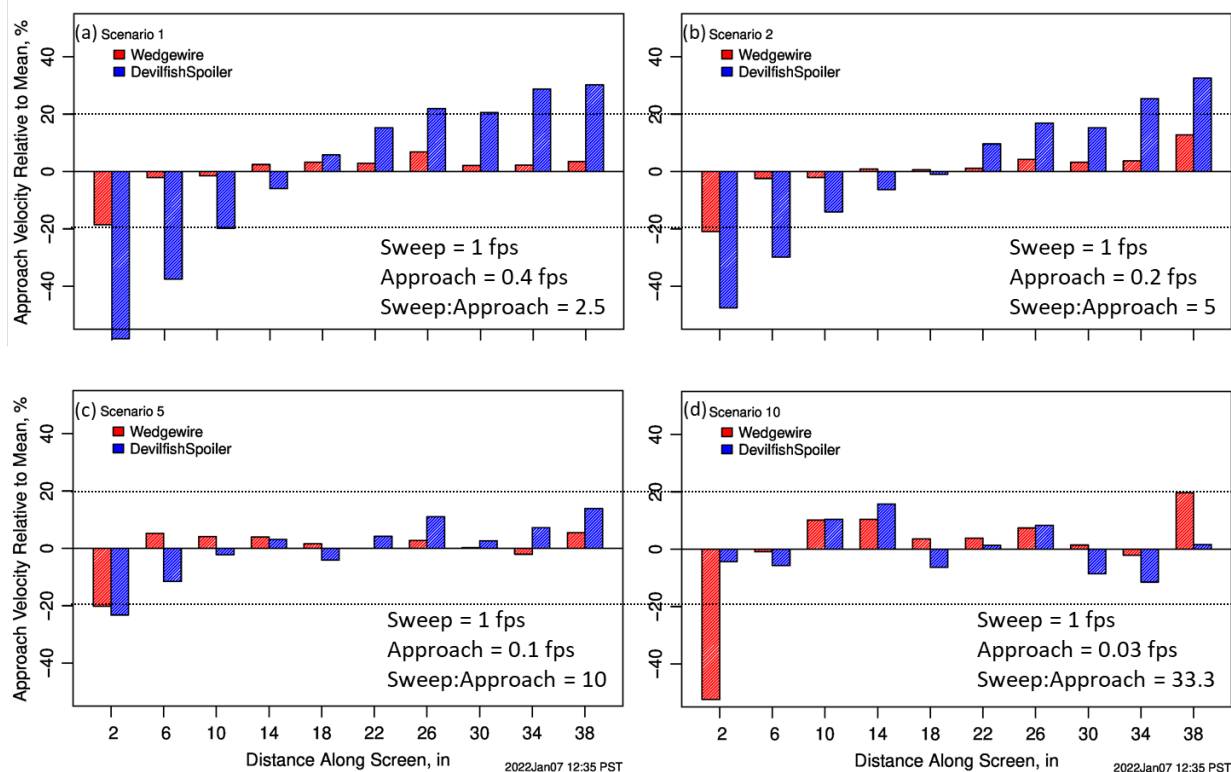


Figure 3.5. Bin-wise approach velocity along the length of the prototype in spoiler mode (blue bars) and wedge wire (red bars) screen types for increasing sweep-to-approach velocity ratio. All scenarios feature a nominal sweep velocity of 1 ft/s; only the water-withdrawal suction was varied). Sweeping flow is left to right.

3.3.2.2 Slot-scale Patterns

At the scale of the screen slots, the flow patterns were similar to patterns simulated by Alden during concept development (e.g., Figure 3.2); specifically, hydraulic restriction of the effective slot size due to the presence of a flow separation zone with the slot. The operating hypothesis is that this interstitial eddy improves exclusion of sub-slot-sized organisms by partial obstruction of the slot.

The interstitial eddy was predicted to form on the downstream side of screen bars in both the prototype and wedge wire. For both screen types, the eddy was predicted to occupy more of the slot width with increasing sweep-to-approach velocity ratio as shown in Figure 3.6 and Figure 3.7 (for scenarios of constant sweep but decreasing approach velocity) and Figure 3.8 and Figure 3.9 (for scenarios of constant approach velocity but increasing sweep velocity).

For the prototype, flow was predicted to round the outward edge of the screen bar and diverge against the upstream face of the next bar downstream. At the divergence point (a.k.a. stagnation point), some flow would move back upward toward the free stream and some flow would move down, continuing through the screen. For all scenarios, the diversion point was predicted to occur on the upward facing aspect of the bar's upstream side, slightly downstream of the "spine" of the bar as shown in Figure 3.6 and Figure 3.8. The location of the divergence point was somewhat insensitive to sweep-to-approach velocity ratio for values less than or equal to ten (Scenarios #1-6; compare Figure 3.6a, b, and c). The point was predicted to move

slightly upward/outward at higher values of the sweep-to-approach velocity ratio as shown in Figure 3.6d (ratio of 33.3) and in the comparison of Scenario #5 (ratio of 10) with Scenario #8 (ratio of 20) shown in Figure 3.8. The location of the flow divergence point is likely key to particle exclusion because this is the point near which particle collisions result in either entrainment or escape. These findings suggest that fish protection is best achieved by the prototype at higher sweep-to-approach velocity ratios so that the particle (organism) encounters the screen outward of the “point-of-no-return” that is the spine of the spoiler-oriented bar.

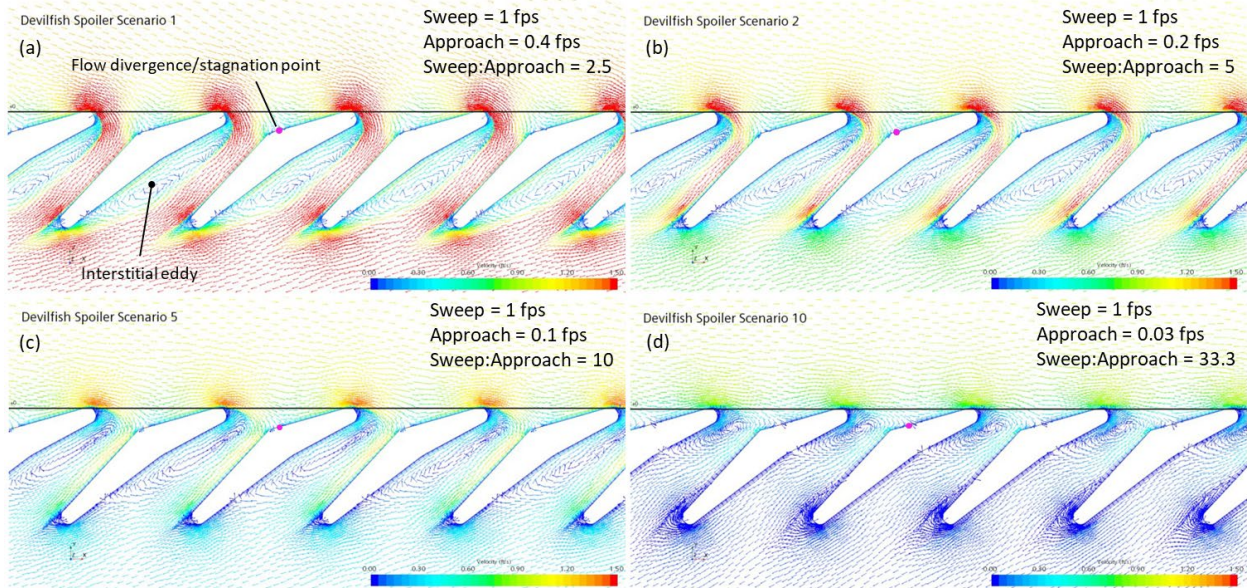


Figure 3.6. Simulated flow patterns through prototype slots (spoiler orientation) for increasing sweep-to-approach velocity ratio. All with **sweep velocity of 1 ft/s**. Flow divergence/stagnation point marked with magenta dot in (a)-(d). Note divergence point is slightly upward/outward in (d) due to high sweep-to-approach ratio. Sweeping flow is left to right.

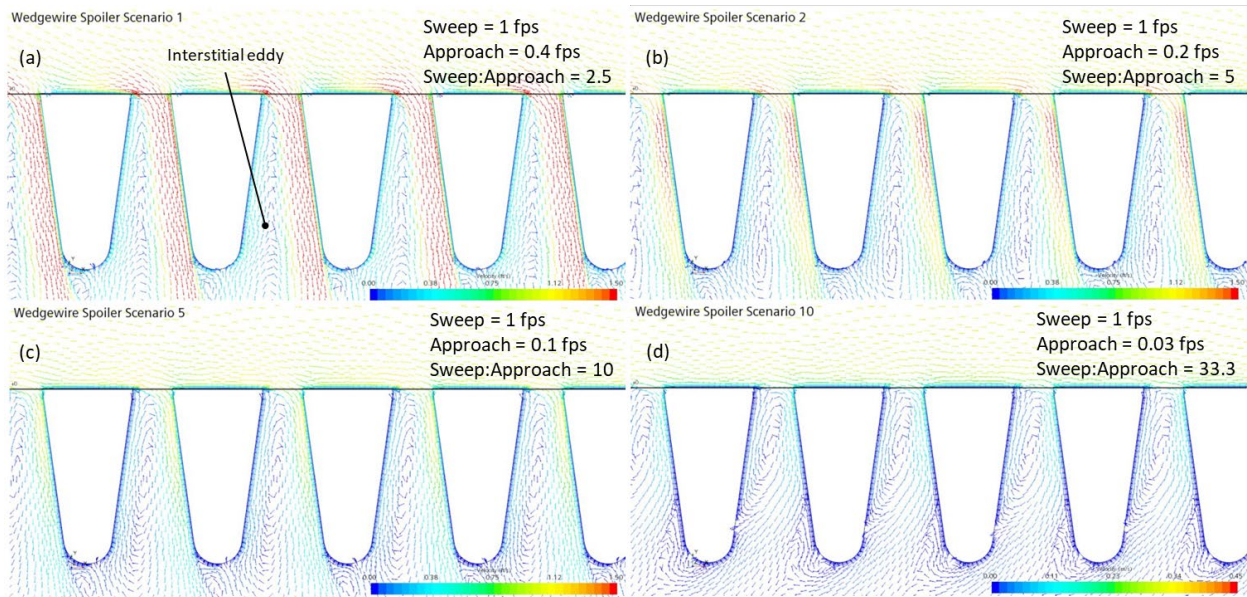


Figure 3.7. Simulated flow patterns through wedge wire slots for increasing sweep-to-approach velocity ratio. All with **sweep velocity of 1 ft/s**.

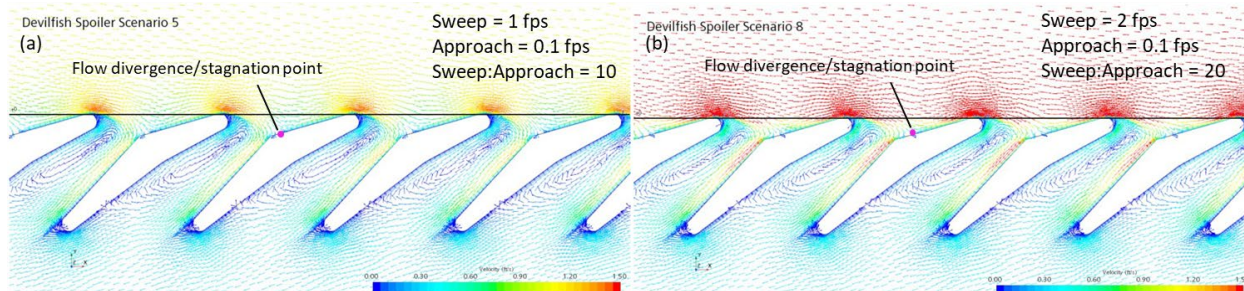


Figure 3.8. Simulated flow patterns through prototype slots (spoiler orientation) for increasing sweep-to-approach velocity ratio. Both with **approach velocity of 0.1 ft/s**. Flow divergence/stagnation point marked with magenta dot in (a) and (b). Note divergence point is slightly upward/outward in (b) due to high sweep-to-approach ratio. Sweeping flow is left to right.

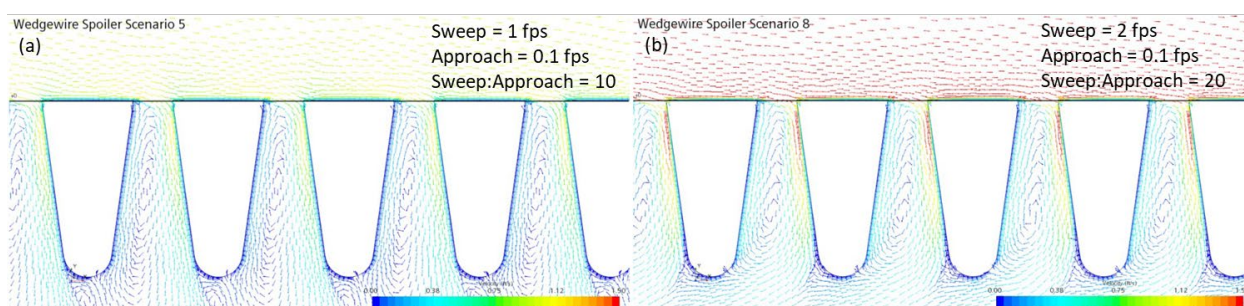


Figure 3.9. Simulated flow patterns through wedge wire slots for increasing sweep-to-approach velocity ratio. Both with **approach velocity of 0.1 ft/s**.

3.3.3 Head loss

Many water withdrawal systems seek to reduce head loss due to frictional resistance in order to maximize flow conveyance, minimize pumping requirements, or maximize turbine output. As such, a goal of prototype development will be to reduce entrainment without overly increasing head loss through the screen.

The drop in static pressure across the two screen types was used to estimate the head loss for the various scenarios (see Appendix A). Due to the more tortuous flow path through the spoiler-oriented prototype slots, pressure drop was predicted to be higher for the prototype screen than for the wedge wire analog; on average, prototype pressure drop was 3.4 times higher than that of the wedge wire. However, pressure drop for both screen types was quite low (average of 0.25 inches for all cases, with maximum of 1.1 inch and minimum of 0.01 inch).

3.3.4 Entrainment

The trajectories of over one thousand particles per simulation were recorded for both the prototype (spoiler orientation) and wedge wire under all ten flow conditions. Particles were predicted to move relatively smoothly toward the screen face before, in the case of “interacting” particles, colliding with the screen face. Following collision, particles were simulated to either become immediately entrained or saltate (skip) along the screen face in a series of subsequent collisions. Some saltating particles eventually became entrained while others escaped to continue on with the flume’s sweeping flow.

Particle trajectories for increasing sweep-to-approach velocity ratio are shown in Figure 3.10 for the prototype and in Figure 3.11 for wedge wire. The simulations shown in these figures (Scenarios #1, #2, #5, and #10) all featured a sweeping velocity of 1 ft/s. Figure 3.12 and Figure 3.13 similarly show the effect of increasing sweep-to-approach ratio, but with approach flow held constant at 0.1 ft/s (Scenarios #5 and #8). These figures show the paths of all particles released, not just those that interacted with the center portion of the screen.

Within the flume portion of the domain, the trajectories were simulated to be smooth and very similar for both screen types for a given velocity ratio as would be expected. Trajectories of entrained particles (on the filtrate side of the screen) differed between screen types due to differences in slot geometry, however, the entrainment rates appear similar based on visual inspection of the trajectories. Other findings include:

- Near immediate entrainment of particles for velocity ratios of 2.5 and 5 (both screen types; Figure 3.10a,b and Figure 3.11a,b).
- Some particle saltation along screen face for velocity ratio of 10 (both screen types; Figure 3.10c and Figure 3.11c).
- Near zero entrainment of particles for velocity ratio of 20 or more (both screen types; Figure 3.10d and Figure 3.11d for ratio of 33.3, Figure 3.12b and Figure 3.13b for ratio of 20). This finding was true even when the sweep velocity was reduced from 2 ft/s (Simulation #8) to 1 ft/s (Simulation #7) as shown in Figure 3.14 for both screen types.

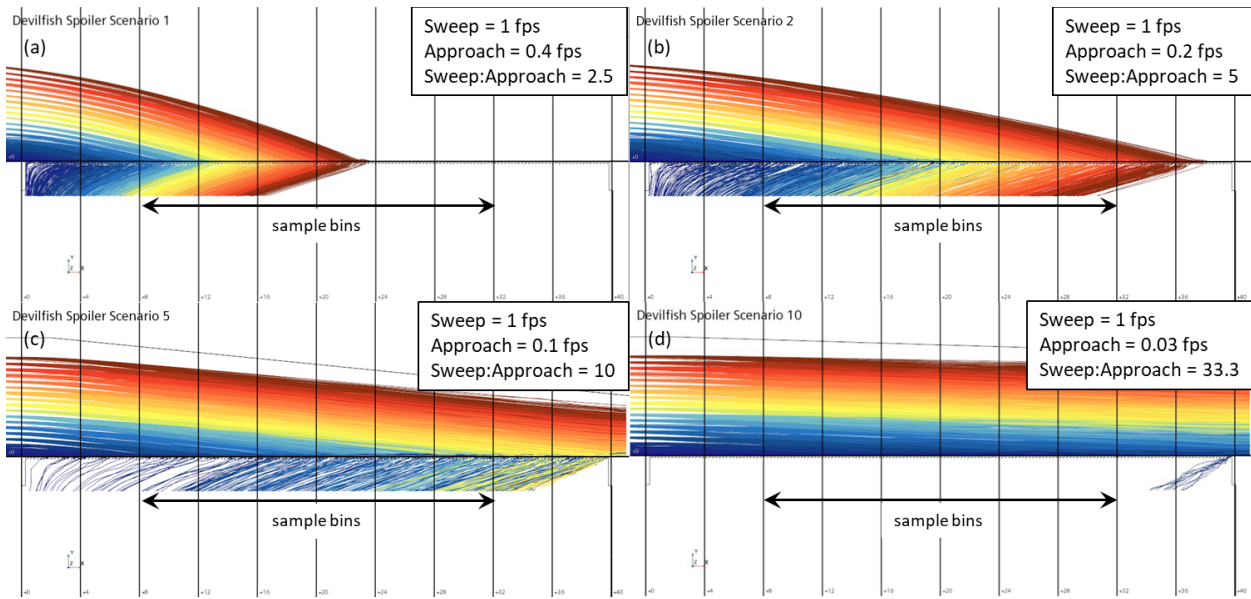


Figure 3.10. Simulated particle trajectories for prototype (spoiler orientation) for increasing sweep-to-approach velocity ratio. All with **sweep velocity of 1 ft/s**. All particle trajectories shown, however, only those interacting within the center bins sampled for entrainment calculations. Coloring is arbitrary. Sweeping flow is left to right.

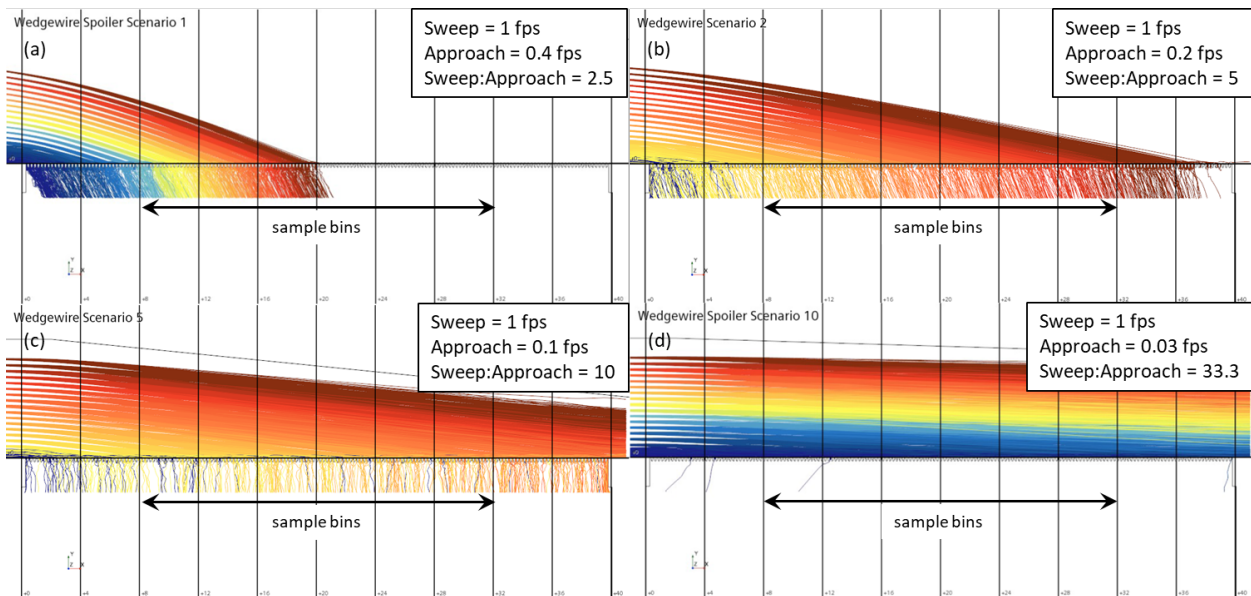


Figure 3.11. Simulated particle trajectories for wedge wire for increasing sweep-to-approach velocity ratio. All with **sweep velocity of 1 ft/s**. All particle trajectories shown, however, only those interacting within the center bins sampled for entrainment calculations. Coloring is arbitrary. Sweeping flow is left to right.

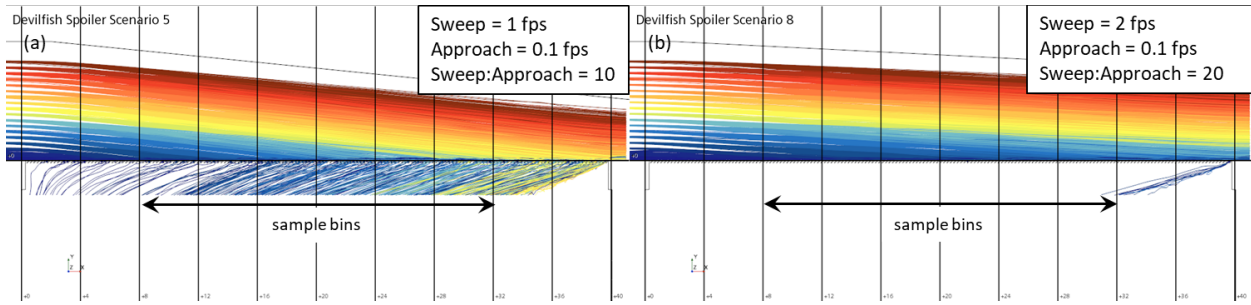


Figure 3.12. Simulated particle trajectories for prototype (spoiler orientation) for increasing sweep-to-approach velocity ratio. Both with **approach velocity of 0.1 ft/s**. Note near complete exclusion for ratio of 20 (b). Sweeping flow is left to right.

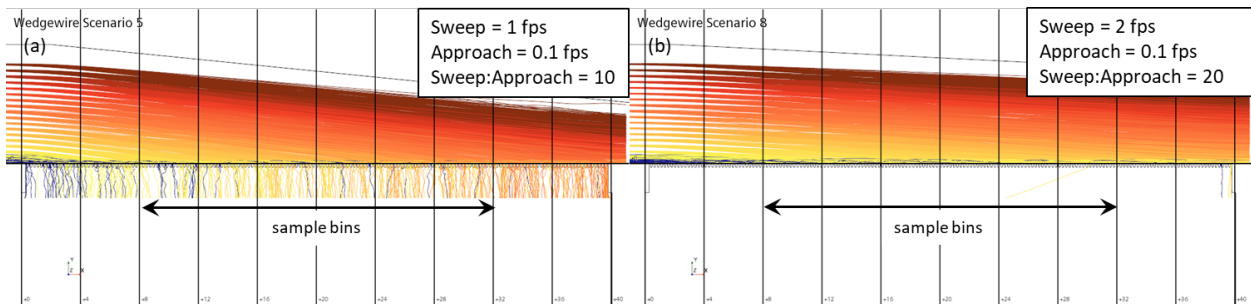


Figure 3.13. Simulated particle trajectories for wedge wire for increasing sweep-to-approach velocity ratio. Both with **approach velocity of 0.1 ft/s**. Note near complete exclusion for ratio of 20 (b). Sweeping flow is left to right.

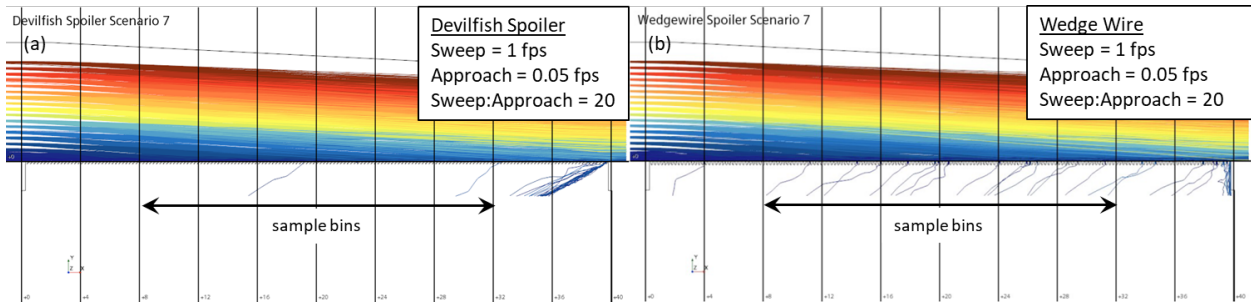


Figure 3.14. Comparison of trajectories for prototype (a) and wedge wire (b) at sweep-to-approach velocity ratio of 20 and a sweep velocity of only 1 ft/s. Note near complete exclusion for is maintained when sweep velocity is reduced from 2 ft/s to 1 ft/s (compare Figure 3.12b with [a] for the prototype, compare Figure 3.13b with [b] for wedge wire).

As discussed in Section 3.2.4, particle trajectories were post-processed to only consider particles that interacted with the screen face, and who's first interaction was within the center 60%, or 24 inches, of the screen length (ignoring particles that never got close enough to the screen to interact and particles who's first interaction was in the first or last eight inches of the test section). With these post-processing filters in place, the entrainment rate for both screen types was calculated for all ten flow scenarios. Results are reported in Table 3.2 and plotted in Figure 3.15.

The entrainment calculations predicted little difference in performance between the baseline prototype in spoiler orientation and the wedge wire analog at the fine-scale and for the flow regimes tested. For both screen types, nearly complete entrainment of interacting particles was predicted for sweep-to-approach velocity ratios of 5 or less and more than 90% exclusion of particles was predicted for ratios of 20 or more. For a velocity ratio of 10, particle entrainment of interacting particles ranged from approximately 30% to 70%, with increasing sweeping velocity leading to less entrainment. This last finding suggests that sweep-to-approach velocity ratio may be a strong predictor of entrainment of sub-slot-sized particles but should not be considered alone when the ratio is ~10. For this regime, other influencing factors may be those related to particle drag, inertia, and collision dynamics. Given the variable performance in this regime, and that many water intakes are characterized by this regime, prototype refinement efforts may be most fruitful if focused here.

Table 3.2. Comparison of particle entrainment in central screen bins. Only considering particles that interacted with the screen face and who's first interaction was within the center 60% of the screen length.

	Scenario #	Sweeping Velocity (fps)	Approach Velocity (fps)	Sweep: Approach Velocity	# Particles Interacted	# Particles Entrained	% of Interacting Particles Entrained
Devilfish Spoiler	1	1	0.4	2.5	804	800	99.5%
	2	1	0.2	5	758	717	94.6%
	3	2	0.4	5	773	715	92.5%
	4	0.5	0.05	10	392	271	69.1%
	5	1	0.1	10	366	193	52.7%
	6	2	0.2	10	380	109	28.7%
	7	1	0.05	20	207	2	1.0%
	8	2	0.1	20	212	0	0.0%
	9	3	0.15	20	212	0	0.0%
	10	1	0.03	33.3	130	0	0.0%
Wedge Wire	1	1	0.4	2.5	639	637	99.7%
	2	1	0.2	5	731	692	94.7%
	3	2	0.4	5	728	674	92.6%
	4	0.5	0.05	10	383	240	62.7%
	5	1	0.1	10	386	195	50.5%
	6	2	0.2	10	390	139	35.6%
	7	1	0.05	20	213	6	2.8%
	8	2	0.1	20	219	1	0.5%
	9	3	0.15	20	212	0	0.0%
	10	1	0.03	33.3	143	0	0.0%

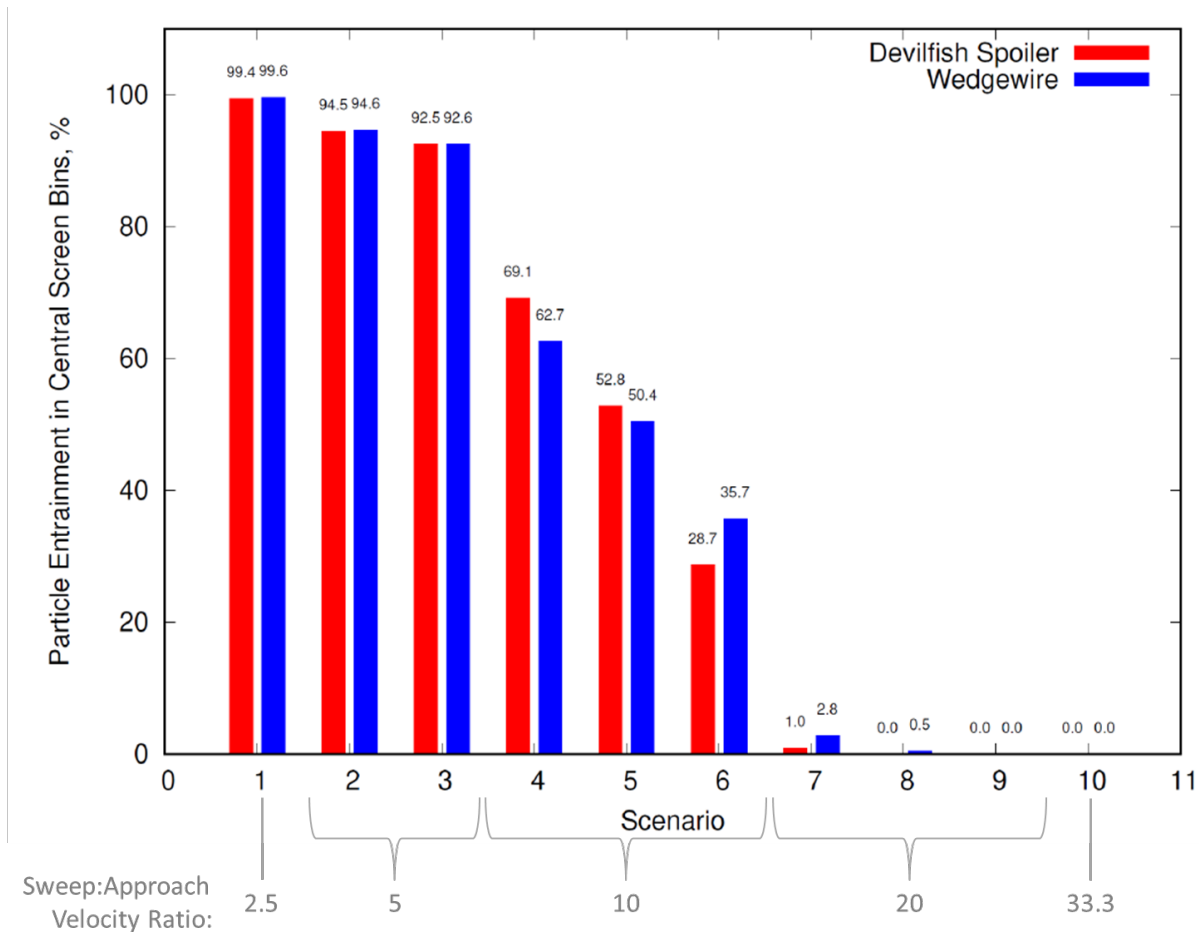


Figure 3.15. Comparison of particle entrainment in central screen bins. Only considering particles that interacted with the screen face and who’s first interaction was within the center 60% of the screen length.

4.0 Prototype Performance in a Laboratory Flume

4.1 Objectives

Laboratory testing was performed on Alden’s Holden, Massachusetts campus where similar screen testing has been performed. The original objectives of the laboratory study were to investigate (i) entrainment and impingement risk, (ii) head loss, and (iii) debris clogging associated with both fine and coarse versions of the prototype along with at least one conventional design (e.g., wedge wire) at matching scales (porosity) for comparison. As in the CFD study, however, only screens at the fine-scale were evaluated. Head loss and debris clogging were considered of secondary importance to entrainment performance and, ultimately, were not performed during the CRADA period. Nor were extensive velocity measurements performed. The CFD effort was intended to inform the laboratory study; therefore, laboratory tests lagged those of the CFD model. As such, only a single flow scenario was fully investigated before sub-freezing temperatures in the laboratory forced a hiatus in the laboratory testing late

in the CRADA term. It is intention of the Alden investigators to continue with laboratory testing when weather permits.

4.2 Methodology

4.2.1 Alden Flume

Alden constructed an 8-inch-wide clear acrylic flume on a closed-loop flow-recirculation system with two pumps as shown in the plan (top) view of Figure 4.1. One pump was used to provide sweeping flow in the flume, while another smaller pump was used to draw flow through the screened test section. The test section was located along the left flume wall 8 ft downstream of the headwater box and had length of 40-inches (matching that simulated with the CFD model). The test section was constructed such that screen panels could be easily interchanged. Average sweeping velocity along the test section was maintained using an adjustable angled guide wall (also matching that of the CFD model). The overall flume depth was 18 inches, however, a water depth of 14 inches was used during testing. Photographs of the flume prior to testing are shown in Figure 4.2.

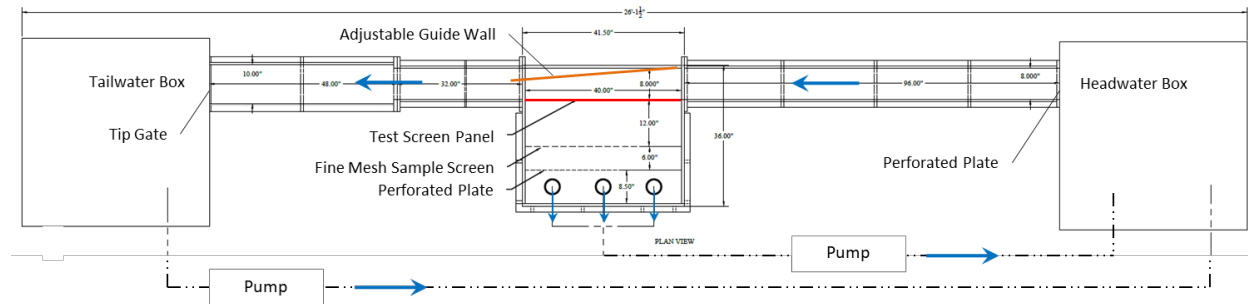


Figure 4.1. Plan view schematic of Alden test flume.

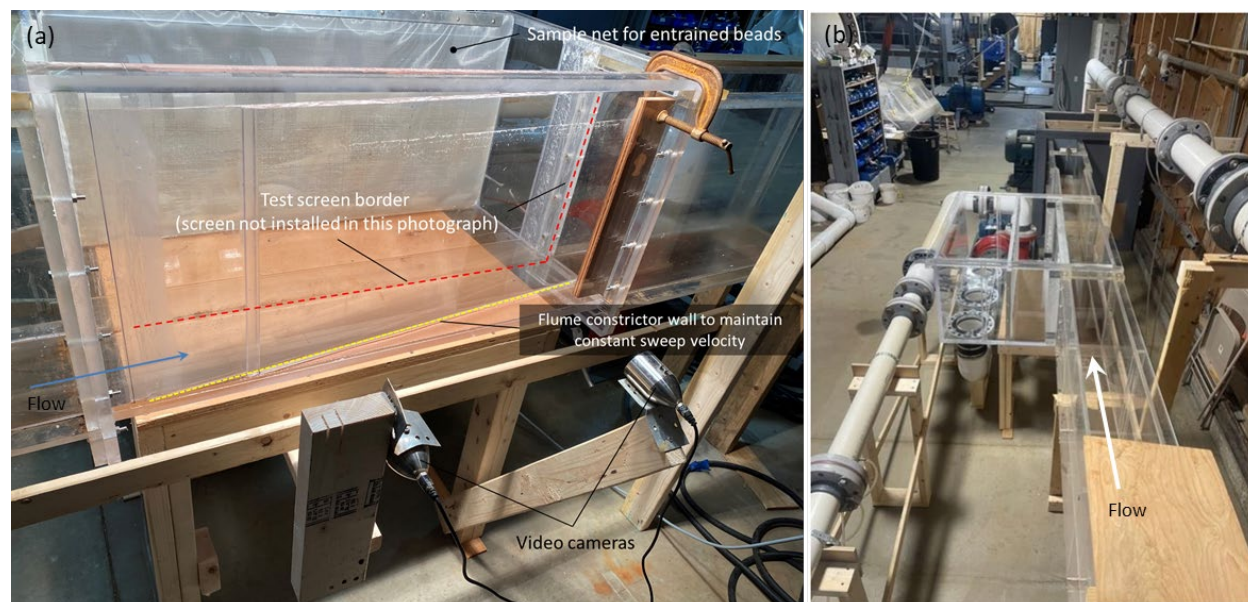


Figure 4.2. Photographs of Alden laboratory flume prior to testing.

4.2.2 Test Screen Panels

PNNL voucher support awarded as part of the Fish Protection Prize was used to fabricate a 40-inch by 18-inch panel of the baseline prototype at the fine-scale for testing in Alden's flume. Screen bar cross-sectional geometry was exactly as simulated in the CFD model (Figure 1.1). PNNL's Prusa i3 MK2S fused filament fabrication 3D printer (0.15-mm layer height) was used to fabricate 12 sub-panels that were joined to compose the full test panel. The test panel was then bordered by an external frame made of 2-inch-wide by 0.25-inch-thick 304 stainless steel bars. The backside of the screen face was supported by a series of 1-inch-wide by 0.105-inch-thick stainless steel support bars, chosen to closely match the wedge wire test panels discussed next. Further details of PNNL's fabrication effort are provided in Appendix B.

Two wedge wire panels were tested to compare with the prototype panel. Rather than have the wedge wire panels fabricated by PNNL, Alden purchased custom-made panels directly from the commercial screen vendor, Johnson Screens (of Aqseptence Group). While the wedge wire panel dimensions were customized to fit the Alden flume test section (40-inches by 18-inches), the wires (bars) themselves were selected from Johnson's existing Vee-Wire® series. Two considerations factored into wire selection (i) desire to approximate the prototype's porosity (29.9%) and (ii) a desire to match a porosity typically used in fish screening applications (~50%). Given these considerations two separate wire geometries were selected, one for each panel. Both Johnson wire types were spaced with 1.75-mm clear spacing to exactly match that of the prototype:

- Johnson #130 Vee-Wire®: 3.3-mm wide by 6.4-mm deep bars: 35% porosity at 1.75-mm clear spacing – selected that best matched prototype porosity of 29.9%.
- Johnson #69 Vee-Wire®: 1.8-mm wide by 4.5-mm deep bars; 49% porosity at 1.75-mm clear spacing – selected to match a typical fish screening application.

Both panels were externally framed with 2-inch-wide by 0.25-inch-thick bars and backed with 0.75-inch by 0.105-inch-thick bars, nearly identically match the support system of the prototype test panel fabricated at PNNL. Photographs of all three test panels are provided in Figure 4.3.

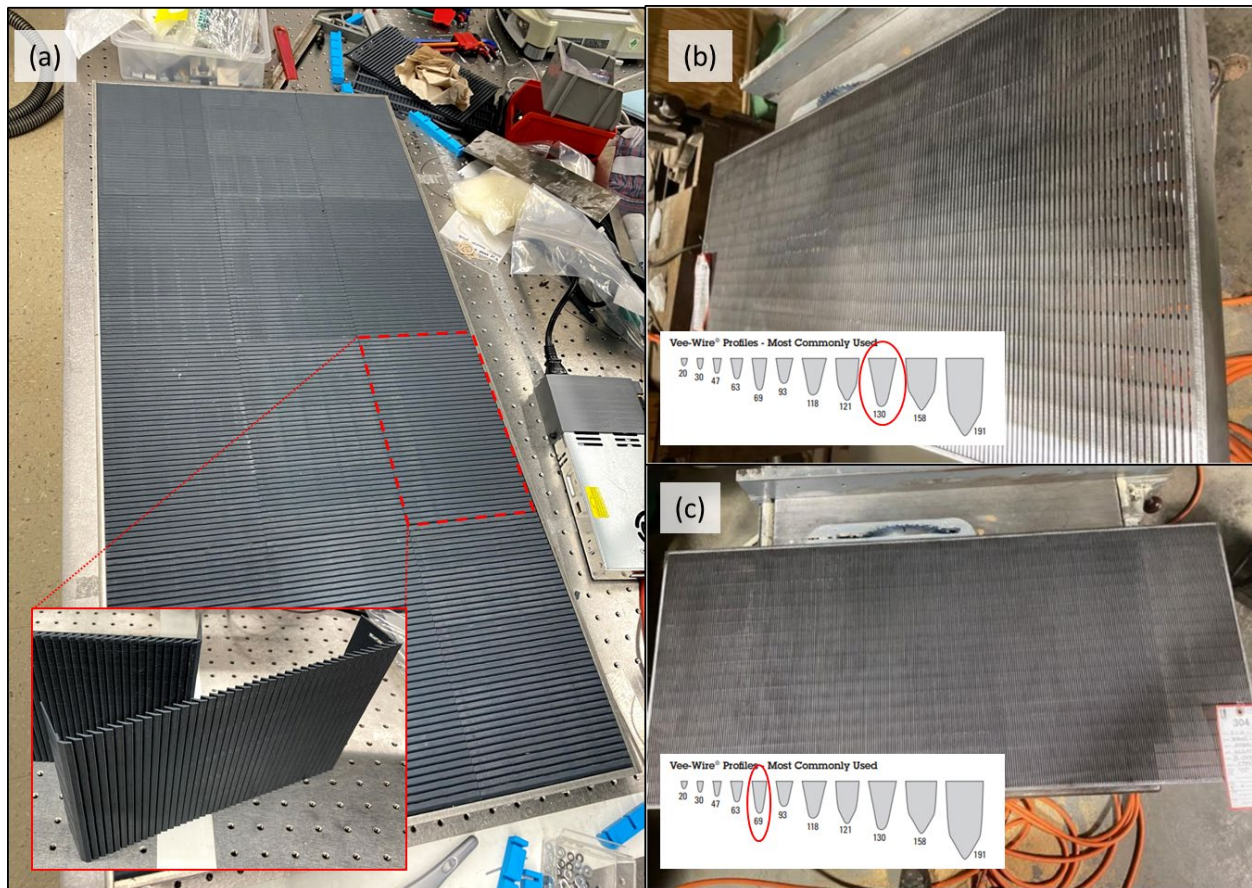


Figure 4.3. Fine-scale prototype test panel fabricated by PNNL (a) and two conventional wedge wire analogs custom-ordered from Johnson Screens: (b) #130 Vee-Wire (35% porosity) and (c) #69 Vee-Wire (49% porosity). All with 1.75-mm clear spacing.

4.2.3 Surrogate Fish Eggs

Like the CFD study, the focus of the laboratory work was to investigate entrainment of very small life stages such as eggs or small larvae. To this end, small plastic beads were used as surrogates. Entrainment performance was evaluated by releasing 0.85-1.0-mm polyethylene beads (density of 1 gram/cm³; commercially-available from Cospheric), closely matching the 1-mm particles of the CFD simulations. Additionally, 2.5-mm nylon beads (density of 1.14 gram/cm³ by Engineering Laboratories) were used to preliminarily investigate impingement.

4.2.4 Simulated Flow Conditions

During the CRADA period, only the flow condition of Scenario #5 (1 ft/s sweeping velocity and 0.1 ft/s approach velocity; Table 3.1) was investigated. The flume's guide wall was set to match that of the CFD model. For this condition, the prototype screen was tested in both wing and spoiler orientation, along with both conventional wedge wire panels. Orifice meters in the pump piping were used to set pumping rates to achieve the steady-state flow rates that would provide the desired sweeping and approach velocity through the test section.

4.2.5 Calculating Entrainment

Both small (~1-mm dia.) and large (~2.5-mm dia.) beads were released at a fixed point upstream of the test section at mid-depth in the flume. To evaluate entrainment, the smaller beads were collected using fine-mesh ichthyoplankton sampling nets in both the filtrate channel (entrained beads) and tailwater box (passing beads). To evaluate impingement, the larger beads that stuck to the screen face were visually counted. Fifty beads of both sizes were released in six replicate tests for the flow rate tested, for a total of 300 beads of each size.

Sources of sample bias related to entrainment estimation were discussed in Section 3.2.4: (i) non-interacting particles and (ii) non-uniform flow conditions along the length of the test section. These same sources of biases (and more) were of concern in the laboratory study. However, unlike in the well-controlled virtual flume of the CFD study, there was no easy way to ignore non-interacting beads or beads that interacted with the ends of the test section where hydraulic conditions were somewhat anomalous. Videography was attempted to determine bead interaction locations, but ultimately proved insufficient due to the beads' small size and fast speed relative to the cameras' resolution. In an effort to "land" beads near the center of the test screen, a single bead release point was determined using dye injection along with trial-and-error bead injections. For the flow condition tested (Scenario #5), a mid-depth release point located 5.5 inches (14 cm) upstream of the leading edge of the screen and 0.5 inches (1.3 cm) from the near wall of the flume was selected and held constant for all six replicate tests.

4.3 Results

4.3.1 Flow Patterns

Flow patterns in an actual flume are much more difficult to visualize than those in the virtual flume of a CFD model due to an inability to sample the entire domain in an instant. Rather than extensive instrumentation of the Alden flume for velocity measurements, basic dye injection tests were performed to qualitatively understand flow patterns. For the condition tested (Scenario #5), these dye tests primarily revealed a higher degree of turbulent dispersion in the flume than in the CFD model (Figure 4.4). This finding was not a surprise given that the CFD model did not explicitly simulate the turbulent motions (as is the case with most industrial CFD applications). Such turbulence would be expected in real-world fish screen environments. The smooth particle trajectories predicted by the CFD model (e.g., Figure 3.10 and Figure 3.11) stand in contrast to the turbulent mixing predicted by the dye tests.

An attempt was made to identify potential vortices associated with prototype screen in wing orientation as were indicated by the CFD model (see Section 3.3.1). Dye traces did indicate that such structures may have been present, although their coherency was apparently disrupted by ambient turbulence in the flume (Figure 4.5). Any increase in turbulence due to such structures could not be identified with the rather crude dye visualization.

Bead dispersion due to turbulence began immediately upon injection (Figure 4.6) and continued downstream through the test section.

More advanced measurements of velocity and turbulence may occur as part of future project work. During the CRADA period, however, the *mean* flow field, i.e., with turbulence smoothed, was assumed to be close to that predicted by the CFD model.

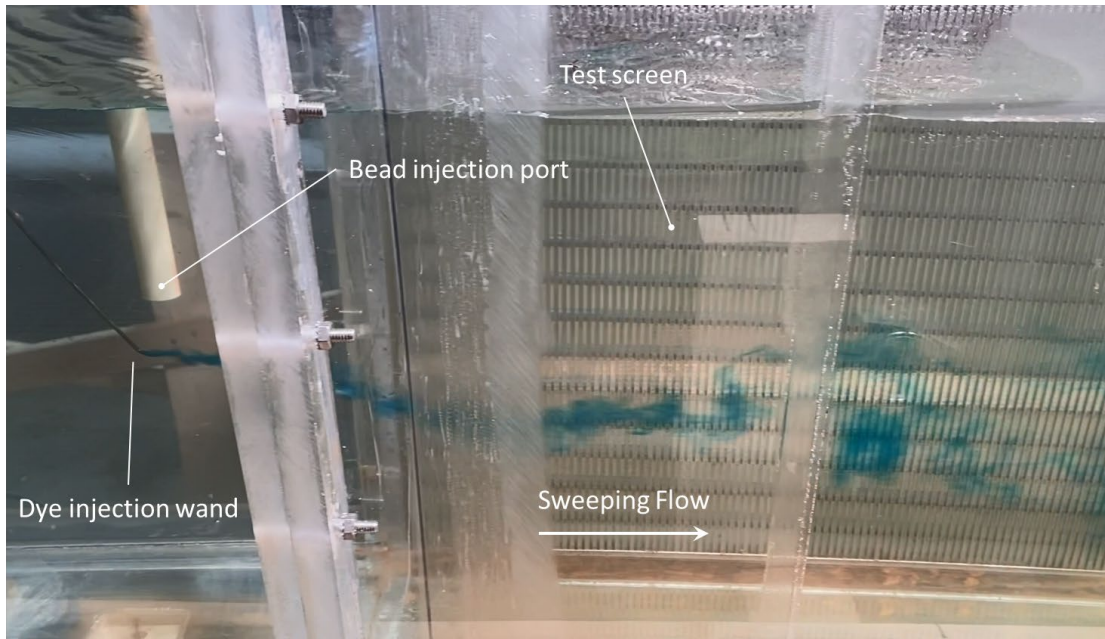


Figure 4.4. Photograph of dye injection revealing considerable turbulent mixing in laboratory flume. Such turbulence would be expected in real-world fish screen environments. Oblique view through flume wall opposite screen face.

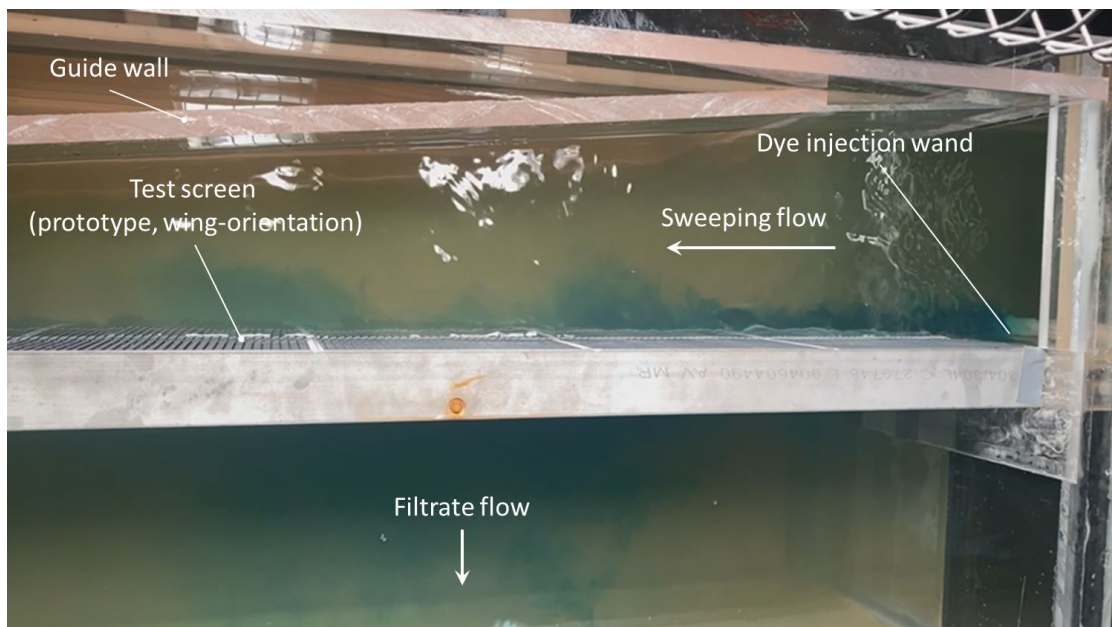


Figure 4.5. Photograph of dye injection revealing considerable turbulent mixing in front of wing-oriented prototype. Further testing needed to confirm presence of vortex generation along screen face as was seen in CFD model. Viewed from above.

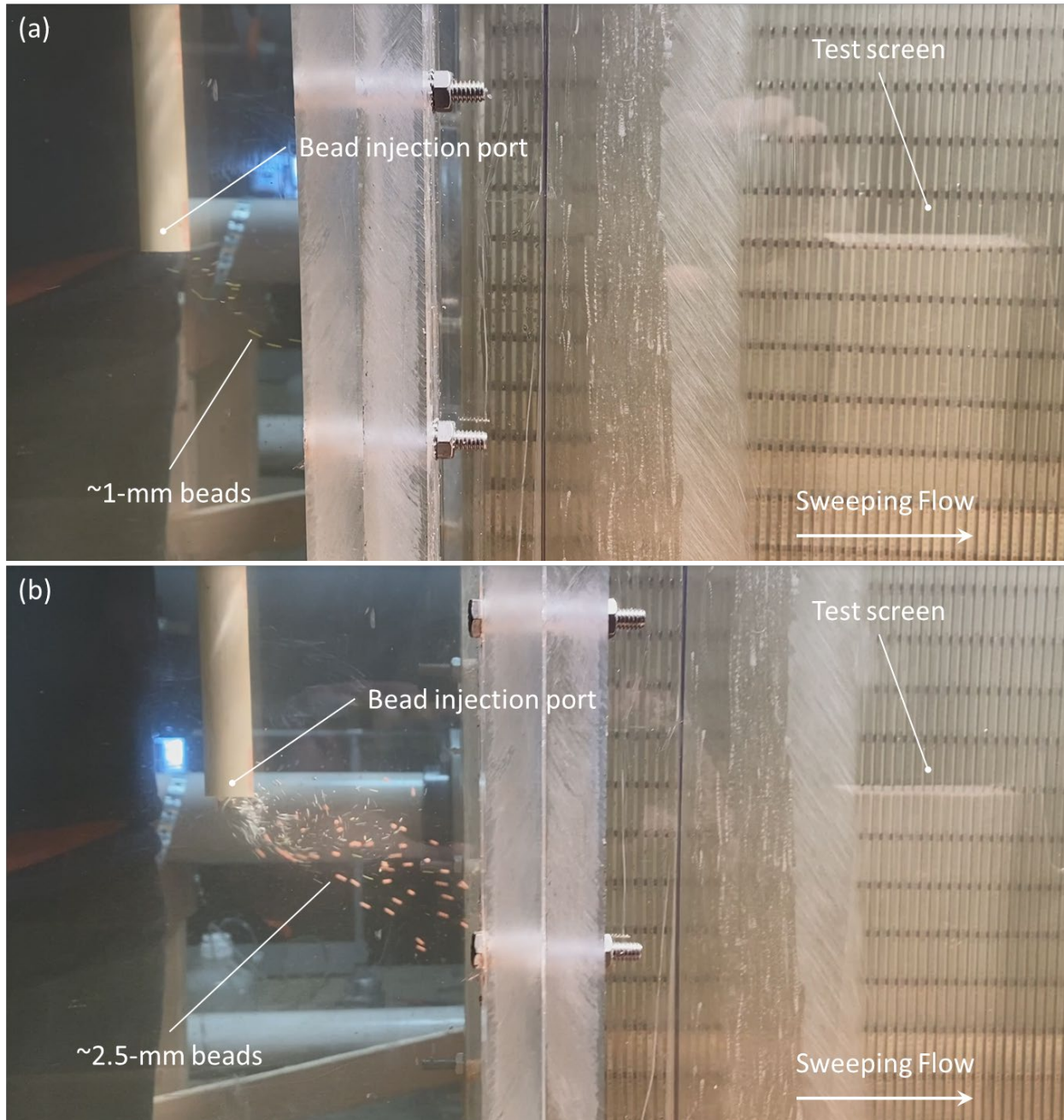


Figure 4.6. Photographs of two bead sizes immediately upon injection into Alden flume. Note turbulent dispersion of particles. Side view through flume wall opposite screen face.

4.3.2 Entrainment

As noted in Section 4.2.5, the small (~1-mm dia.) beads were released at a point which provided the best opportunity for beads to interact with the screen face mid-way down the test section. The turbulent dispersion noted above, however, made this task quite difficult. With that caveat in mind, the entrainment percentages for the fine-scale, baseline prototype and the two wedge wire screens are presented in Figure 4.7 for the Scenario #5 flow condition.

Variation in entrainment across the six test repetitions (50 beads each) was considerable, as shown in Figure 4.7a. For this flow condition and bead release point, most beads were predicted to be entrained by the prototype screen and the wedge wire screen of similar porosity (#130 Vee-Wire). The average entrainment rates for these three configurations were from 66% to 82%, with differences likely being within uncertainty bounds due to turbulence and other factors.

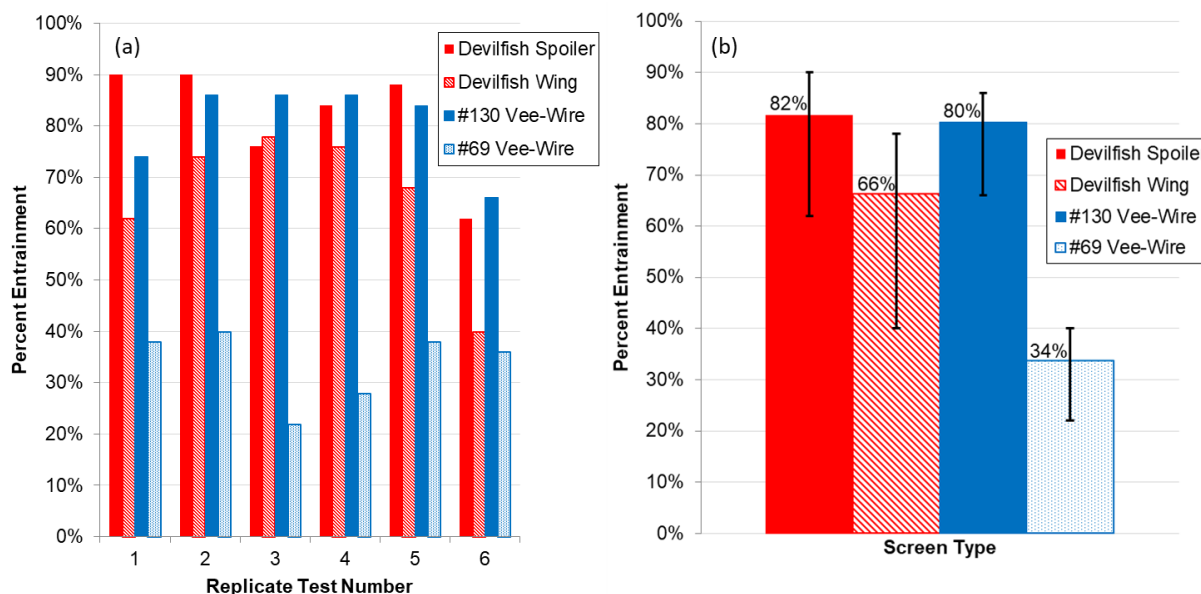


Figure 4.7. Comparison of 1-mm bead entrainment in laboratory flume testing of prototype (spoiler and wing orientations) and two wedge wire panels for flow Scenario #5 (1 ft/s sweeping velocity, 0.1 ft/s approach velocity): (a) Comparison for each of six repeated test (50 beads each); (b) Comparison after averaging over six test replicates, with error bars to show observed ranges. 1.75-mm slot size for all screens.

While the prototype and its conventional wedge wire analog of similar porosity (30-35% porosity) were predicted to perform similarly with regard to entrainment, the performance of the #69 Vee-Wire (49% porosity) was improved, with an average entrainment rate of 34% within a relatively narrow variability range of approximately 20-40% entrainment across the six test repetitions. This apparently significant finding is likely due to screen porosity; higher porosity results in lower slot velocity for the same approach velocity. As such, the more porous #69 Vee-Wire panel was associated with lower slot velocity. Beads interacting with the screen face, therefore, experienced less tractive force (drag) acting to pull them into the screen slots. The nominal slot velocities for the three screen types are provided in Table 4.1. Note that drag goes like the square of velocity, therefore, small changes in slot velocity would lead to relatively large changes in drag force pulling the beads into the slot. Beads would have to be very near slots to experience this phenomenon.

The hypothesis that increased porosity leads to decreased entrainment of sub-slot-sized particles is somewhat counter-intuitive until the argument above for decreased slot velocity is made. However, this hypothesis is incomplete. Surely, as porosity is further increased, there comes a point when particles simply drift through the screen without much interaction with the screen wires at all. In the limit, this would be a 100%-porous screen with the lowest slot velocity possible! Of course, this cannot be the answer. The answer likely comes from an optimization

problem wherein slot velocity is minimized while particle-screen interactions are maximized. The goal of future work will be to address this problem through revised screen bar geometry and pore-scale flow patterns.

Table 4.1. Comparison of 1-mm bead entrainment and 2.5-mm bead impingement in laboratory flume testing of prototype (spoiler and wing orientations) and two wedge wire panels for flow Scenario #5 (1 ft/s sweeping velocity, 0.1 ft/s approach velocity). 1.75-mm slot size for all screens. Porosity and nominal slot velocity noted.

Screen Type	% Entrained (Avg.)	% Entrained (Max)	% Entrained (Min)	% Impinged* (Avg.)	Porosity	Slot Velocity (ft/s)
Devilfish Spoiler	82%	90%	62%	1.7%	0.299	0.334
Devilfish Wing	66%	78%	40%	0.3%	0.299	0.334
#130 Vee-Wire	80%	86%	66%	0.0%	0.346	0.289
#69 Vee-Wire	34%	40%	22%	0.0%	0.493	0.203

*Only considering beads impinged against middle 60% of test section

4.3.3 Impingement

Entrainment of sub-slot-sized organisms (~1-mm) was the key focus of this study; however, preliminary consideration was given to impingement of larger organisms in the form of the 2.5-mm beads. These larger beads were injected at the same location as the smaller beads and similarly affected by turbulence, albeit a bit less so. Particles trapped against the screen face were visually counted for the prototype (wing and spoiler orientation) and the two wedge wire panels for the flow conditions of Scenario #5.

Impingement risk against all screen types was found to be very low for Scenario #5 flow conditions. In the case of the prototype in spoiler orientation, a total of 19 beads were impinged against the screen face out of 300 beads released over the six tests. 15 of those 19 beads were impinged on either the upstream or downstream-most 8 inches of the screen face – likely due to the anomalous hydraulic conditions noted in the CFD effort – leaving just four out of 300 beads impinged in the center 60% of the test section (~1-2% impingement). In the case of the prototype in wing orientation, only a single bead out of 300 was impinged. In the case of the wedge wire analog screens, no impingement was observed. In all cases, saltation of beads along the screen face was common.

4.3.4 Comparison with CFD

The laboratory and CFD results may be compared on the basis of Scenario #5 (1 ft/s sweeping velocity, 0.1 ft/s approach velocity), wherein nominal flow rates and geometry were identical for the numerical and physical flumes. For this flow condition, the CFD model predicted approximately 50% entrainment of 1-mm particles that interacted with the center portion of the screen for both screen types, while the laboratory study found a somewhat higher entrainment at 66%-82% for the screens of similar porosity (prototype and #130 Vee-Wire). Neither study estimated a meaningful difference across screen types of similar porosity.

Recall, however, that beads were released at a single point in the flume, whereas, particles were released across the entire channel width in the CFD model. Moreover, the CFD model results only consider particles that interacted in the center portion of the screen face – away from the hydraulically-anomalous end sections. The somewhat higher entrainment predicted by

the laboratory study may reflect end-effect bias; when the CFD injection point nearest the laboratory injection point is considered in isolation, nearly all injected particles were entrained in the CFD model prior to reaching the center portion of the screen (58 out of 64 DEM particles never made it to the center portion of the prototype screen and none of 64 particles made it to the center portion of the wedge wire screen). Turbulent motions in the flume likely allowed injected particles to make their way further down the screen face in the laboratory tests.

As was noted in Section 4.3.1, turbulent motions in the laboratory flume led to erratic particle paths that were not captured in the CFD model. This was to be expected given that the CFD model represented the mean flow field wherein the effects of turbulence are parameterized using a turbulence model. The utility of the CFD model lies in its ability to rapidly test various scenarios, but under the assumptions that the erratic motions are essentially smoothed over. While the free stream trajectories of beads in the real world are considerably more complex than those in the CFD flume, the particle-screen interaction dynamics are likely captured with enough accuracy so as to make CFD a valuable comparative tool for future concept refinement.

5.0 Is It Worth It? Marketability

5.1 Objectives

This study was largely a proof-of-concept investigation, but was carried out with an eye toward potential commercialization of the conceptual fish-protection screen at some point in the future. Therefore, a market simulation tool (spreadsheet) was developed by PNNL as part of the Fish Protection Prize voucher award. The objective of the effort was to develop a tool that would estimate potential costs and benefits of the new technology compared to existing technology.

5.2 Methodology

In essence, the market simulator developed by PNNL estimates potential savings associated with a new flat-plate-style fish screen over an assumed 20-year lifetime. The model assumes that savings may take the form of reduced capital, operations, and maintenance costs, but leaves the degrees of improvement in these areas as a user inputs. In the case of the devilfish concept, these costs are likely similar to those of conventional screens, although some maintenance cost benefits are perhaps possible through improved debris shedding (to be determine by future research). Data on screen type and size distribution as well as costs from PNNL's experience in the Yakima River basin and elsewhere were used to provide a basis for typical costs. Data from the Bonneville Power Administration were used to estimate the potential number of annual screen deployments in coming years and, thus, market opportunity for the new technology.

The market model also estimates cost saving due to reduced fish mortality – again leaving the percent reduction as a user input. It is in this comparison that the devilfish concept likely has the most potential for savings. However, the benefits of reduced mortality are difficult to quantify and reach beyond the realm of economics. For simplicity (although still not that simple), the model estimates mortality savings in terms of improved harvest of commercially harvested species.

Many factors will affect the economic return from any new fish screen technology, including site-specific conditions and target fish species. For this reason, the model is designed as a Monte Carlo simulation in which triangular distributions are assigned to all important model inputs and

the model is recalculated 10,000 times to simulate and summarize all possible combinations of inputs from these distributions. Further details of the tool are provided in Appendix C: Fish Screen Life-Cycle Cost Model.

5.3 Results

The main result of the market study was development of the Monte Carlo simulator tool. At this point, values for key user inputs to the model are unknown. Key missing inputs include percent improvement in fish protection over existing technology and, perhaps, percent reduction in maintenance cost. Future work is needed to optimize the devilfish concept further (see Section 7.0) and will hopefully lead to a screen design that shows meaningful improvements in protection against entrainment, impingement, and debris fouling. At such a time, the model will be a valuable tool for communicating likely savings with potential investors. Conversely, the model will make a good tool for understanding the performance improvement needed to make the screen commercially viable. This exercise has yet to be carried out, but will provide a target for further design refinement and a sanity check: is the performance improvement needed for commercial viability within the realm of technical/physical possibility?

Finally, one thing the model does not explicitly consider is the influence that regulatory agencies have on the fish protection market. Since the implementation of Section 316(b) of the Clean Water Act, thousands of industrial facilities using large volumes of water from natural water bodies to cool their plants have had to adopt fish protection measures. Similar government-issued protective measures have been required of water withdrawal for agricultural use and desalination intakes, especially those located in Critical ESA-designated habitat. In the U.S. West with sea-run salmonids and abundant irrigation-water withdrawals, the National Marine Fisheries Service has strict criteria for screen design and performance. Screening measures are typically required to be the best technology available for minimizing adverse environmental impact. If shown to out-perform conventional screen designs in the protection of aquatic and marine life without compromising hydraulic performance (e.g., head loss, debris fouling), the economic value of the prototype screen in government-regulated settings could be much increased over market-model predictions.

6.0 Discussion of Findings

The general objectives of the CRADA-related work were to investigate the prototype and a conventional, commercially available, fish-protection screen using computer modeling and laboratory testing. These objectives were accomplished, as documented above, with an emphasis on entrainment of sub-pore-scale particles in lieu of fish eggs or small life stages (1-mm spheres). The fine-scale (1.75-mm slot), baseline (un-optimized) prototype was examined alongside a conventional wedge wire-style screen with identical slot size.

In summary, this multi-pronged study suggests that there appears to be no meaningful difference in entrainment performance between the baseline prototype screen and a conventional wedge wire screen of similar porosity for the flow regimes investigated. The study did, however, generate valuable information that can be used for concept refinement and may have broader impact for the fish screening industry. Key findings include:

- i. CFD modeling is a valuable tool for investigating small-scale particle-screen hydraulics and interactions. In employing CFD, consideration should be given to ensure sufficient

mesh resolution, and results should be interpreted with the understanding that real-world turbulence would superimpose considerable noise on the CFD predictions.

- ii. CFD modeling predicted flow regimes relevant to entrainment of sub-slot-sized organisms. These regimes likely apply to most slotted fish-protection screens with slots oriented normal to sweeping flow:
 - a. Near 100% entrainment for sweep-to-approach velocity ratios $\lesssim 5$. Near immediate entrainment; no saltation/ricocheting along screen face.
 - b. Decreasing entrainment risk for sweep-to-approach velocity ratios from 5 to 20. Saltation/ricocheting becoming important to reduce entrainment.
 - c. Near 0% entrainment for sweep-to-approach velocity ratios $\gtrsim 20$. Saltation/ricocheting prevents entrainment.
- iii. Agreement with previous work. The prototype mimics the filter elements of an actual devil ray which were evolved to operate at high sweep-to-approach velocity ratio (~ 30 ; Divi et al., 2018). The CFD predictions of highly effective cross-flow filtration were in agreement with those of Divi et al. for this flow regime.
- iv. Laboratory testing was in approximate agreement with CFD results pertaining to entrainment rate and particle behavior (saltation/ricocheting along the screen face for all screen types).
- v. Laboratory testing suggested near 0% impingement of particles just larger than screen slot size (2.5-mm) for a sweep-to-approach velocity ratio of 10 (for all screen types).
- vi. Laboratory testing revealed the importance of porosity relative to entrainment. *Increasing* porosity from $\sim 30\%$ to $\sim 50\%$ was shown to *decrease* entrainment of 1-mm particles through 1.75-mm slots by more than a factor of two (half the entrainment at 50% porosity vs. 30% porosity) – likely due to decreased slot velocity at higher porosity.

7.0 Future Research

The prototype and its conventional wedge wire analog fish-protection screen were found to provide similar protection against entrainment of sub-slot-sized particles and against impingement of slightly larger particles. Future work is needed to optimize the prototype. Motivating research questions include:

Flow Regimes?: In the context of entrainment, near equivalence between the prototype and the conventional screen held over a wide range of sweeping and approach velocities typical of fish protection screening applications. When sweeping flow is very high or very low compared to the approach velocity, nuances in screen bar/slot shape probably matter little. However, for intermediate values of the sweep-to-approach velocity ratio (~ 10), many particles entrain while many escape, suggesting that details of particle-screen interactions could be manipulated to improve entrainment protection. This intermediate flow regime will be a focus of future design improvement.

The clearly demonstrated advantage of a high ratio of sweeping velocity to approach velocity for minimizing entrainment suggests that enhancing sweeping velocity could improve screen performance of existing intakes (having fixed approach velocity mandated by needed water withdrawal volumes) as well as newly designed ones. Velocity enhancement could be accomplished passively by arrangements of baffles in the source stream or actively by directed pumped-water flow.

Porosity?: Future efforts will also focus on the importance of porosity to entrainment protection. Increasing porosity was shown to reduce entrainment risk of sub-slot-sized particles, mostly likely due to reduced slot velocity. An optimal porosity likely exists that minimizes slot velocity while maximizing particle-screen interactions that send particles back toward the free stream.

Scale?: It is worth noting that the ~1-mm particles investigated here are somewhat small compared to most ichthyoplankton that is at risk of being entrained in natural water bodies. The spherical shape of the particles may also be overly simplistic – especially when considering fish larvae that have round head capsules but elongated bodies. It is likely that actual organism-screen interactions are more complicated than the sphere interactions investigated so far. The interactions probably become increasingly complex as larger slot sizes and correspondingly larger and more varied body shapes are considered. If so, screen bar shape may likely become more important at coarse scales. Future work will investigate opportunities for concept refinement at these larger scales.

Debris Fouling?: As noted in Section 5.0, operation and maintenance costs can be considerable for fish protection screens, with those costs heavily influenced by debris, biofouling, and/or sediment. Future work to improve the prototype's ability to shed organisms will likely be compatible with the goal of reducing clogging by small debris and perhaps biofouling. Debris and sediment fouling potential can be tested in the Alden flume. Alden also has outdoor facilities that could be employed to investigate biofouling.

Turbulence?: Finally, the role of turbulence should not be ignored. Drifting ichthyoplankton are often small compared to the boils, bursts, sweeps, ejections, eddies, vortices, and other colorfully-named and erratic flow patterns in a freely-flowing waterbody – especially near screen faces and other boundaries. As such, their trajectories are equally erratic. The vortex shedding off the wing-oriented prototype screen predicted by the CFD model, suggests that near-screen turbulence could be manipulated through screen bar shape. It is possible that manipulating turbulence in such a way could lead to improved protection against entrainment or impingement. It is also possible that manipulation of near-screen turbulence could lead to improved avoidance behavior of motile life stages that take their cues from turbulent motions. Future work will further investigate the role of turbulence using the Alden's test flume.

8.0 References

Divi, R. V., J. A. Strother, and E. W. M. Paig-Tran. 2018. "Manta rays feed using ricochet separation, a novel nonclogging filtration mechanism." *Sci Adv* 4 (9): eaat9533. <https://doi.org/10.1126/sciadv.aat9533>. <https://www.ncbi.nlm.nih.gov/pubmed/30263959>.

Appendix A CFD Evaluation of Devilfish-Inspired Fish Exclusion Screening

January 2022

William A Perkins, PNNL
Rajesh K Singh, PNNL
Andre A Rahrooh, PNNL
Kenneth D Ham, PNNL
Benjamin Mater, Alden

Summary

A team from Alden Research Laboratory, LLC, (Alden) was selected as one of three grand prize winners of the Fish Protection Prize challenge (<https://americanmadechallenges.org/fishprotection/index.html>). Their winning concept involved using the food filtering structures of devilfish (*M. tarapacana*) to inform the design of screens to reduce entrainment of the various life stages of fish. Winning teams were awarded funds to support the development of their concept in collaboration with Pacific Northwest National Laboratory (PNNL). This report summarizes the efforts of computational fluid dynamics investigations of particle-flow simulations through novel devilfish and typical wedge wire screen designs at various flow scenarios. CFD-DEM simulations predict the resulting entrainment of particles representing fish eggs as an indicator of screen performance.

Acronyms and Abbreviations

2D	Two dimensional
Alden	Alden Research Laboratory, LLC
CFD	computational fluid dynamics
DEM	discrete element method
FFT	Fast fourier transform
PIC	PNNL institutional computing
PNNL	Pacific Northwest National Laboratory

Appendix A Contents

Summary.....	A.1
A.1 Introduction	A.7
A.2 Methods	A.7
A.2.1 Screen Designs and Flow Scenarios	A.7
A.2.2 Flow Simulation	A.7
A.2.2.1 Simulation Domain.....	A.8
A.2.2.2 Guide Wall Taper.....	A.9
A.2.2.3 Mesh.....	A.10
A.2.2.4 Scenarios.....	A.10
A.2.3 Particle Simulations.....	A.11
A.3 Results	A.12
A.3.1 Flow Simulation	A.12
A.3.1.1 Guide Wall Taper.....	A.12
A.3.1.2 Mesh Independence Test	A.14
A.3.1.3 Devilfish Wing Orientation	A.17
A.3.1.4 Flow Scenario Comparison.....	A.18
A.3.2 Particle Simulation.....	A.24
A.4 References.....	A.31

Appendix A Figures

Figure A.1.	Fish Screen Cross-sectional Geometries Provided by Alden: Wedge Wire, Devilfish Spoiler Orientation, and Devilfish Wing Orientation.....	A.7
Figure A.2.	Dimensions of the Two-dimensional Flow Channel Used in CFD Simulations.....	A.9
Figure A.3.	Velocity Probe Locations used for the Mesh Independence Study.....	A.10
Figure A.4.	Locations Where Particles Were Injected.....	A.12
Figure A.5.	Screen Sweep and Approach Velocity for Various Guide Wall Taper Configurations.....	A.13
Figure A.6.	Background and Screen Mesh Base Size and Cell Count.....	A.14
Figure A.7.	Relative Change in Simulated Screen Sweep and Approach Velocity and Normalized Velocity Measured at 3 and 1 inches Upstream of the Screen for Each Mesh Case.....	A.15
Figure A.8.	Simulated Screen Gap Velocity Profiles and Relative Change in Maximum Gap Velocity in Each Mesh Resolution Case.....	A.15
Figure A.9.	Relative Change in Simulated Screen Pressure Drop in Mesh Resolution Cases.....	A.16
Figure A.10.	Mesh Used for the Devilfish Spoiler Screen Simulation.....	A.16
Figure A.11.	Mesh Used for the Wedge Wire Screen Simulation.....	A.17
Figure A.12.	Vortex Shedding Observed in the Simulation of the Devilfish Screen in Wing Orientation.....	A.18
Figure A.13.	Velocity Fluctuation Frequencies Observed for the Wing Mode Orientation of the Devilfish Screen for Scenarios #5 and #7.....	A.18
Figure A.14.	Simulated Velocity Around the Devilfish Spoiler Screen Bars.....	A.19
Figure A.15.	Simulated Velocity Around the Wedge Wire Screen Bars.....	A.20
Figure A.16.	Distribution of Approach Velocity Magnitude Along the Wedge Wire and Devilfish Spoiler Screens.....	A.22
Figure A.17.	Approach Velocity Relative to the Mean Along the Wedge Wire and Devilfish Spoiler Screens.....	A.23
Figure A.18.	Simulated Wedge Wire and Devilfish Spoiler Screen Head Loss for All Scenarios.....	A.24
Figure A.19.	Particle Tracks Simulated for the Devilfish Spoiler Screen.....	A.25
Figure A.20.	Closer View of Particle Tracks Simulated for the Devilfish Spoiler Screen.....	A.26
Figure A.21.	Particle Tracks Simulated for the Wedge Wire Screen.....	A.27
Figure A.22.	Closer View of Particle Tracks Simulated for the Wedge Wire Screen.....	A.28
Figure A.23.	Comparison of Particle Interaction and Entrainment Between the Wedge Wire and Devilfish Spoiler Screens for the 10 Flow Scenarios.....	A.29
Figure A.24.	Comparison of Particle Entrainment In the Central Part of the Screen.....	A.31

Appendix A Tables

Table A.1.	Background Channel Dimensions Used in Simulation Cases	A.8
Table A.2.	Tested Guide Wall Taper Configurations	A.13
Table A.3.	Mesh Independence Test Results.....	A.14
Table A.4.	Particle Count Summary	A.30

A.1 Introduction

As part of this work, Pacific Northwest National Laboratory (PNNL) performed a series of computational fluid dynamics (CFD) simulations of screen designs provided by Alden Research Laboratory, LLC (Alden). The primary objective of the effort was to evaluate the performance of a baseline conceptual screen design (proof of concept). Performance metrics included hydraulic resistance (head loss) and particle exclusion rate. The performance of the devilfish-inspired screen concept was compared to that of a conventional wedge wire fish exclusion screen design. CFD results were intended to augment Alden's laboratory evaluation of these screen types, but with more particles and across a wider range of conditions than would be practical with the laboratory apparatus alone.

A.2 Methods

A.2.1 Screen Designs and Flow Scenarios

Alden provided PNNL geometry for two novel screen designs based on the devilfish and one wedge wire design (Figure A.1). Alden provided ten flow conditions for CFD simulation in terms of sweep and approach velocity (Table A.1). The details of screen configuration flow scenarios are presented later in this report.

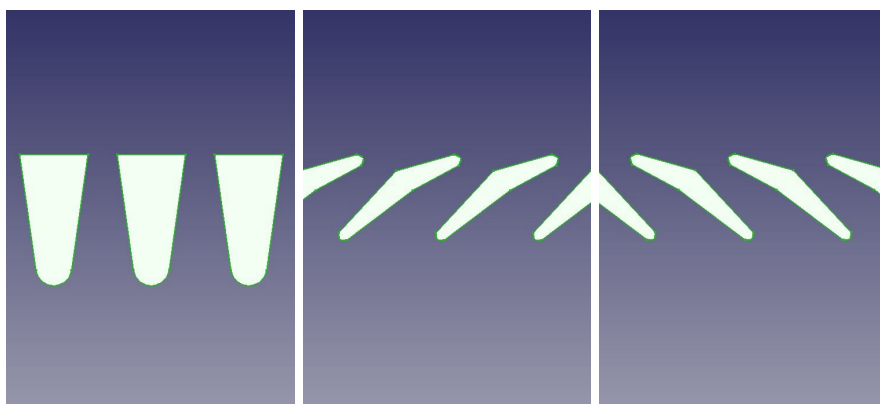


Figure A.1. Fish Screen Cross-sectional Geometries Provided by Alden: Wedge Wire (left), Devilfish Spoiler Orientation (center), and Devilfish Wing Orientation (right). Sweeping flow is from left to right, and screen approach flow is from top to bottom of these images.

A.2.2 Flow Simulation

The commercial CFD software, STAR-CCM+ (Siemens Digital Industries Software 2021), was used for flow simulations. Two-dimensional turbulent unsteady flow simulations were conducted to investigate the flow across the concept and traditional screen types for a variety of flow scenarios. The realizable $k - \epsilon$ turbulence model was used as the turbulence closure in the flow simulations. Details of the turbulence model can be found in the user guide of the software.

Table A.1. Background Channel Dimensions Used in Simulation Cases. In all cases, the screen width was 40 in.

Scenario	Screen Velocity		Inlet		Outlet	
	Sweep (fps)	Approach (fps)	Width (in)	Length	Width (fps)	Length (fps)
1	1.0	0.40	24.0	120.0	8.0	24.0
2	1.0	0.20	24.0	120.0	16.0	48.0
3	2.0	0.40	24.0	120.0	16.0	48.0
4	0.5	0.05	8.0	40.0	4.0	12.0
5	1.0	0.10	8.0	40.0	4.0	12.0
6	2.0	0.20	8.0	40.0	4.0	12.0
7	1.0	0.05	8.0	40.0	6.0	18.0
8	2.0	0.10	8.0	40.0	6.0	18.0
9	3.0	0.15	8.0	40.0	6.0	18.0
10	1.0	0.03	8.0	40.0	6.8	20.4

A.2.2.1 Simulation Domain

The simulation domain was set up to represent Alden's laboratory flume, but only in 2 dimensions (a horizontal cross-section). Domain dimensions are shown in Figure A.2. Parameterized dimensions were used to ensure a physically correct domain for each flow case. A fraction of the inflow was extracted through the screen outlet channel. The guide wall was tapered to keep the velocity the same at the inlet and outlet (V_{in}) to maintain a constant sweep velocity across the screen. The screen length, (W_s), was kept fixed at 40 inches for all cases. Given an inlet width, (W_{in}) and velocity (V_{in}), the outlet width (W_{out}) was calculated by mass conservation.

$$W_{in}V_{in} = W_sV_s + W_{out}V_{out} \quad (1)$$

As stated above, the sweep velocity across the screen was to be the same all along the screen, which means:

$$V_{sweep} \approx V_{in} \approx V_{out} \quad (2)$$

Plugging 2 into 1 and rearranging

$$W_{out} = W_{in} - W_s \frac{V_s}{V_{in}} \quad (3)$$

To keep any boundary issues well away from the screen, each of the channel lengths were set to several multiples of the channel width:

$$L_{in} = 5.0W_{in}$$

$$L_s = 5.0W_s$$

$$L_{out} = 3.0W_{out}$$

Domain dimensions for each flow scenario are shown in Table A.1.

Uniform velocity magnitude was imposed as the inlet of flow domain. A fixed outward mass flux was imposed at the screen outlet, meaning the outward velocity could vary over the boundary, but the total flux was fixed. The outlet boundary was left as a normal outlet, which was necessary to maintain mass balance. The StarCCM+ "All-y+" wall model was applied at the flow domain walls and surface of the screen.

A.2.2.2 Guide Wall Taper

A systematic examination of the effects of the guide wall taper relative to the screen was performed. The taper is bounded by two points nominally directly across the main channel from the screen ends (Figure A.2). These points may need to be placed (at O_{in} and O_{out} in Figure A.2) up or downstream of the screen end in order to maintain a consistent sweep velocity along the entire screen length.

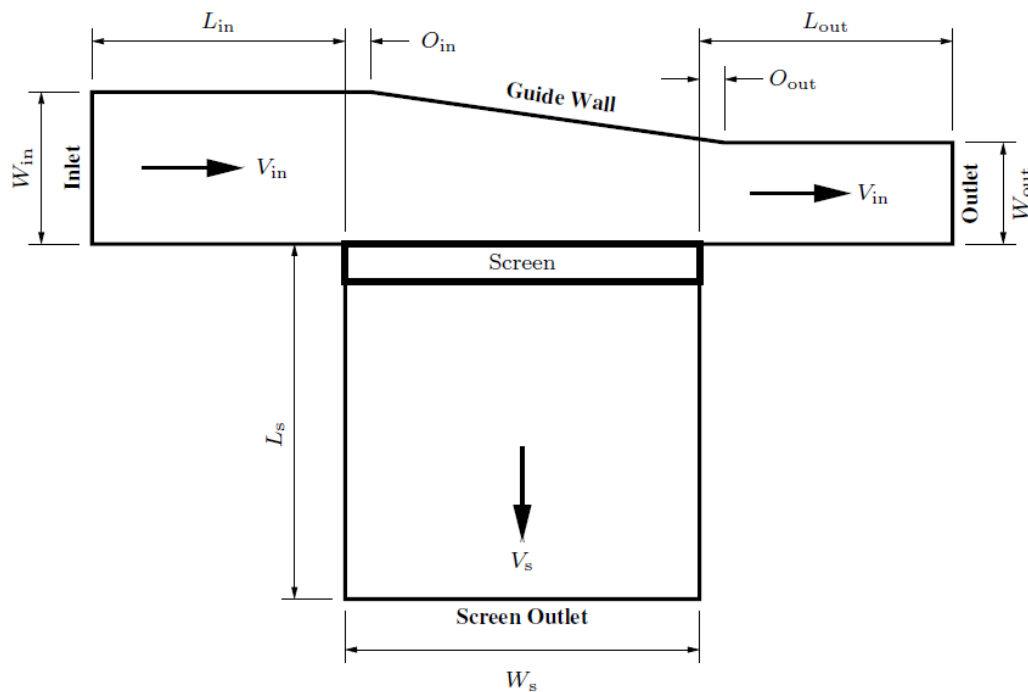


Figure A.2. Dimensions of the Two-dimensional Flow Channel Used in CFD Simulations

Several guide wall taper configurations (Table A.2) were devised and tested to determine the effect on sweep velocity. Sweep velocity was measured at a distance of 1 in. from the screen surface. Simulations used the standard wedge wire screen and flow scenario #5 (Table A.1). The guide wall taper simulations were completed prior to the mesh independence test (Section A.2.2.3), but the mesh resolution was adequate.

Simulated screen sweep and approach velocities were measured at a series of 50 locations along a line 1 inch upstream and parallel to the screen (Figure A.3). These simulations allowed an appropriate guide wall taper to be chosen.

A.2.2.3 Mesh

The computational mesh was generated using the STAR-CCM+ overset mesh capability. Two meshes were used. The background mesh was used for the flume channels. The screen, and a small area around the screen, was a separate mesh. For a single screen, the background mesh was generated according to the dimensions necessary for the flow scenario (Section A.2.2.1) while leaving the screen mesh the same.

A 2D polygonal mesh was used for both the background and screen meshes. Mesh generation parameters were largely the StarCCM+ defaults except that maximum cell size was limited in the screen mesh and in a region around the screen in the background mesh. Near wall boundaries, the mesh was composed of prismatic cell layers to capture potentially steep gradients. After establishing these limitations, a single parameter, Base Size, controlled mesh density.

The lack of validation data made a mesh independence study necessary (Roache, Ghia, and White 1986). The initial simulation included the devilfish spoiler orientation with an overly coarse mesh under flow scenario #5 for 60 s at a time step of 0.05 s. A subsequent simulation was performed with the “Base Size” for both the background and screen meshes reduced by a factor of two. Sweep, approach, and gap velocities were extracted and compared to the previous simulation. When the change in those velocities between simulations was reduced to a few percent, the flow solution was considered mesh independent.

Locations of velocity measurements are shown in Figure A.3. Simulated sweep and approach velocity were measured at several locations along lines 1 and 3 inches upstream of the screen. Simulated velocity was also measured across the narrowest part of the gap between screen elements.

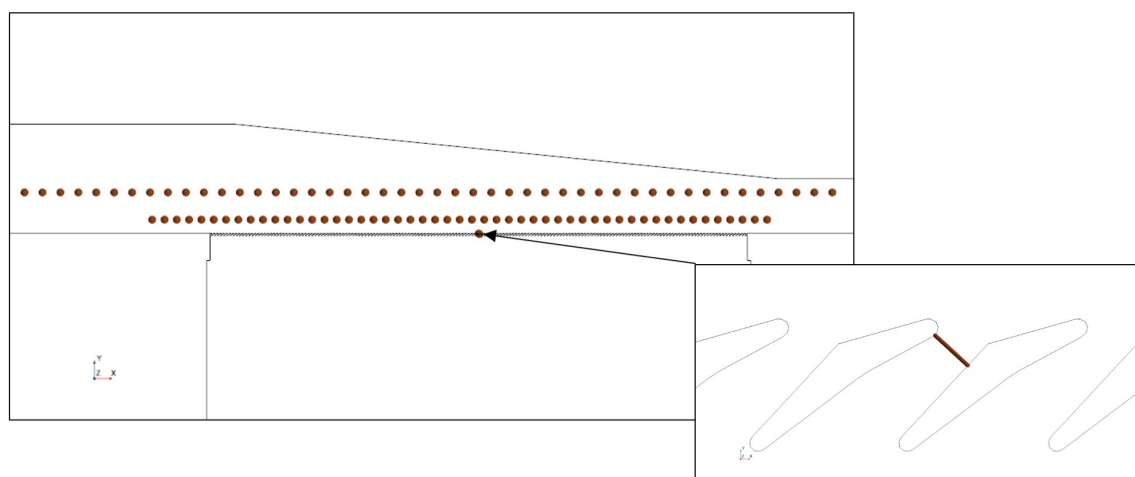


Figure A.3. Velocity Probe Locations used for the Mesh Independence Study. The locations 1 inch upstream of the screen were also used for the guide wall taper simulations.

A.2.2.4 Scenarios

Each scenario and screen type was simulated for 60 s with a 1 ms time step. Simulated flow fields were analyzed to understand the distribution of approach velocity across the screen. Velocity was sampled along a series of 1000 points placed very close (~1 mm) to the upstream

of the screen. The screen was divided into 10bins with a size of 4 inches each. Velocity at the sample points was used to compute an area-weighted average velocity in each bin. These bins were numbered 1 through 10 starting at the upstream edge of the screen ($x = 0$). Additionally, simulated pressure was sampled and integrated along the upstream and downstream sides screen frame. The head loss through the screen was computed as the difference between these two pressures.

A.2.3 Particle Simulations

The CFD-discrete element method (DEM) was employed to simulate the fate of transported particles in the flow fields. In all scenarios, particles were released at 18 locations placed perpendicular to the screen and 14 cm (5.5 in) upstream of the leading screen edge (Figure A.4). Injector 0 was placed 0.5 cm from the wall and injectors 1 through 17 were placed at 1 cm intervals starting at 1 cm from the wall. At these locations, 21 particles/s were injected over 3 s, which resulted in 1152 particle tracks. This low particle injection rate was used to avoid unnecessary particle-particle interaction. To match the laboratory tests at the Alden research lab, the particles were 1 mm in diameter. Material properties of the CFD particles were chosen to be similar to materials being used in the laboratory testing:

- density: 1028.15 kg/m³
- Poisson's ratio: 0.32
- Youngs's modulus: 3.275E9 Pa

Because particles were comparable in size to the screen slot size, the influence of particles on the flow field needed to be captured. Therefore, two-way coupled CFD-DEM simulation was used in the flow investigation. Under this condition, the effects of particle motion and inter-particle collision were accounted for in the computation of fluid flow. This produced a more realistic representation of particle-screen collisions. Since the current work focuses on particle motion in the turbulent flow, the exact eddy interaction model for turbulent dispersion was used to affect turbulent velocity fluctuations on the particle's trajectory. To lower computational requirements for efficient simulations, a parcel depletion model was used in which particles were eliminated if they pass out of the domain of interest such as beyond the downstream edge of the screen.

Further, particle trajectories were analyzed to determine the location of two possible events:

1. "screen interaction": the point at which the particle is in close proximity, but still upstream, of the screen; and
2. "entrainment": the point at which the particle passes through the screen.

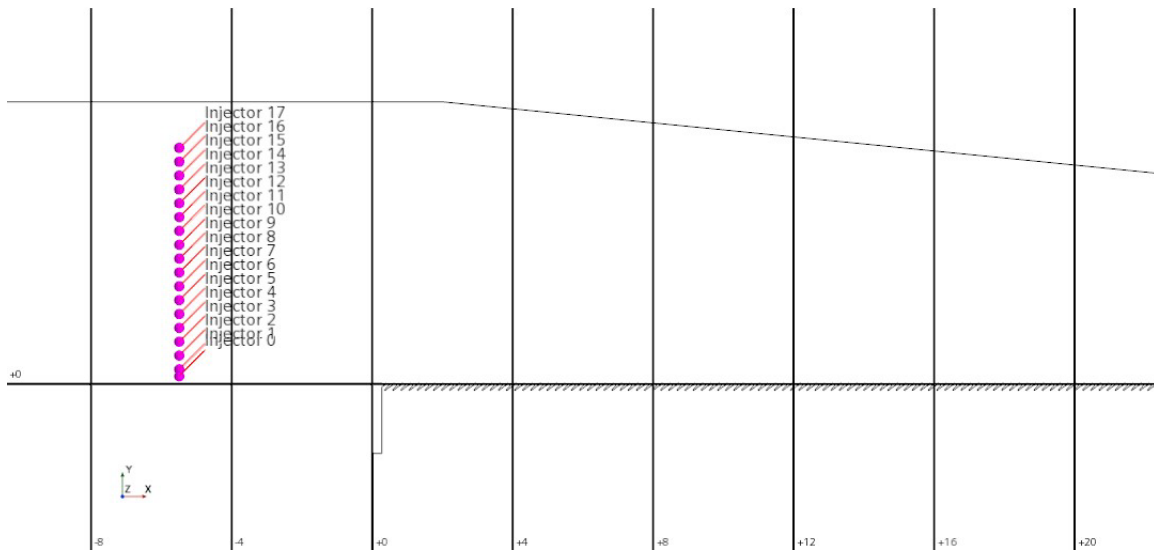


Figure A.4. Locations Where Particles Were Injected

A particle was considered to have “interacted” with the screen the first time its center came within 5 particle diameters of the screen surface. A particle was considered entrained if it passed a plane 2 particle diameters downstream of the screen surface. This included particles trapped in recirculations just below the screen surface.

These events were sampled using the 10 bins used in Section A.2.2.4. It was noted that the flow field became nonuniform at either end of the screen. In this context, center of the screen would be more representative of a screen of arbitrary length and the 6 central bins ($x = 8$ to 32 in) were used for analyses.

Using the central bins altered the definition of particle interaction and entrainment rates. The analysis was limited to particles whose first interaction was in the central bins, so as to avoid bias due to non-uniform flow conditions at the screen ends.. Only those could be considered for entrainment. If a particle’s first interaction with the screen was outside the central bins, but it passed the screen in the central bins, it was not considered “entrained” and ignored.

A.3 Results

A.3.1 Flow Simulation

A.3.1.1 Guide Wall Taper

Figure A.5 shows how the distribution of screen sweep and approach velocity changed with various arrangements of the guide wall (Table A.2). In general, the screen approach velocity was relatively consistent regardless of guide wall position. However, the sweep velocity was significantly affected by the guide wall placement. Of the guide wall configurations tried, a 5% downstream shift maintained a sweep velocity along the screen closer to the nominal than other configurations. This configuration was used for all subsequent flow simulations and utilized in Alden’s laboratory flume testing..

Table A.2. Tested Guide Wall Taper Configurations. Positive offsets are downstream, negative are upstream. Sweep velocity was measured 1 in above the screen.

Case Name	Taper Offset			Sweep Velocity				Screen Head Loss (in H ₂ O)
	Inlet (in)	Outlet (in)	Mean (fps)	Min (fps)	Max (fps)	Range (fps)	Dev (%)	
No Offset	0.0	0.0	1.044	1.031	1.094	0.063	4.8	0.0365
Upstream (5%)	-2.0	-2.0	1.070	1.047	1.110	0.063	3.7	0.0377
Upstream (10%)	-4.0	-4.0	1.098	1.056	1.134	0.079	3.9	0.0390
Downstream	2.0	2.0	1.021	0.996	1.085	0.089	6.2	0.0353
Longer	-2.0	2.0	1.050	1.003	1.105	0.102	5.2	0.0368
Shorter	2.0	-2.0	1.039	1.014	1.088	0.049	4.7	0.0360

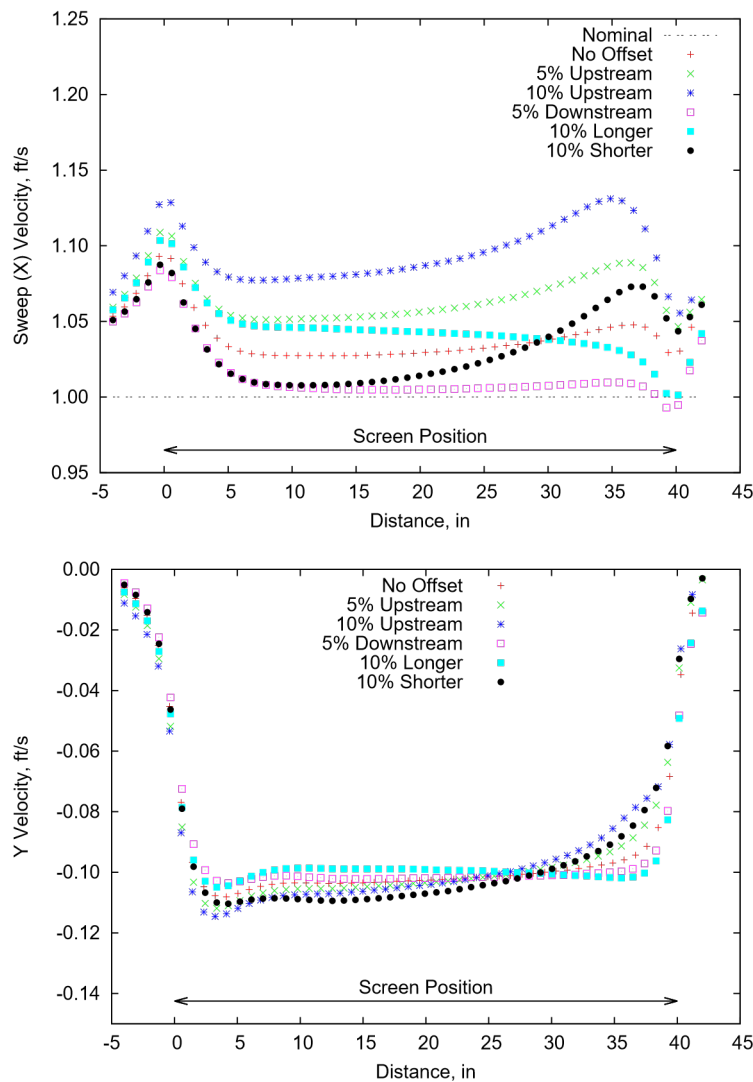


Figure A.5. Screen Sweep (above) and Approach (below) Velocity for Various Guide Wall Taper Configurations. Velocity was probed 1 in upstream of the screen.

A.3.1.2 Mesh Independence Test

Five mesh resolutions were used to perform the grid independence test. Mesh resolutions, sizes and corresponding number of cells are shown in Table A.3 and Figure A.6. Results for the grid independence test were analyzed in terms of screen sweep and approach velocity (Figure A.7), screen gap velocity (Figure A.8), and screen head loss (Figure A.9). As evident from Figures 7-9, the predicted velocity using mesh 5 were less than 1% different than those computed from mesh 4. Since the use of mesh 5 had little effect on velocity fields, the flow simulations using mesh 4 were considered to be mesh independent and used for all subsequent simulations. Figure A.10 and Figure A.11 show the mesh used for the devilfish spoiler and wedge wire screens respectively. As evident from Figures 10 and 11, a prism layer mesh was used to capture the flow field near the wall. The remaining region was meshed with polyhedral mesh.

Table A.3. Mesh Independence Test Results.

Case	Mesh Size		Normalized Maximum Velocity Change above Screen						Screen Head Loss (Pa)
	Background		Screen		3 in		1 in		
	Base (mm)	Cells	Base (mm)	Cells	Sweep	Normal	Sweep	Normal	
1	2.0	65k	2.0	129k					23.8
2	1.0	164k	1.0	225k	2.16E-02	3.45E-02	5.70E-02	8.64E-01	25.1
3	0.5	460k	0.5	405k	1.54E-02	3.32E-02	3.61E-03	3.09E-02	27.0
4	0.25	1450k	0.25	522k	1.05E-02	2.29E-02	2.21E-03	1.70E-02	26.8
5	0.125	4988k	0.125	968k	7.05E-03	8.18E-03	1.75E-03	7.42E-03	26.6

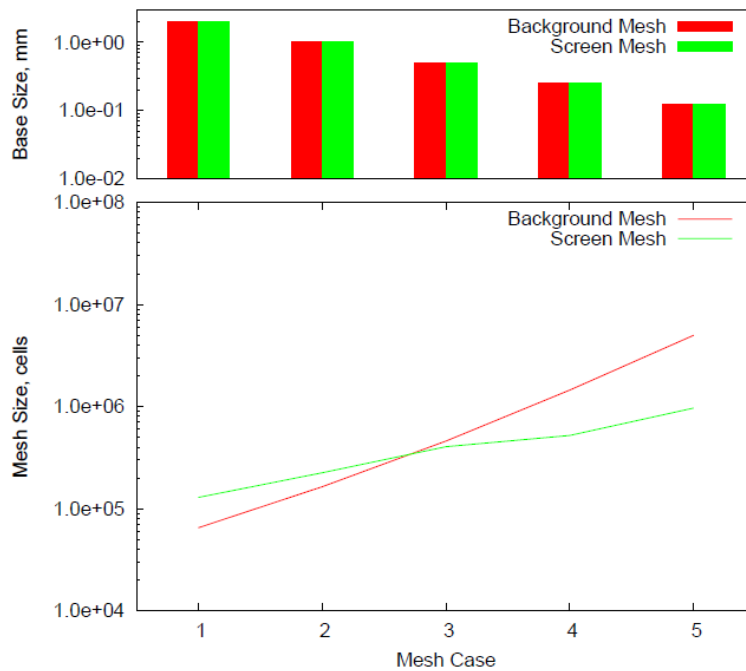


Figure A.6. Background and Screen Mesh Base Size (above) and Cell Count (below)

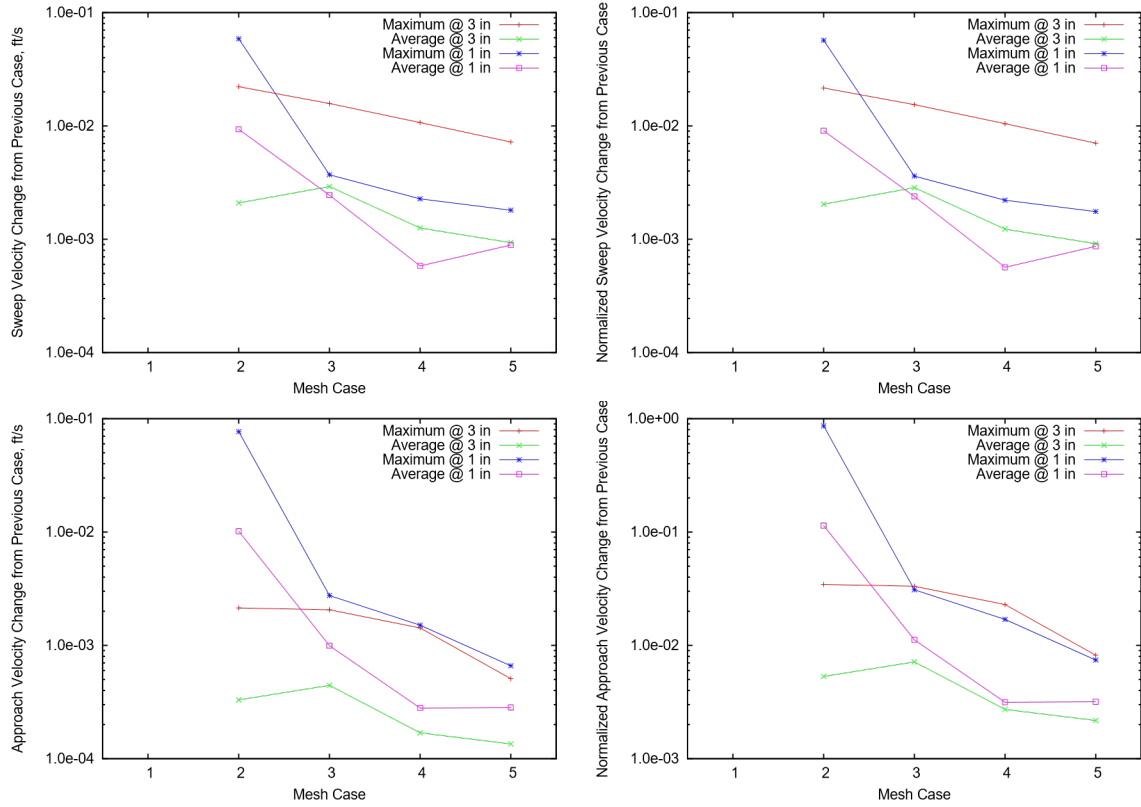


Figure A.7. Relative Change in Simulated Screen Sweep (above) and Approach (below) Velocity (left) and Normalized Velocity (right) Measured at 3 and 1 inches Upstream of the Screen for Each Mesh Case

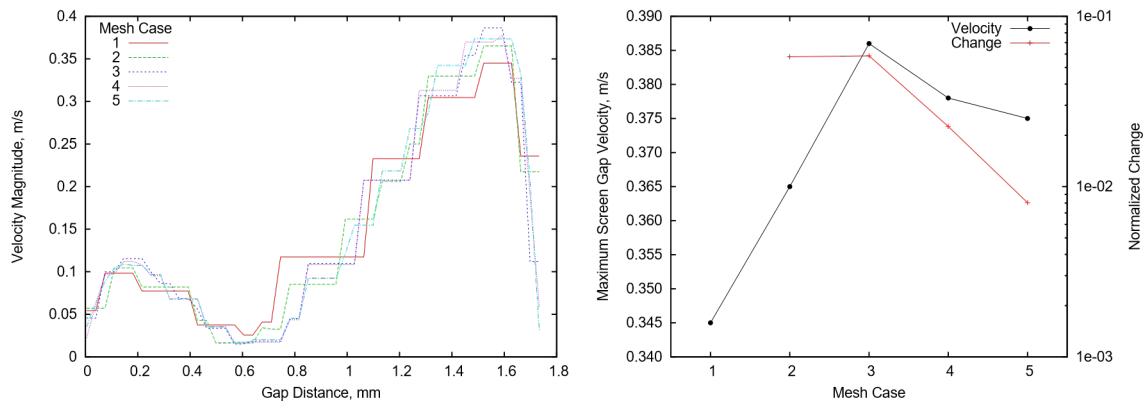


Figure A.8. Simulated Screen Distance Gap Velocity Profiles (left) and Relative Change in Maximum Gap Velocity (right) in Each Mesh Resolution Case

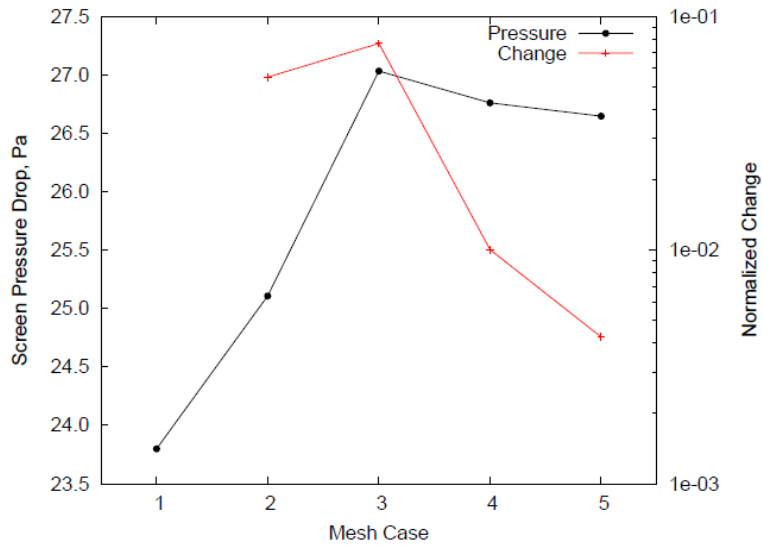


Figure A.9. Relative Change in Simulated Screen Pressure Drop in Mesh Resolution Cases

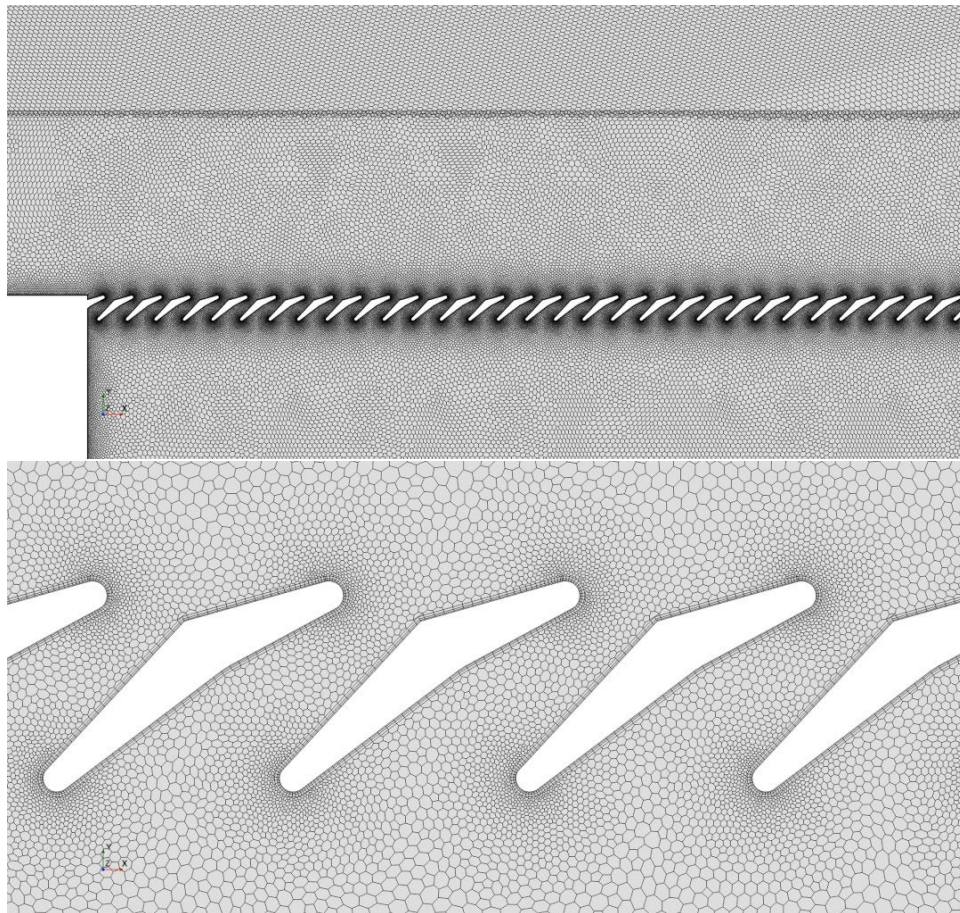


Figure A.10. Mesh Used for the Devilfish Spoiler Screen Simulation

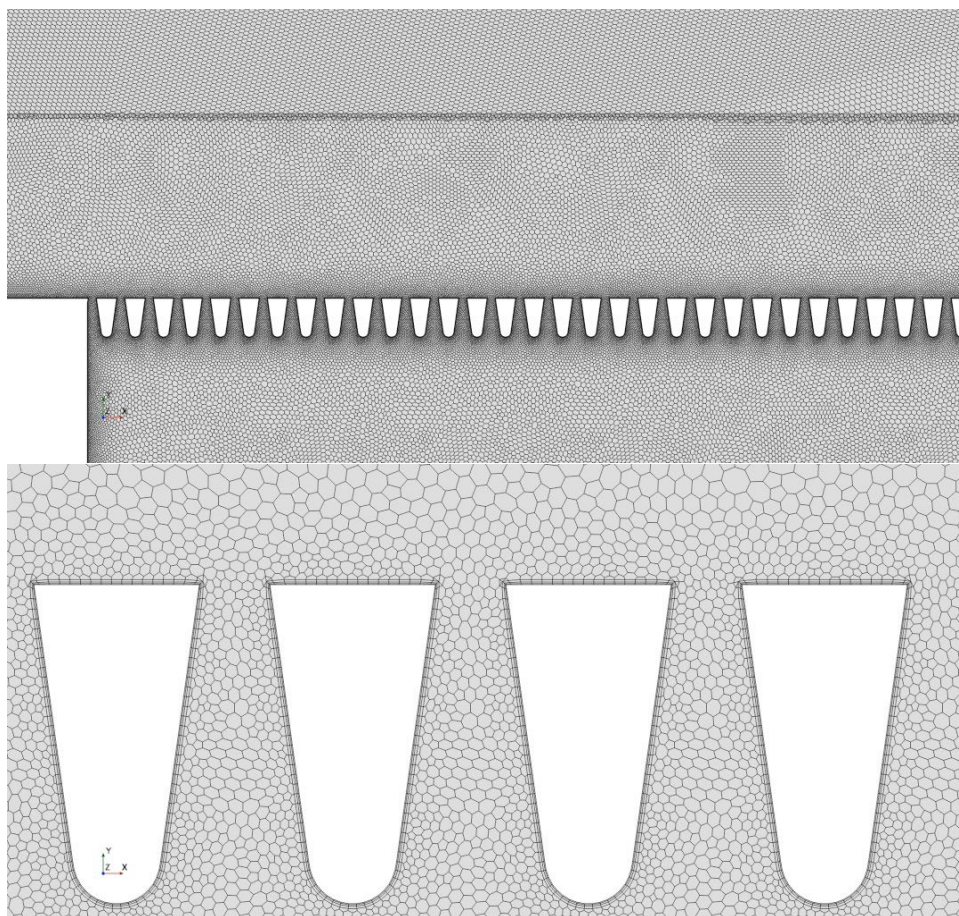


Figure A.11. Mesh Used for the Wedge Wire Screen Simulation

A.3.1.3 Devilfish Wing Orientation

Early flow simulations for the devilfish screen in the wing orientation showed very large oscillations in the flow field emanating from the leading edge of the screen (Figure A.12). These were first observed in simulations of the baseline scenario #5. Similar behavior of flow instability was also observed in the Scenario #7 because of low approach velocity. An analysis of vortex shedding was also performed. Vortex shedding frequency was computed by placing probes above the screen to measure temporal variation of velocity at intervals of 4 inches (see Figure A.12). A Fast Fourier Transform (FFT) was performed from 10-15s in simulation time to get the vortex shedding frequency (Figure A.13). It is observed that the frequency of oscillation stays constant until approximately 16 in, where it then breaks apart and has multiple frequencies. This finding suggests that the wing orientation may induce considerable turbulence near the screen face. Near-screen turbulence may have both negative implications (e.g., screen vibration) and positive implications (e.g., behavioral deterrence of fish). However, because turbulence was not explicitly simulated by the model, the wing orientation was excluded from further CFD investigation.

Solution Time 30 (s)

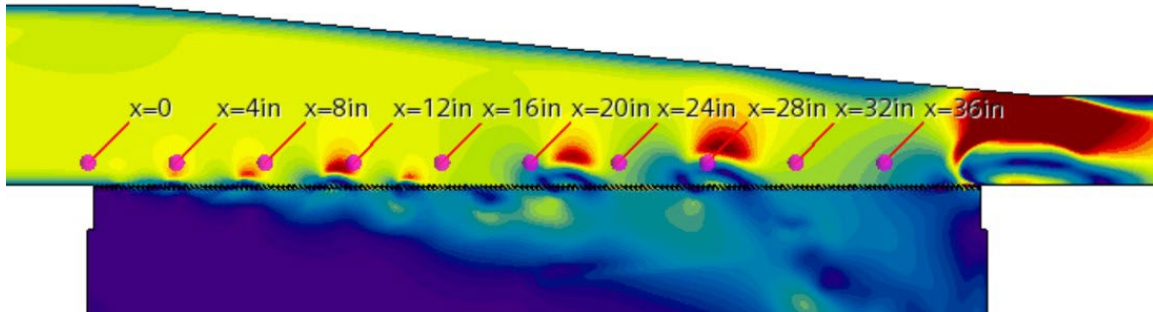


Figure A.12. Vortex Shedding Observed in the Simulation of the Devilfish Screen in Wing Orientation (Scenario #5). Simulated velocity was extracted at the probe locations noted and used for a frequency analysis.

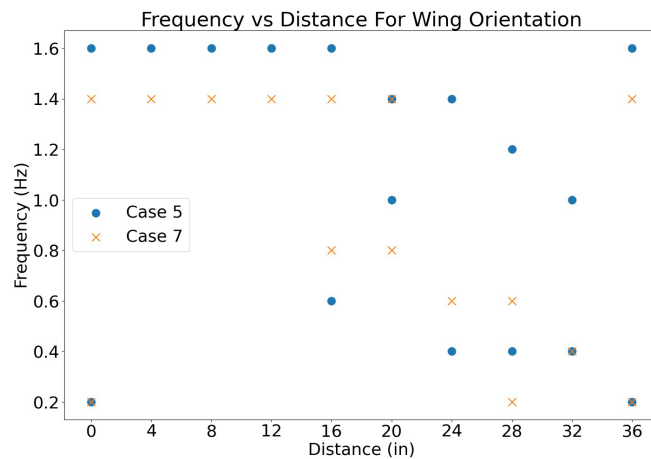


Figure A.13. Velocity Fluctuation Frequencies Observed for the Wing Mode Orientation of the Devilfish Screen for Scenarios #5 and #7

A.3.1.4 Flow Scenario Comparison

As noted in Section A.2.2, an outward flux was imposed at the screen channel outlet. In an attempt to increase flow uniformity through the screen, an alternative approach was tested whereby a uniform outlet velocity was imposed at the screen outlet. This did not significantly affect flow patterns downstream of the screen, nor considerably increase screen flow uniformity.. Therefore, predicted results shown here used the original fixed flux condition.

Flow simulations were carried out for the devilfish spoiler orientation and wedge wire screens under the 10 flow scenarios. Figure A.14 and Figure A.15 show predicted velocity fields near the screen bars. Figure A.16 compares the distribution of approach velocity for the wedge wire and devilfish spoiler screens. Figure A.17 shows a similar comparison but relative to the mean approach velocity. The latter highlights differences in the absolute velocities shown in the former.

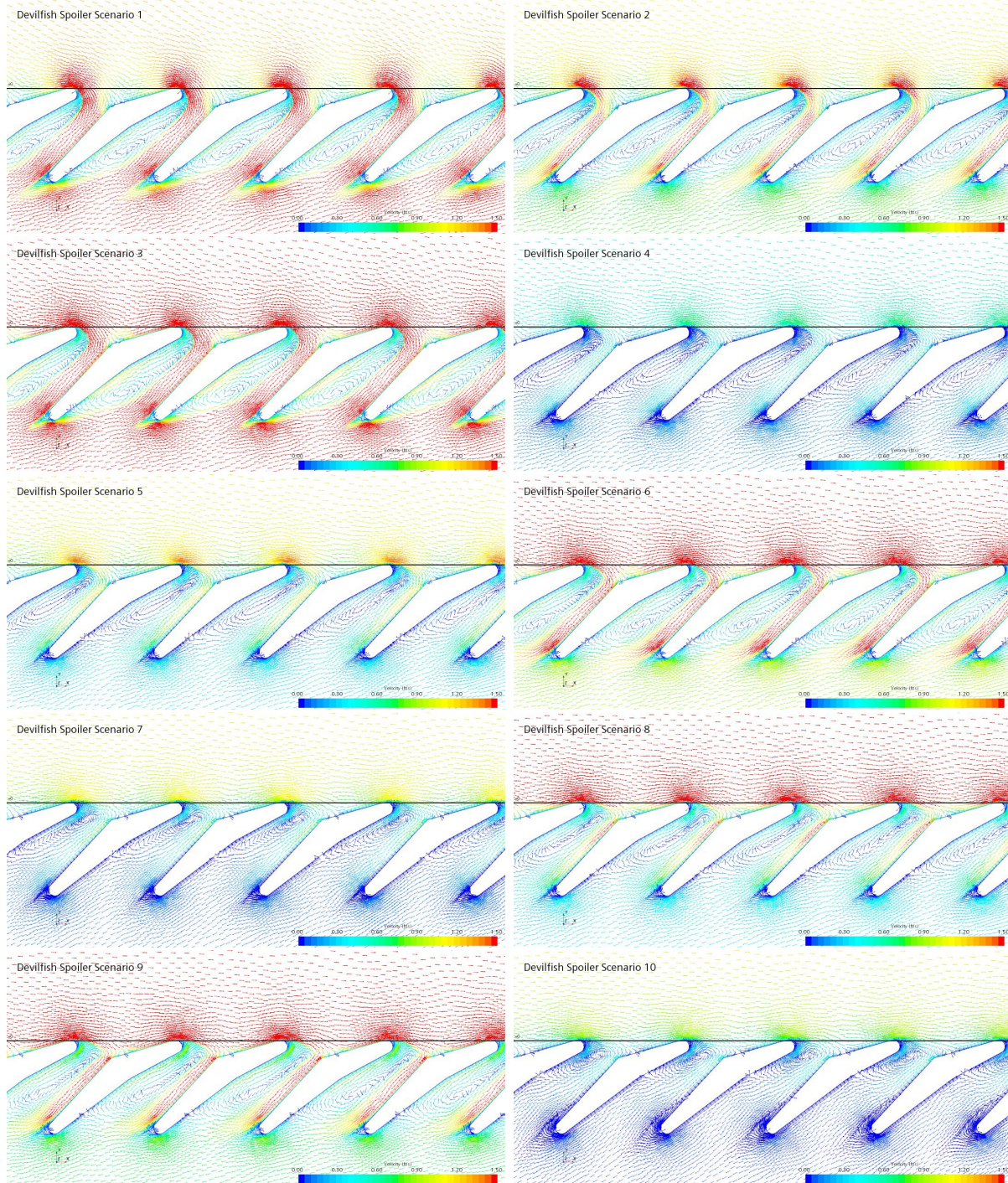


Figure A.14. Simulated Velocity Around the Devilfish Spoiler Screen Bars

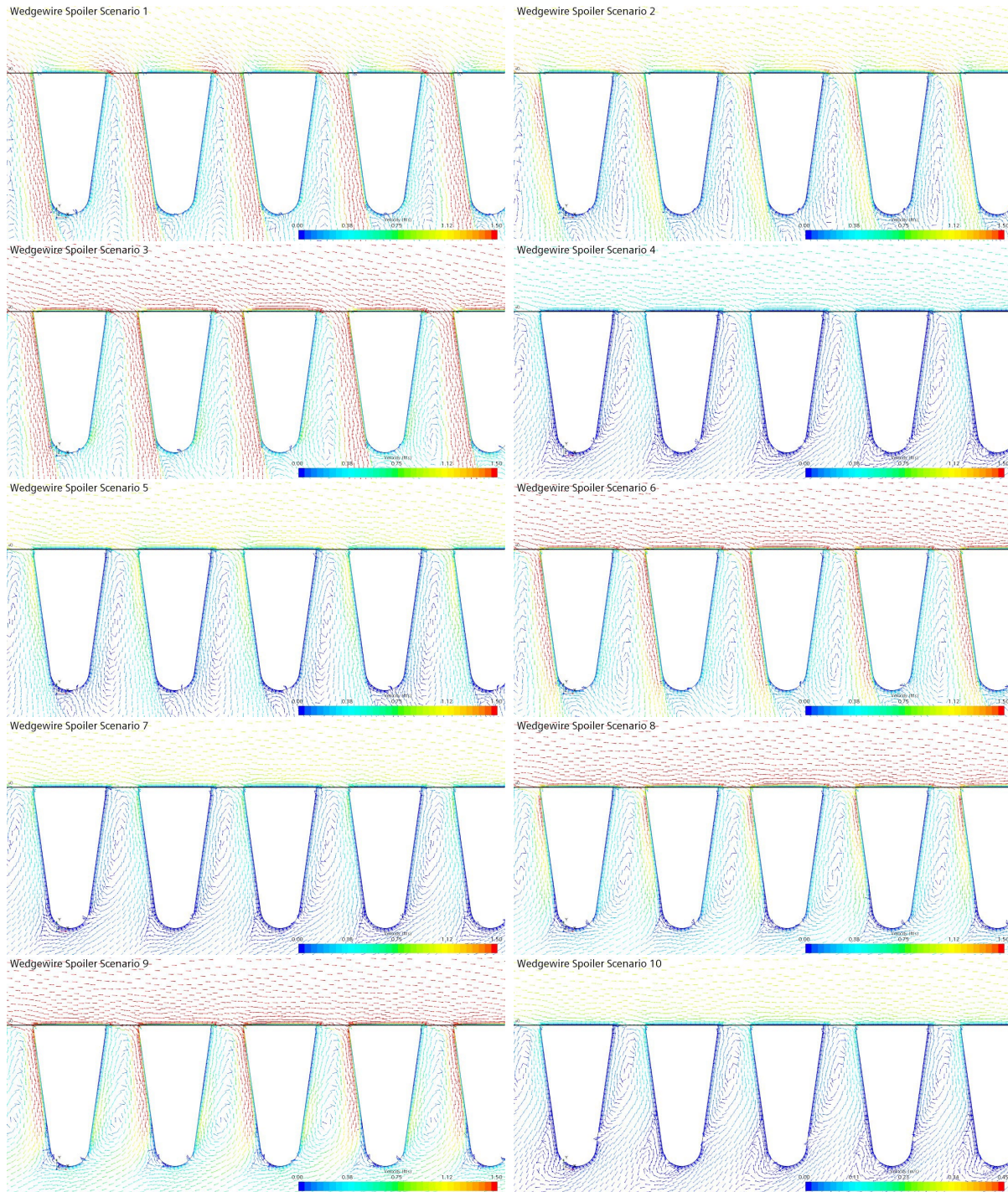


Figure A.15. Simulated Velocity Around the Wedge Wire Screen Bars

In general, the distribution of approach velocity with the wedge wire screen was constant across the screen, with the exception of the upstream 4 inch of the screen. Approach velocity in this first bin is significantly lower than the remainder of the screen.

In contrast, variation in the approach velocity distribution through the devilfish spoiler screen is relatively high. When the average approach velocity was low (scenarios 4,5,7-10), variation in

the approach velocity from the mean approach velocity was seemingly random. In those scenarios with a relatively high mean approach velocity, velocity through the upstream half of the screen was much lower than the downstream half, with a relatively consistent distribution.

Figure A.18 shows the predicted head loss across the screen for all simulated scenarios. The head losses are very small, less than 1 inch of water head in all but one scenario. However, the devilfish spoiler screen produces a significantly higher head loss than the wedge wire screen in all scenarios.

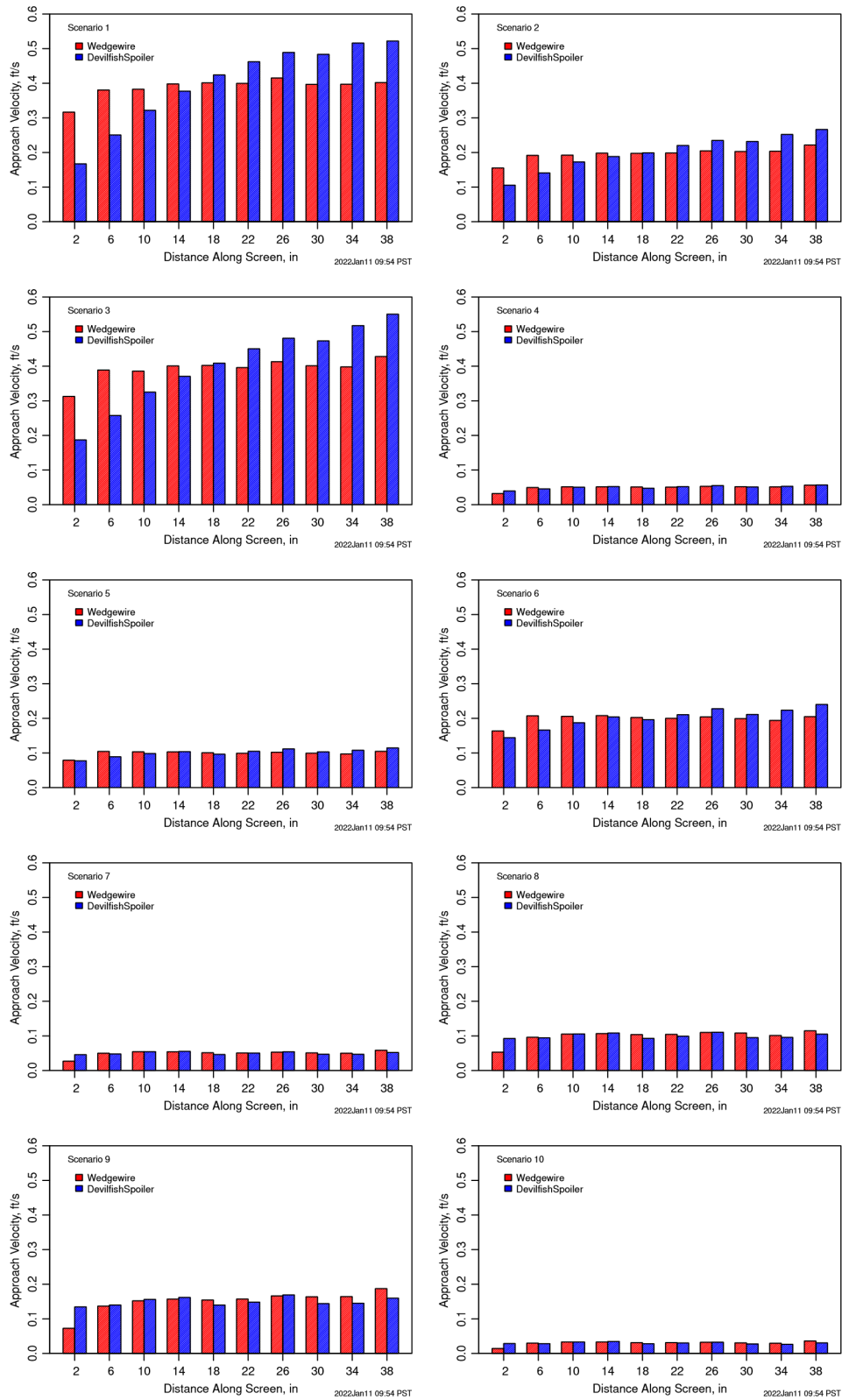


Figure A.16. Distribution of Approach Velocity Magnitude Along the Wedge Wire and Devilfish Spoiler Screens

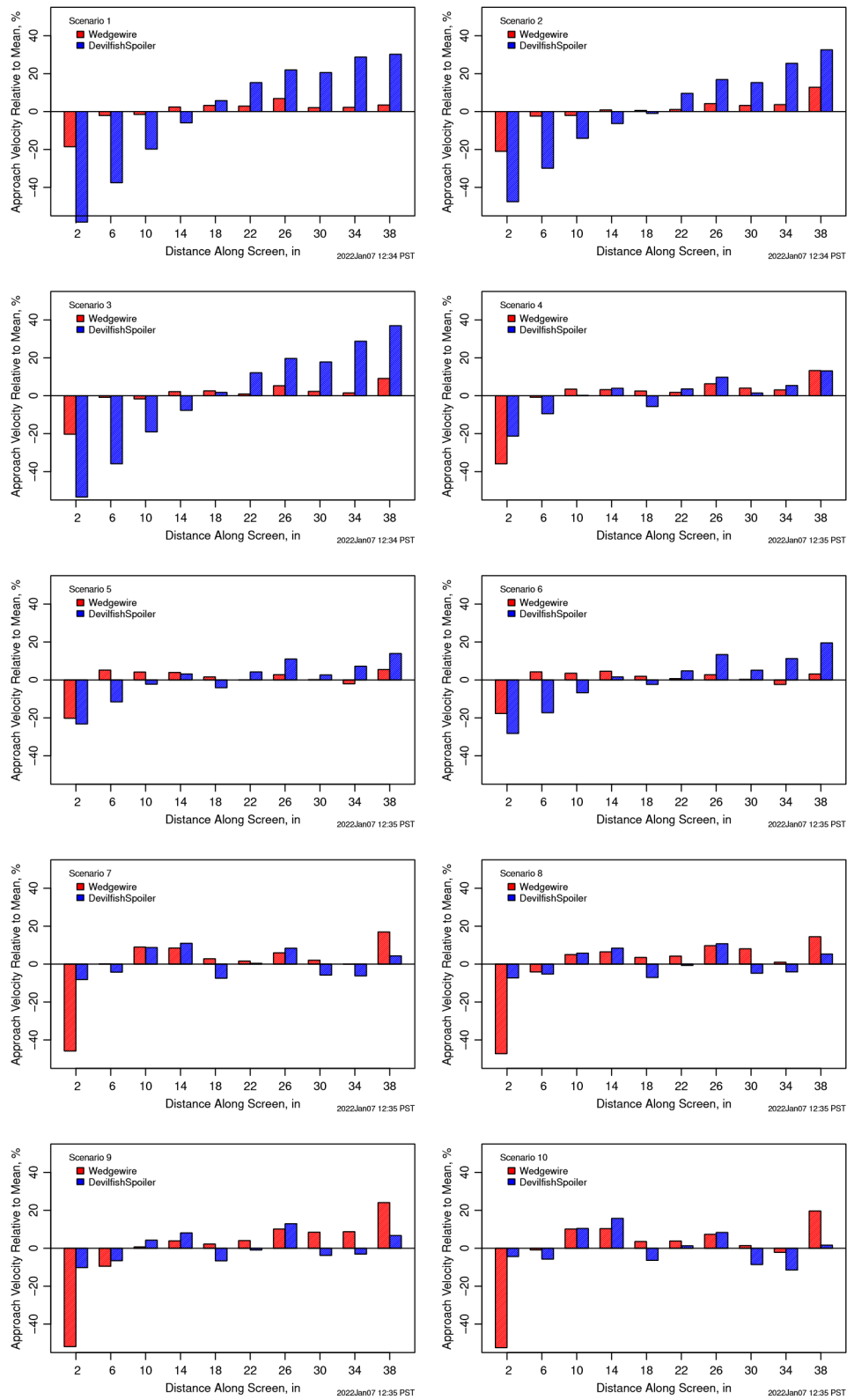


Figure A.17. Approach Velocity Relative to the Mean Along the Wedge Wire and Devilfish Spoiler Screens

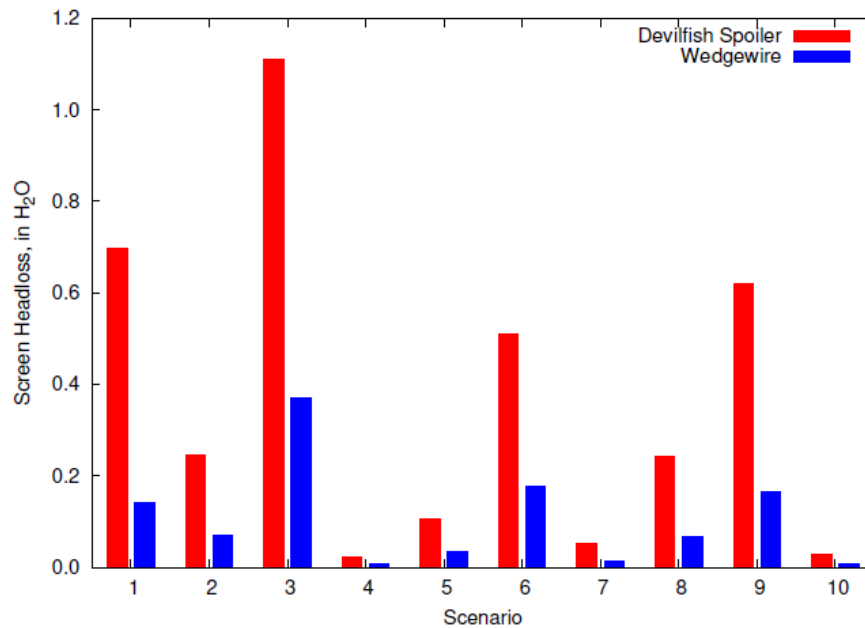


Figure A.18. Simulated Wedge Wire and Devilfish Spoiler Screen Head Loss for All Scenarios

A.3.2 Particle Simulation

CFD-DEM simulations were performed for both screens under the 10 flow scenarios. Figure A.19 shows particles' trajectory colored by injectors' location for the devilfish spoiler screen. Figure A.20 shows some tracks in detail around a few screen bars. Figure A.21 and Figure A.22 show tracks for the wedge wire screen. The vertical lines in those figures mark the edges of the bins for which screen interaction and entrainment were analyzed. Figure A.23 compares the distribution of particle interaction and entrainment over the central part of the screen (8-32 inch). Particle fate counts are shown in Table A.4. Overall entrainment in the central part of the screen is compared in Figure A.24. As would be expected, the distribution of particles interacting with the screen is nearly the same for either screen. Although the overall entrainment was similar with both screens, entrainment with the devilfish screen was usually higher at the downstream section of screen. This might be due to the distribution of velocity across the devilfish screen (Figure A.17).

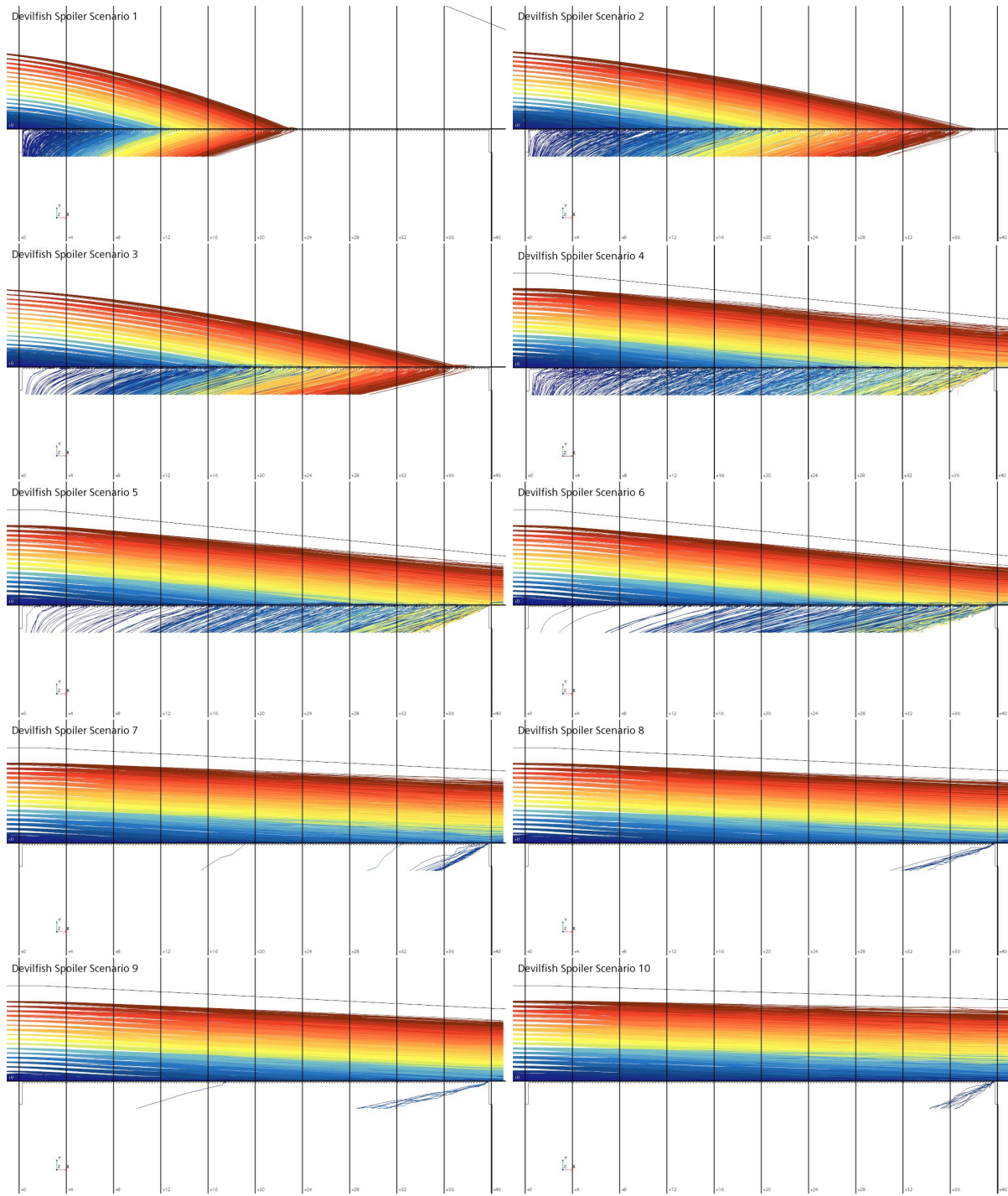


Figure A.19. Particle Tracks Simulated for the Devilfish Spoiler Screen. Tracks are colored by an arbitrary injection point index.

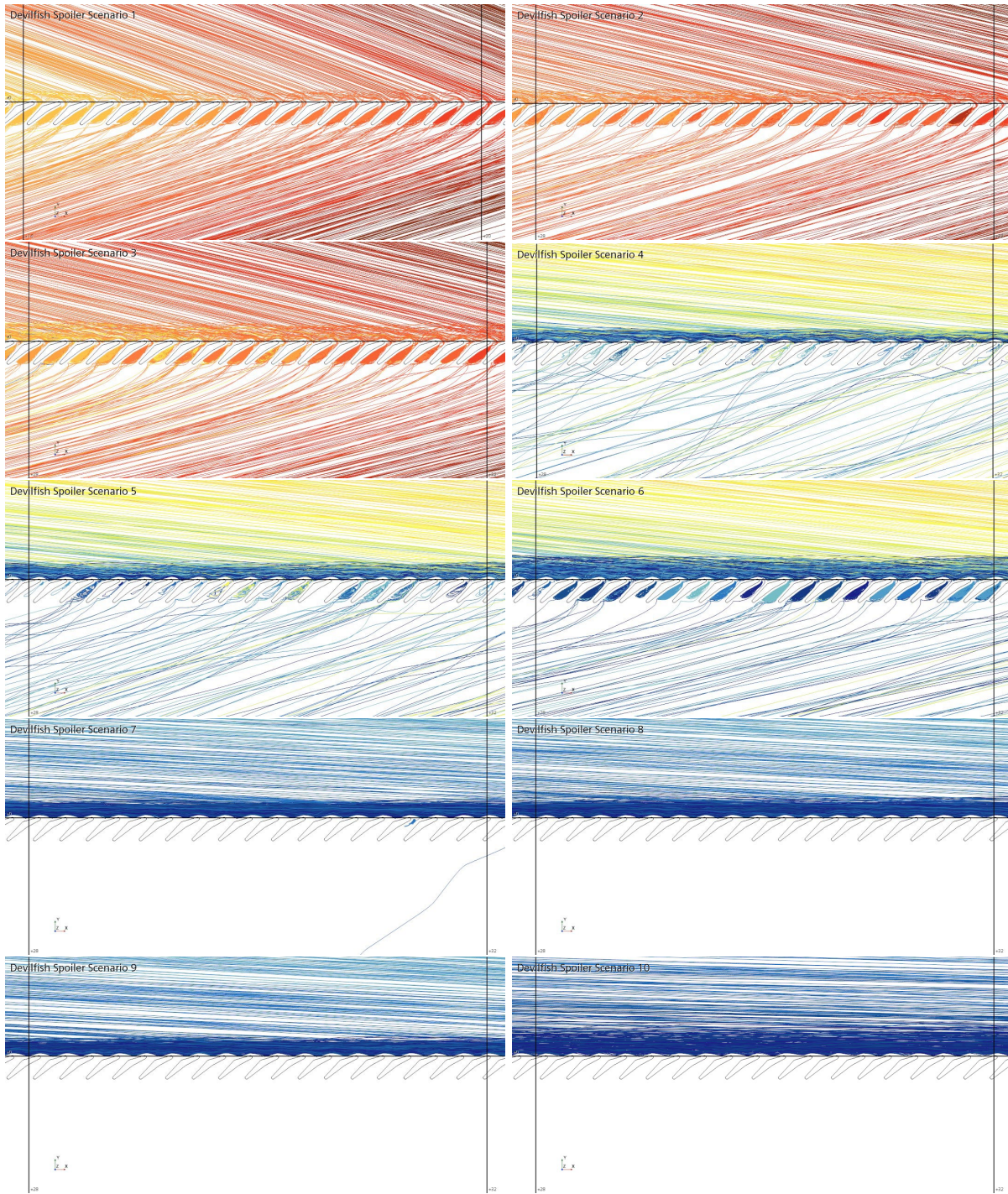


Figure A.20. Closer View of Particle Tracks Simulated for the Devilfish Spoiler Screen

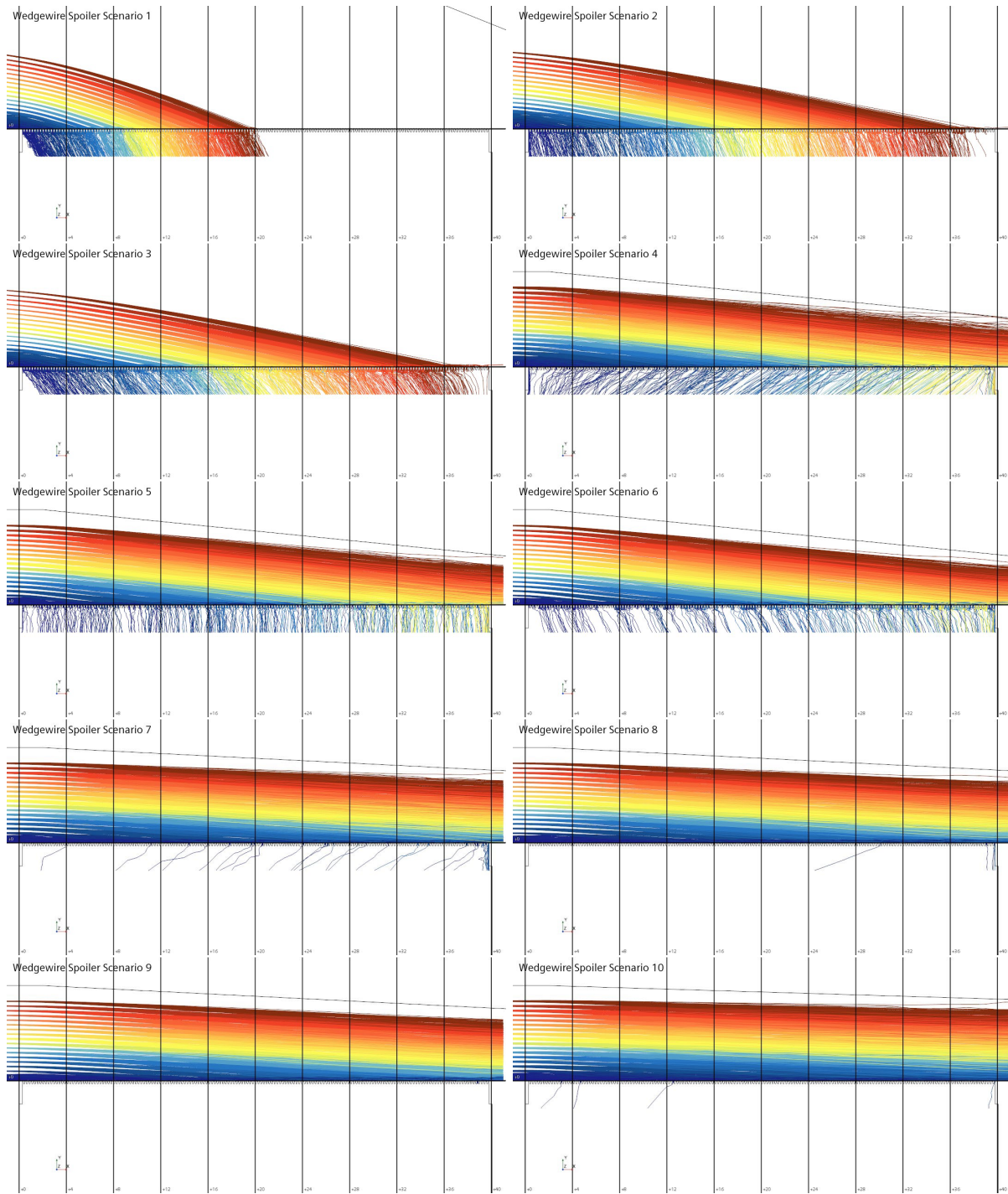


Figure A.21. Particle Tracks Simulated for the Wedge Wire Screen. Tracks are colored by an arbitrary injection point index.

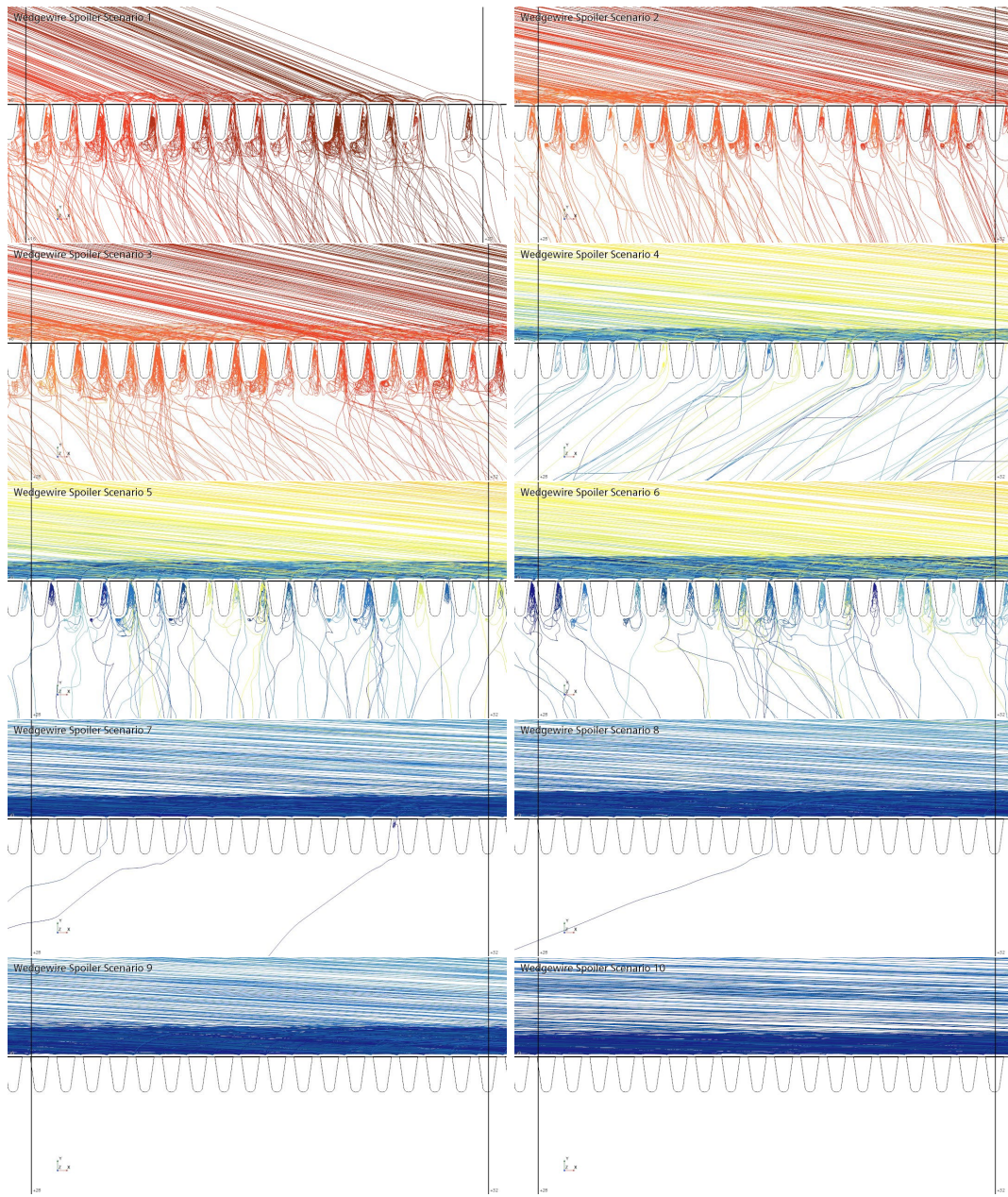


Figure A.22. Closer View of Particle Tracks Simulated for the Wedge Wire Screen

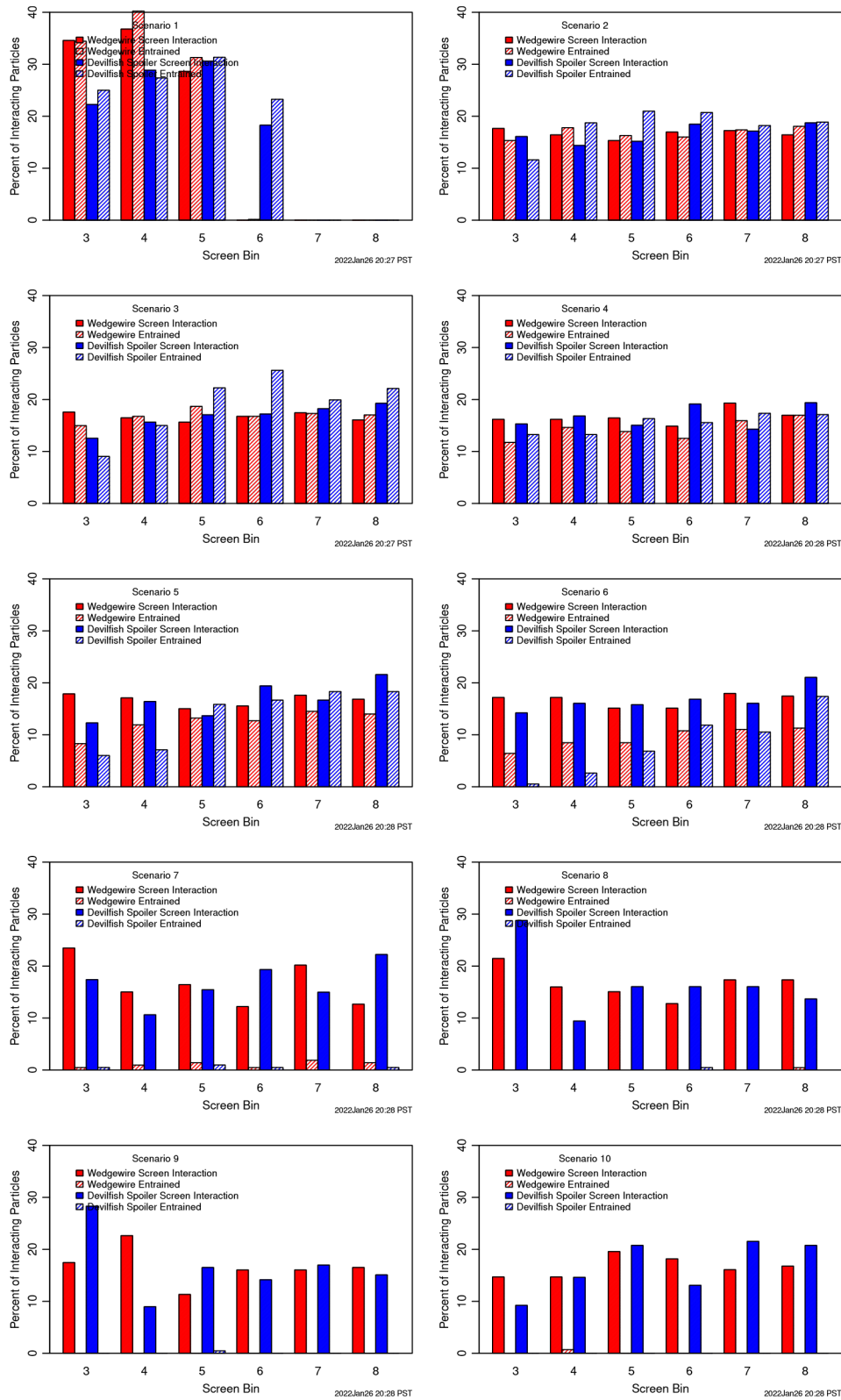


Figure A.23. Comparison of Particle Interaction and Entrainment Between the Wedge Wire and Devilfish Spoiler Screens for the 10 Flow Scenarios. Only particles whose first screen interaction was in the central part of the screen (8-32 in) were considered.

Table A.4. Particle Count Summary

Scenario	Total Tracks	Particle Count			
		Entire Screen		Central Bins	
		Interacted	Entrained	Interacted	Entrained
Devilfish Spoiler					
1	1152	1152	1148	804	800
2	1152	1152	1150	758	717
3	1152	1152	1152	773	715
4	1152	711	595	392	271
5	1152	711	517	366	193
6	1152	714	413	380	109
7	1152	396	33	207	2
8	1152	393	12	212	0
9	1152	391	11	212	0
10	1152	282	12	130	0
Wedge wire					
1	1152	1152	1146	639	637
2	1152	1152	1147	731	692
3	1152	1152	1138	728	674
4	1152	709	552	383	240
5	1152	710	522	386	195
6	1152	707	398	390	139
7	1152	396	34	213	6
8	1152	390	5	219	1
9	1152	388	1	212	0
10	1152	276	4	143	0

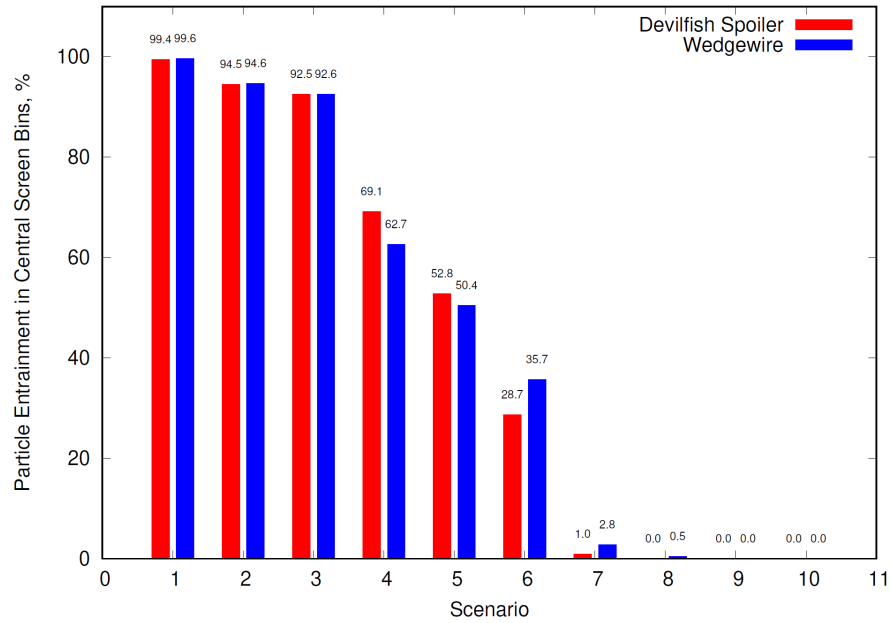


Figure A.24. Comparison of Particle Entrainment In the Central Part of the Screen (8-32 in). In this plot, only those particles whose first screen interaction was within the central bins were considered.

A.4 References

Roache, P. J., K. N. Ghia, and F. M. White (1986, 03). Editorial policy statement on the control of numerical accuracy. *Journal of Fluids Engineering* 108(1), 2–2.

Siemens Digital Industries Software (Siemens 2021). Simcenter STAR-CCM+, version 2021.1.

Appendix B
Additive Manufacturing

January 2022

Sef Christ, PNNL

This appendix outlines the fabrication and design of the test fin array based on the concept submitted to the Fish Protection Prize.

B.1 Fin Panel Design

Figure B.1. shows the cross-sectional profile of the fin design. In the fin array, each fin is spaced at 6.31 mm, leaving an approximately 2.0 mm flow gap between adjacent pins. The fin array was specified to be 40 inches by 18 inches. The chosen means for fabrication was FDM 3D printing. Due to the size limitation of the available printer, the full panel array had to be broken down into 12 equal subarrays as seen in Figure B.2. These subarrays can be combined in a 3x4 array to create the full panel assembly as seen in Figure B.3. The subpanels have cross-bars printed in to later be attached to the metal frame. The wings on either end of the subarrays were added to improve the printing process and were removed during the assembly of the full panel.

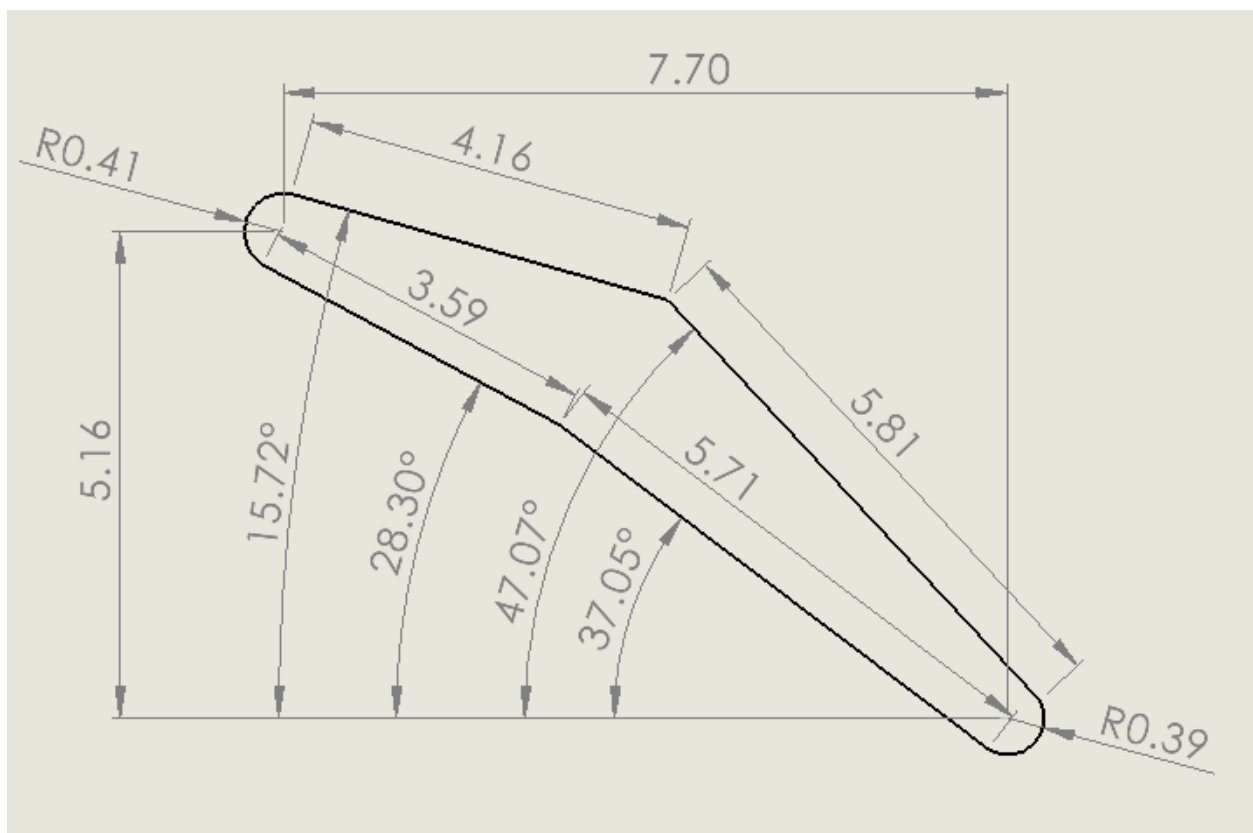


Figure B.1. Fin Cross-section (units in millimeters)

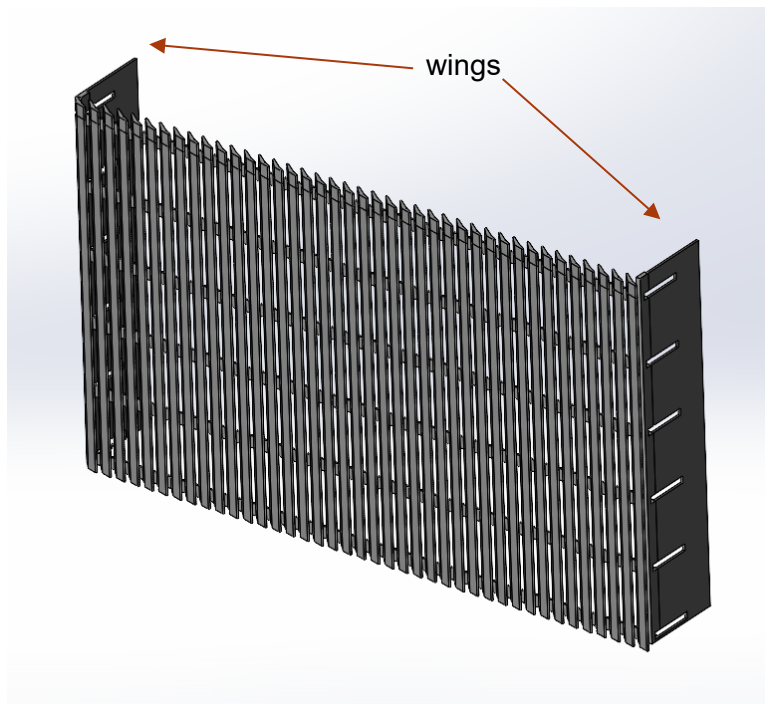


Figure B.2. Single Subarray Panel

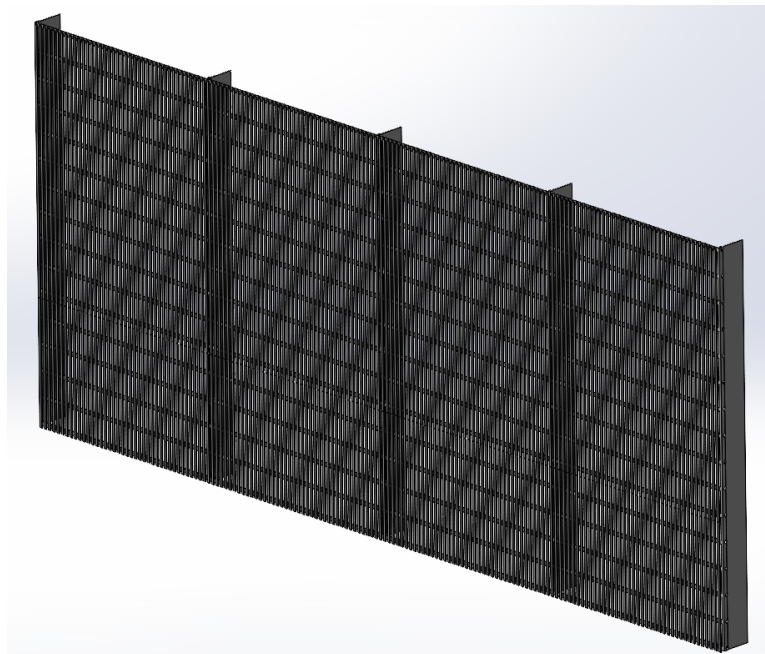


Figure B.3. Full Fin Array

B.2 Printing Parameters

The printer used to print the subarray panels was a Prusa i3 MK2S. The material used was MatterHackers' Pro PLA. The printer used a 300 micron nozzle printing at a 150 micron layer height. The following figures, B.4 through B.6, show the resultant printed components.

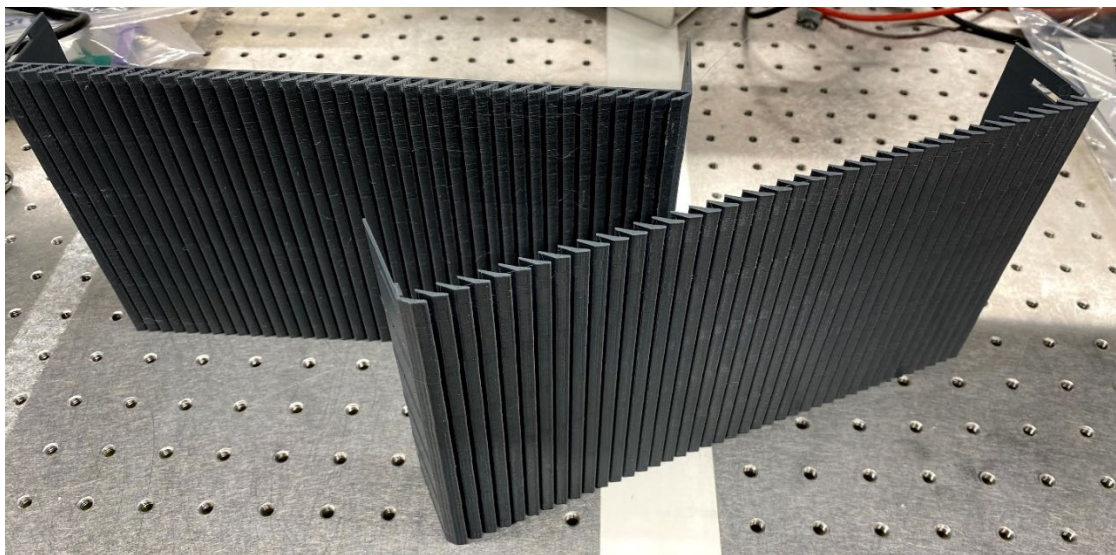


Figure B.4. Set of printed subarray panels



Figure B.5. Rear of subpanel



Figure B.6. Full panel array - before installation

B.3 Full Assembly

The full assembly consist of the 3x4 array of subarray panels attached via 2-part epoxy to the 304 stainless steel frame. This frame consisted of an external frame made of 2-inch-wide by 0.25-inch-thick 304 stainless steel bars and a series of 1-inch-wide by 0.105-inch-thick support bars. Figure B.7 gives an illustration of this frame while Figure B.8 shows the final assembly prepped for shipping.

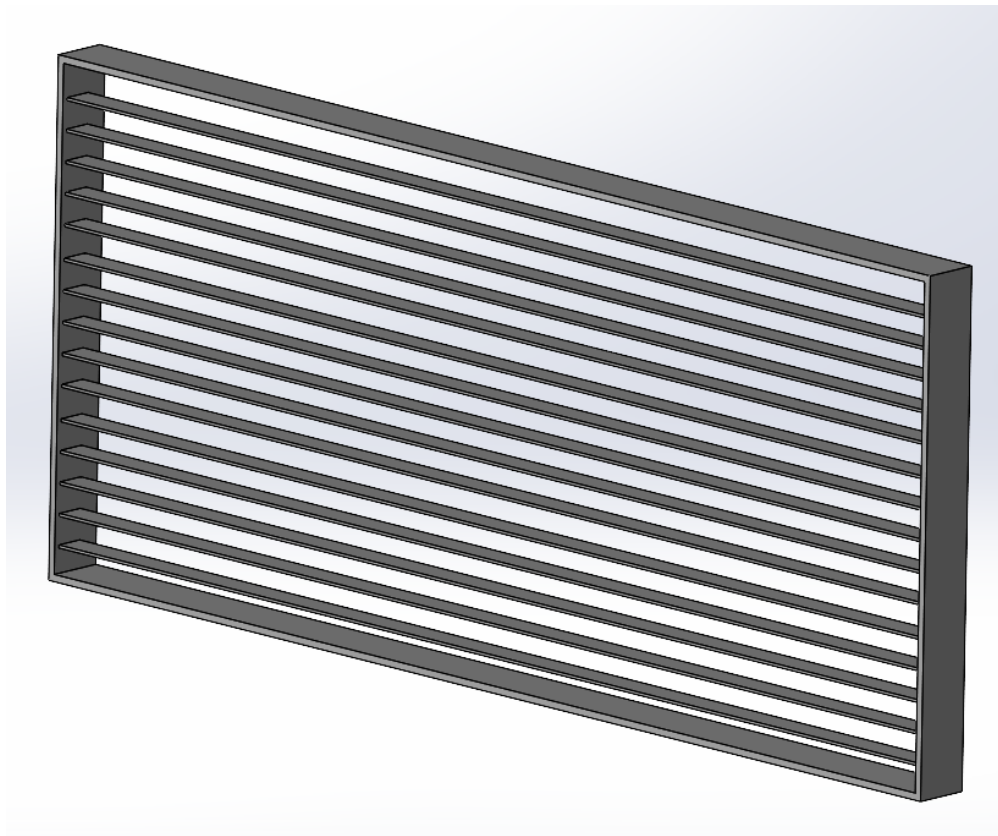


Figure B.7. Stainless Steel Frame



Figure B.8. Fully assembled Array

Appendix C
Fish Screen Life-Cycle Cost Model

January 2022

Dave Anderson, PNNL
Brittany Tarufelli, PNNL
Bob Mueller, PNNL

Summary: PNNL designed this model to be used in technical support of the Mater team's efforts as part of the WPTO Fish Exclusion Challenge for Hydropower. It provides economic valuation in terms of life-cycle cost analysis of the Mater screen technology compared to existing comparable diversion screening technology (flat plate screens) for relatively small diversions ranging from 15-100 cfs. The results can be used to articulate potential costs and benefits offered by new technology compared to baseline screen technology.

Best efforts under the funding constraints were made to identify citable sources for costs and other economic variables used to develop the analysis. Technology economic benefits result from reduced capital and operations and maintenance costs. Additional economic benefits result in the form of reduced mortality of early life-stage fish species attributable to the technology design. Though not currently paid to beneficiaries, these mortality benefits can be substantial over the lifetime of screen installations.

Model results are applicable to the states west of the Great Plains in the United States. Additional refinement would permit extension of the model to all waterways of the US which utilize flat plate screen technology.

Note: The market analysis model is provided as a separate Excel workbook with an integrated instruction manual.

Pacific Northwest National Laboratory

902 Battelle Boulevard
P.O. Box 999
Richland, WA 99354
1-888-375-PNNL (7665)

www.pnnl.gov